



POLITECNICO
MILANO 1863

SCUOLA DI INGEGNERIA INDUSTRIALE
E DELL'INFORMAZIONE

Experimental investigation on hemicellulose and biomass mixture pyrolysis: a study on devolatilization and speciation

TESI DI LAUREA MAGISTRALE IN
CHEMICAL ENGINEERING¹ AND ENERGY ENGINEERING² –
INGEGNERIA CHIMICA¹ E INGEGNERIA ENERGETICA²

Authors: **Eleonora Benedetto¹, Alessandro Roda²**

Student IDs: 995603, 990075

Advisor: Alessandra Beretta

Co-advisor: Veronica Piazza

Academic Year: 2022-23

Abstract

In recent decades, unprecedented economic and technological advancements have led to increased energy consumption and heightened environmental awareness. In this context, the untapped potential of second-generation biomass plays a pivotal role, presenting an eco-friendly alternative to fossil fuels and a versatile resource with applications in biofuel, biogas, and chemical production. The intricate nature of this raw material demands advanced technologies for efficient conversion and a comprehensive understanding of the behavior of its macro-constituents. This thesis focuses on pyrolysis, a process that subjects biomass to high temperatures in an oxygen-free environment, employed to investigate the behavior of hemicelluloses, selecting and comparing three specific types (xylan, arabinoxylan, glucomannan) alongside cellulose. This research comprises two phases. The first investigates hemicellulose devolatilization through thermogravimetric analysis (TGA), in which biomass undergoes pyrolysis under varied heating ramps (3°C/min, 20°C/min, and 100°C/min) to understand the impact of operating conditions and provide valuable insights to ultimately formulate kinetic models. This phase of the study reveals that hemicellulose exhibits lower stability compared to cellulose, resulting in a higher yield of char and demonstrating intricate devolatilization pathways. The second phase focuses on qualitative and quantitative pyrolysis product speciation using online Mass Spectrometry (MS), offline Gas Chromatography (GC), and Orbo™ sorbent traps. This exploration aims to unravel the intricate landscape of pyrolysis product yields and distribution resulting from hemicellulose degradation. The key findings highlight xylan as the hemicellulose exhibiting the highest yields of water and residual char, while glucomannan stands out for the highest amount of bio-oil, particularly enriched in C5 and C6 compounds. These analytical protocols are applied both to single components and mixtures, in order to investigate potential synergistic effects and to enhance our understanding of complexities arising from the coexistence of hemicellulose with other components. An additive behavior both in terms of mass loss trends and product speciation is generally confirmed. To conclude, data derived from experiments conducted within a fixed bed reactor configuration will also be presented, allowing for a comparative analysis and discussion of the results obtained from the two distinct experimental setups. Through such exploration, this research aims to enhance our knowledge of pyrolysis reactions applied to hemicelluloses, contributing valuable insights to the broader field of biomass utilization.

Key-words: Pyrolysis, biomass, hemicellulose, devolatilization, speciation, thermogravimetric analysis, mass spectrometry, gas chromatography.

Abstract in italiano

Negli ultimi decenni, progressi economici e tecnologici senza precedenti hanno portato a un aumento del consumo di energia ed a una maggiore consapevolezza ambientale. In questo contesto, il potenziale della biomassa di seconda generazione svolge un ruolo fondamentale, presentando un'alternativa ecologica ai combustibili fossili e una risorsa versatile per la produzione di biocarburanti, biogas e prodotti chimici. La complessità di questa materia prima richiede tecnologie avanzate per una conversione efficiente e una comprensione approfondita del comportamento dei suoi macro-costituenti. Questa tesi si concentra sulla pirolisi, un processo che sottopone la biomassa a temperature elevate in un ambiente privo di ossigeno, per investigare il comportamento delle emicellulose, selezionando e confrontando tre tipi specifici (xilano, arabinoxilano, glucomannano) insieme alla cellulosa. Questa ricerca è suddivisa in due fasi. La prima indaga sulla devolatilizzazione dell'emicellulosa attraverso l'analisi termogravimetrica (TGA), in cui la biomassa è sottoposta a diverse rampe di riscaldamento per comprendere l'impatto delle condizioni operative e fornire informazioni per formulare modelli cinetici. Questa fase dello studio rivela che l'emicellulosa mostra una stabilità inferiore rispetto alla cellulosa, risultando in un maggior residuo solido e mostrando una devolatilizzazione più complessa. La seconda fase si concentra sulla speciazione qualitativa e quantitativa dei prodotti di pirolisi utilizzando la spettrometria di massa (MS), la gascromatografia (GC) e le trappole sorbenti Orbo™. Questa esplorazione svela le complessità di rese e distribuzione dei prodotti di pirolisi derivanti dalla degradazione delle emicellulose. Le principali scoperte evidenziano lo xilano come l'emicellulosa che presenta le rese più elevate di acqua e residuo solido, mentre il glucomannano si distingue per la quantità più elevata di bio-olio, particolarmente arricchito in composti C5 e C6. Questi protocolli analitici sono stati applicati anche a miscele, al fine di indagare potenziali effetti sinergici e approfondire aspetti legati alla coesistenza dell'emicellulosa con altri componenti. Un comportamento additivo, sia in termini di perdita di massa che di speciazione dei prodotti, è generalmente confermato. Infine, verranno presentati dati derivati da esperimenti condotti in un reattore a letto fisso, consentendo un'analisi comparativa e una discussione dei risultati ottenuti dai due differenti settaggi sperimentali. Attraverso questa approfondita indagine, l'obiettivo della ricerca è migliorare la nostra comprensione delle reazioni di pirolisi applicate alle emicellulose, contribuendo con importanti intuizioni al vasto campo dell'utilizzo della biomassa.

Parole chiave: Pirolisi, biomassa, emicellulosa, devolatilizzazione, speciazione, analisi termogravimetrica, spettrometria di massa, gas cromatografia.

Contents

Abstract	i
Abstract in italiano.....	iii
Contents	v
Introduction.....	1
1 State of art.....	3
1.1. Biomass as renewable feedstock.....	3
1.2. Biomass characterization	4
1.3. Biomass valorization	8
1.3.1. Combustion	9
1.3.2. Liquefaction	10
1.3.3. Gasification	10
1.3.4. Pyrolysis.....	11
1.4. Experimental set-up for pyrolysis investigations	18
1.4.1. Thermogravimetric analyzer.....	18
1.4.2. Fixed bed reactor.....	19
1.4.3. Micro-pyrolizer	19
1.5. Kinetic models for biomass pyrolysis.....	21
1.6. Thesis outline.....	24
2 Materials and methods	27
2.1. Materials.....	27
2.2. TG device	29
2.3. MS device	32
2.4. GC device.....	35
2.5. Syringes for GC analysis of light oxygenates	39
2.6. Orbo™ traps for GC analysis of heavy oxygenates.....	39
3 Tuning of experimental procedures.....	41
3.1. Calibration for quantitative analysis.....	42
3.1.1. Mass flow controller calibration	43
3.1.2. Mass spectrometer calibration	44
3.1.3. Gas chromatograph calibration	47

3.2.	Devolatilization kinetics.....	49
3.2.1.	Before the experiment	49
3.2.2.	Biomass pyrolysis in the TG analyzer.....	50
3.2.3.	Data processing	51
3.3.	Speciation of pyrolysis products.....	53
3.3.1.	Speciation of pyrolysis gases and heavy oxygenates	53
3.3.2.	Speciation of pyrolysis light oxygenates	62
3.3.3.	Char quantification	66
3.3.4.	Final quantification	66
3.4.	Pyrolysis of mixtures	67
3.5.	Optimization of GC analysis	67
3.6.	Choice of Orbo™ trap for heavy oxygenates analysis.....	70
3.7.	NTNU campaign.....	72
3.7.1.	NTNU setup.....	72
3.7.2.	NTNU procedure	73
4	Investigation on hemicellulose pyrolysis	75
4.1.	Effect of carrier flowrate and sample mass on TG curves	76
4.1.1.	Carrier flow rate influence.....	76
4.1.2.	Mass influence	78
4.2.	Devolatilization trends.....	80
4.2.1.	Investigation on heating rate.....	81
4.3.	Speciation of pyrolysis products.....	84
4.3.1.	Glucomannan	85
4.3.2.	Xylan	93
4.3.3.	Comparison between Glucomannan and Xylan	100
5	Biomass mixtures pyrolysis	103
5.1.	Mixtures devolatilization.....	103
5.2.	Speciation of pyrolysis products.....	112
5.2.1.	Xylan and Glucomannan mixture	113
5.2.2.	Xylan and Cellulose mixture	116
6	Experiments in packed bed reactor	119
6.1.	Xylan, Glucomannan and Cellulose comparison.....	120
6.2.	Xylan and Glucomannan mixture	122
6.3.	Xylan and Cellulose mixture	125
7	Conclusion.....	129
	Bibliography.....	133

List of Figures.....	139
List of Tables.....	145

Introduction

Over the past century, with the world experiencing unparalleled levels of development, a multitude of challenges emerged. Among these challenges, the escalating global CO₂ emissions appear as a one of the most important concerns for both society and the environment.

Global CO₂ emissions can be grouped into four main sectors: building, transport, industry and power.

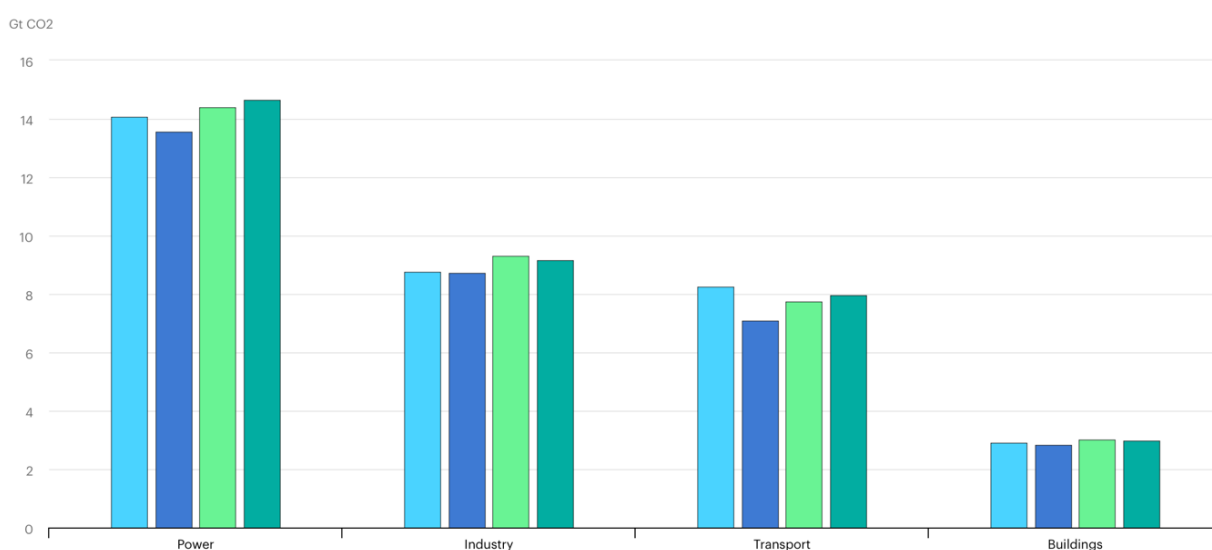


Figure 0.1: IEA, Global CO₂ emissions by sector, 2019-2022 [1]

As it is shown in figure 0.1, it is evident that the energy sector alone is responsible for the 42% of emissions and it is therefore fundamental to find alternative approaches to reduce its environmental impact and to maximize the effectiveness of the economic investments. [1]

Renewable energy sources can be considered a greener solution to reduce the emissions in the short term and move towards the decarbonization of the energy and industrial sectors in the mid/long term. Solar, wind and hydro energy are the most common renewable sources and their importance in the reduction of the use of fossil fuels it's undeniable, but they cannot cover the whole consumption for different reasons, such as the intermittent availability or the low energy density. Addressing the energy challenge requires a multifaceted approach, extending beyond established technologies, and exploring diverse and less mature renewable energy sources.

1 State of art

1.1. Biomass as renewable feedstock

In recent years, the use of biomass has gained interest as a promising alternative to fossil-based feedstock. Biomass, derived from organic materials, offers a range of advantages. It not only reduces our reliance on finite fossil fuels but also mitigates greenhouse gas emissions, as the carbon dioxide released during its conversion, is compensated by the CO₂ abated during the natural carbon cycle (Fig.1.1). [2]

Moreover, its versatility makes it a viable candidate for producing various forms of renewable energy, including biofuels and biogas, as well as bio-based chemicals, thereby offering a promising pathway towards a more environmentally responsible and sustainable energy future.

Biomass can be divided in four different generations:

- 1st generation biomass from edible feedstock (corn, sugar cane, seed oil)
- 2nd generation biomass from non-edible feedstock (lignocellulosic biomass, food and agricultural waste and residues)
- 3rd generation biomass from algal biomass
- 4th generation biomass from genetically engineered feedstocks

Nowadays first-generation biomass remains the most prevalent choice due to its abundant availability, straightforward harvest, and versatility in conversion into a variety of products, ranging from energy carriers to specialty chemicals. First-generation biomass has played a significant role in the development of renewable energy and biofuels; however, one key concern is the potential competition with food production, which can lead to issues such as rising food prices and land-use conflicts. Additionally, the overall efficiency and sustainability of first-generation biomass can vary, making it essential to explore more advanced and environmentally friendly alternatives, such as second and third-generation biomass sources.

Second-generation biomass represents a more sustainable and diverse feedstock for bioenergy and bio-based products. Unlike first-generation biomass, it primarily comprises non-food materials such as agricultural residues, wood chips, and dedicated fast growing energy crops. The key advantages lie in its reduced competition with food production, lower environmental impact, and the possibility of

exploiting waste material that otherwise would be thrown away. Many challenges however arise in its employment due to its complex structure, requiring advanced and often innovative conversion technologies, such as biochemical and thermochemical processes, to efficiently extract valuable energy and chemical components.

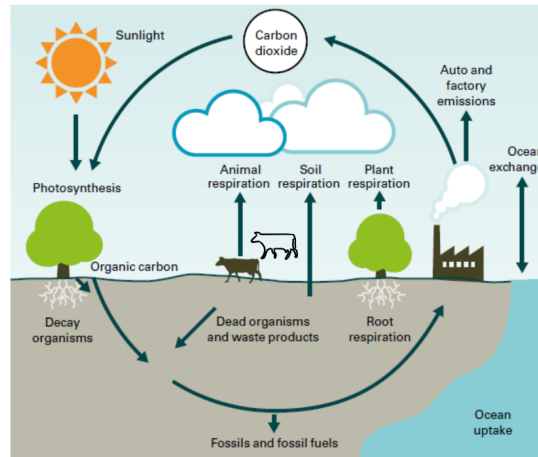


Figure 1.1: CO₂-neutral cycle [2]

1.2. Biomass characterization

Biomass has several key components, each with distinct characteristics and roles in various applications. Understanding the composition of biomass is crucial for its efficient conversion as it guides the selection of appropriate processing methods and technologies.

Carbohydrates are the main constituents of biomass and can be defined as biomolecules consisting of carbon (C), hydrogen (H) and oxygen (O) atoms [3,4]. They can be divided into:

- Storage carbohydrates (starch, sucrose), mainly present in first generation biomass as energy reserve.
- Structural carbohydrates (cellulose, hemicellulose), mainly present in second generation biomass as structural component.[3]

Starch and cellulose are constituted by the same repeating glucose units linked together by an acetalic bond (Fig.1.2).

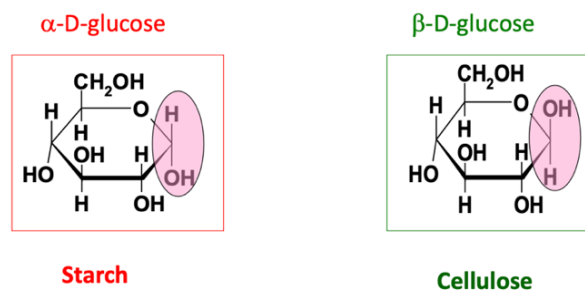


Figure 1.2: Starch and cellulose [3]

- Starch is characterized by an alfa glycosidic bond, which makes the molecule edible, branched and amorphous.
- Cellulose is characterized by a beta glycosidic bond, which makes the molecule not edible, linear and crystalline.[3]

Lignocellulosic biomass is constituted primarily of cellulose, linked together with hemicellulose and lignin.

Cellulose is an abundant natural polymer that serves as a fundamental building block of plant cell walls, providing structural rigidity and support to plant cells, giving them strength and integrity. It is a polysaccharide consisting of linear chains of several hundred to many thousands of $\beta(1\rightarrow4)$ linked D-glucose units with a general formula of $(C_6H_{12}O_5)_n$ (Fig.1.3). The repeating unit of this natural polymer is a dimer of glucose, known as cellobiose. [3,4] Cellulose is a linear syndiotactic homopolymer, which features highly crystalline zones, contributing to its strength, but also amorphous regions, contributing to a certain degree of flexibility and accessibility for transformation. Due to the intricate network of hydrogen bonds keeping the structure together, cellulose is also water insoluble and resistant to hydrolysis. Its thermal decomposition, occurring at 240-350°C, produces mainly anhydrocellulose and levoglucosan [3,4].

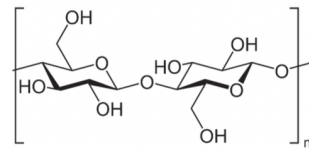


Figure 1.3: Cellulose structure [3]

Hemicellulose is another important component of plant cell walls and acts as interfacial agent between cellulose and lignin. It is a branched polymer composed of various sugar monomers. The specific composition of hemicellulose can vary among different plant species and tissues and this variability contributes to the diversity of hemicellulosic materials. The monomers are linked together through various types of glycosidic bonds, resulting in an amorphous structure with shorter chains if compared to cellulose (Fig.1.4).

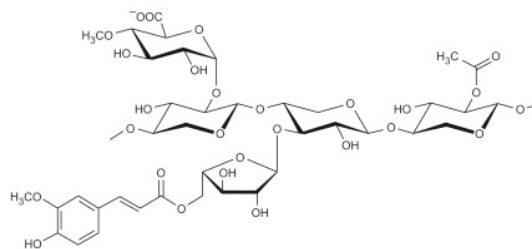


Figure 1.4: General hemicellulose structure [3]

A range of analytical techniques and methods have been used to elucidate the chemical composition and structural features of hemicellulose. As shown in table 1.1, the functional groups (building blocks) of hemicelluloses include pentoses (d-xylose and l-arabinose), hexoses (d-mannose, d-galactose, and d-glucose), hexuronic acids (4-O-methyl-d-glucuronic acid, d-glucuronic acid, and d-galacturonic acid), as well as small amounts of l-rhamnose and l-fucose. These functional groups can assemble into a range of various hemicellulose polysaccharides with diverse structures from linear to highly branched.[22] The structure of the main monomeric units is also shown in figure 1.5. [26]

Table 1.1: Monomeric composition of hemicellulose [22]

Hemicellulose	Monomeric composition (a)							
	Man	Glu	Gal	Ara	Xyl	Rha	GluUA	GalUA
Spruce wood	49	19	19	5	<1	<1	4	3
Brewery's spent grain	-	11	3	26	54	2	4	-
Wheat straw	0.37	17.8	-	13.8	62.9	0.41	7	-
Xylan	-	1.6	1.3	0.5	95.9	0.8	-	-
Glucomannan	62	-	38	-	-	-	-	-
Arabinoxylan	4.4	6.5	1.6	36	51	-	-	-

(a) Abbreviations: Man, mannose; Glu, glucose; Gal, galactose; Ara, arabinose; Xyl, xylose; Rha, rhamnose; GluUA, glucuronic acid; GalUA, d-galacturonic acid

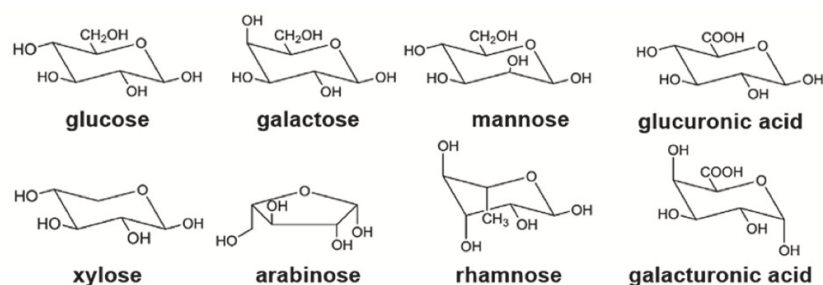


Figure 1.5: Main monomeric units of hemicellulose [26]

Moreover hemicellulose, unlike cellulose, is generally water-soluble, exhibits lower molecular weight and decomposes at lower temperatures, which makes it more accessible for various industrial processes, making it an important component in processes like biofuel production. [3,4]

Finally, lignin (Fig.1.6) constitutes the matrix of the plant cell wall, providing structure and rigidity, acting as barrier against microbial attack and enabling water and nutrient transport through plant tissues. It is an amorphous, irregular, three-dimensional, and highly branched alkyl-aromatic polymer, constituted by three main building blocks: p-coumaroyl alcohol, sinapyl alcohol, coniferyl alcohol. Being the only source of aromatics in nature, it can be considered as a valid alternative to fossil sources for various value-added products, which can be obtained from the monomeric units constituting it.

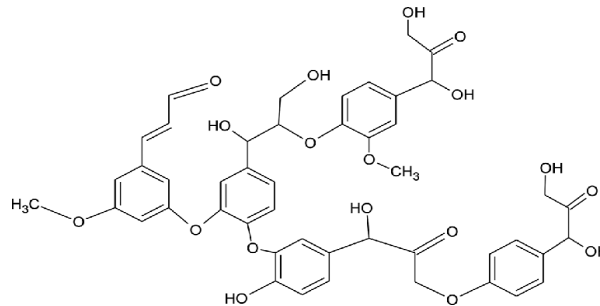


Figure 1.6: Lignin general structure [5]

Lignin transformation includes the cleavage of ether and carbon-carbon linkages, yielding a variety of phenolic products. However, it is probably considered the most problematic constituent of biomass due to the multitude of challenges it poses during processing. Its robust and cross-linked structure is quite resistant to decomposition, requiring temperatures as high as 450°C and thus more demanding process conditions. Its complexity, irregularity, and heterogeneity make it difficult to control the reactions to produce specific target compounds and avoid the formation of undesirable by-products. Moreover, lignin is typically insoluble in most common solvents, making it challenging to work with in solution-based processes. [4,5]

Due to their huge variety, lignocellulosic materials present very different compositions. In the following table (Tab.1.2), an example of the different composition of lignocellulosic material of some biomasses is shown [4]:

Table 1.2: Biomass composition

Plant material	Lignocellulose content [%]			Extractives & Ashes
	Hemicellulose	Cellulose	Lignin	
Orchard grass	40	32	4.7	23.3
Rice straw	27.2	34	14.2	24.6
Birchwood	25.7	40	15.7	18.6

1.3. Biomass valorization

Biomass valorization refers to the process of extracting, transforming, and utilizing biomass resources to create valuable products or energy, thereby harnessing the full potential of these renewable materials. It plays a crucial role in promoting sustainability, reducing environmental impact, and addressing energy and resource challenges in a more eco-friendly and economically beneficial manner. The opportunity behind the exploitation of biomass resides in the fact that it contains carbon and hydrogen and can be processed in several ways to obtain valuable products in different forms (i.e., vapor, liquid and solid).

Nowadays however, a significant fraction of biomass is discarded due to high costs of processing and low end-product values. This fraction, which includes agricultural wastes, dedicated plants, spent grains, de-oiled seed cakes, forestry wastes, food wastes, municipal wastes, and digested residues, represents a key component for sustainable utilization of renewable sources and could represent an effective alternative to decouple the industrial and energy sectors from fossil sources. In 2016, forestry was the main biomass feedstock in all Europe and represented more than 60% of the total mass. Beside this, agricultural biomass featured a share of almost 27% and other biological wastes like municipal solid waste, industrial waste etc. account for the remaining 12.4%. [6]

The utilization of this kind of biomass comes not without its challenges. Such wastes in fact generally contain few digestible compounds (i.e., fatty acids and sugars, typical of first-generation biomass), and more proteins and lignin, which require more severe reaction conditions to extract valuable compounds. Due to this complexity, a variety of different conversion processes have been developed for biomass valorization (Fig.1.7). On the one hand, biochemical routes to produce biodiesel and value-added chemicals are employed to process vegetable oil through several reactions, including transesterification, esterification, hydrogenation, hydrolysis, etc. Furthermore, sugary plants have been used to produce bioethanol via fermentation. On the other hand, biomass has been directly converted into biofuels via thermochemical processes including pyrolysis, gasification and liquefaction.

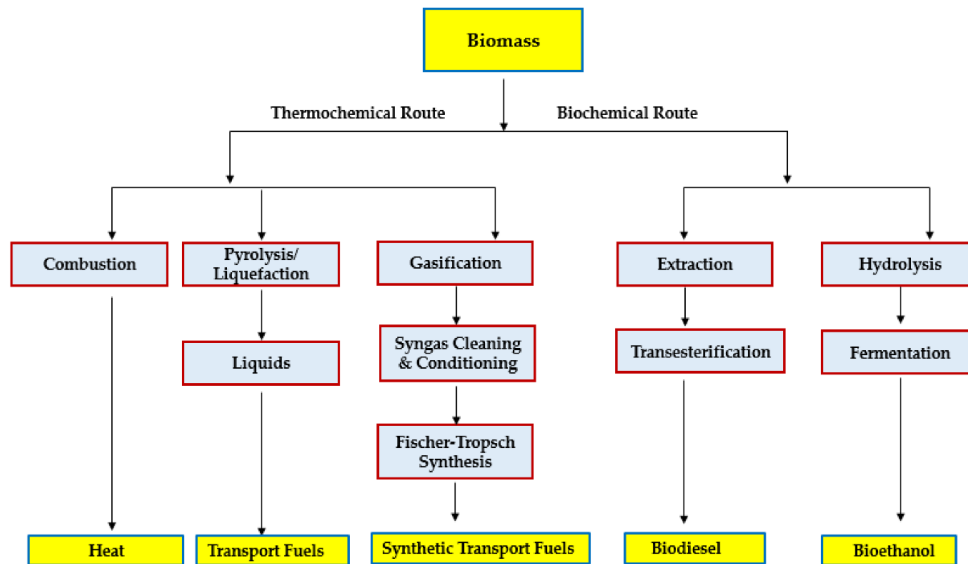


Figure 1.7: Biomass valorization routes [7]

In recent years, there has been a growing interest in the thermochemical conversion of biomass, particularly when applied to lignocellulosic feedstocks. This increased attention is driven by the numerous advantages associated with this process. Unlike biological processes, that can convert only limited components of the biomass, thermochemical processes are capable of converting all the carbon in the feedstock. Thermochemical conversion technologies produce a wide range of products including gases, condensable vapors and solids. These condensable vapors represent bio-oil, a valuable product which can then be upgraded to biofuels and chemicals. [8]

In an energy sector increasingly focused on emissions reduction and sustainability, biofuels are emerging as a pivotal component, highlighting their growing significance. For instance, under the European Union (EU) 2030 energy framework and climate actions, a 27% increase in the share of renewable fuels and 40% reduction in greenhouse gases are targeted by 2030. [9]

Recently, several technologies have been reported for thermochemical valorization of biomass including torrefaction, hydrothermal liquefaction, pyrolysis, and gasification which can readily convert biomass into bio-oil, syngas, heat, and charcoal. [7]

1.3.1. Combustion

Biomass combustion encompasses a sequence of chemical reactions in which carbon is oxidized into carbon dioxide and hydrogen into water (Fig.1.8). Oxygen deficiency leads to the formation of various products of incomplete combustion, whereas an excess of air favors complete combustion. These chemical reactions release heat as they are exothermic, primarily occurring in the vapor phase due to the elevated

temperatures involved. Presently, combustion serves as the primary method for harnessing heat energy from initial biomass sources. [10]

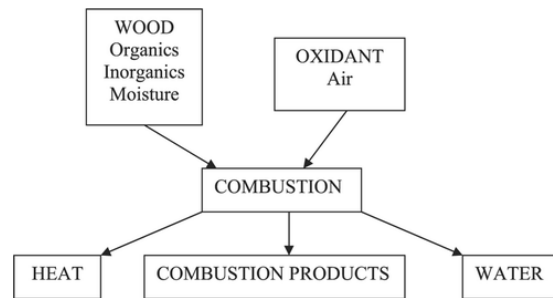


Figure 1.8: Biomass combustion [10]

1.3.2. Liquefaction

Liquefaction is a thermochemical process during which the biomass is converted into three products, i.e. a bio-oil fraction (target product), a gas fraction and a solid residue fraction. This process works at low-temperature (250–400 °C) and high-pressure (5–20 MPa), in water or another suitable solvent. As depicted in figure 1.9, the basic reaction pathways for the liquefaction of biomass can be described as: (i) depolymerization of the biomass into biomass monomers; (ii) decomposition of biomass monomers by cleavage, dehydration, decarboxylation and deamination, forming light fragments of small molecules, which are unstable and active; (iii) rearrangement of light fragments through condensation, cyclization and polymerization, leading to new compounds. [11]

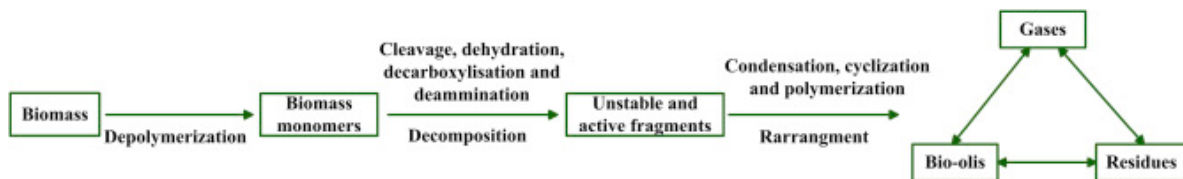


Figure 1.9: Basic reaction pathway for the liquefaction of biomass [11]

1.3.3. Gasification

The biomass gasification process consists in the conversion of a solid/liquid organic compound in a gas/vapor phase and a solid phase, generally carried out in the presence of a gasifying carrier, such as air, oxygen, steam or carbon dioxide. The gaseous product, usually called "syngas", has a high heating power and can be used for power generation or biofuel production. It is a mixture of carbon monoxide (CO), hydrogen (H₂), methane (CH₄) and carbon dioxide (CO₂) as well as light hydrocarbons, such as ethane and propane, and heavier hydrocarbons, such as tars, that condense at temperatures between 250 and 300 °C. The lowest heating value (LHV) of the syngas ranges from 4 to 13 MJ/Nm³, depending on the feedstock, the gasification technology and the operational conditions. The solid product, called "char", includes the organic unconverted fraction and the inert material present in the treated biomass. The amount

of unconverted organic fraction mainly depends on the gasification technology and the operational conditions, while the amount of ash depends on the biomass treated. The LHV of the char ranges from 25 to 30 MJ/kg, depending on the amount of unconverted organic fraction. The principal gasification reactions are endothermic and the necessary energy for their occurrence is, generally, granted by the oxidation of part of the biomass. Considering an auto-thermal system, gasification can be seen as a sequence of several stages. A simplified schematic representation of gasification is reported in figure 1.10. The main steps of the gasification process are oxidation (exothermic stage), drying (endothermic stage), pyrolysis (endothermic stage), reduction (endothermic stage). [12]

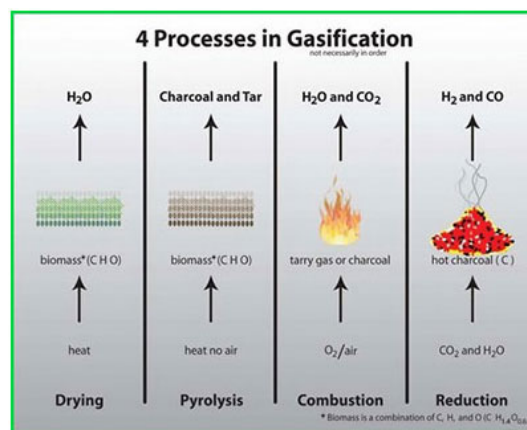


Figure 1.10: Processes in biomass gasification [12]

1.3.4. Pyrolysis

Besides the already mentioned processes, another possible method for biomass valorization is pyrolysis, a process consisting in heating up the biomass in an inert atmosphere (e.g., nitrogen or helium), degrading the initial mass in a mix of gas, oil and char. It is one of the most promising biomass utilization methods, characterized by easy operation and high compatibility with diverse feedstocks. [4] In the absence of oxygen and at elevated temperatures, organic material undergoes thermochemical decomposition. This process, also called destructive distillation, is an irreversible process, which leads to change in chemical composition and physical state of organic matter.[13]

Generally, pyrolysis of organic substances produces three phases of matter [13,14]:

- gaseous products including carbon monoxide and hydrogen, methane, short hydrocarbon chain gases, and carbon dioxide.
- liquid products (known industrially and economically as bio-oil and tars), including aliphatic and aromatic compounds, phenols, aldehydes, hydrocarbon chains, and water.
- a solid residue rich in carbon (known as char or biochar). The solid phase may contain also some impurities, e.g., aromatic compounds.

A number of parameters affect the biomass pyrolysis process, yields and properties of products. These include the biomass type, biomass pretreatment (physical, chemical, and biological), reaction atmosphere, temperature, heating rate and vapor residence time. [15]

During biomass pyrolysis, a large number of reactions take place in parallel and series, including dehydration, depolymerization, isomerization, aromatization, decarboxylation, and charring. It is generally accepted that the pyrolysis of biomass comprises three main stages:

- (i) drying, starting at very low temperature ($T < 100^{\circ}\text{C}$), consisting in heating up of biomass and initial evaporation of free moisture,
- (ii) an intermediate stage called primary decomposition, covering temperatures between 200°C and 400°C , where dehydration of biomass is completed and biomass decomposition takes place leaving behind char as solid residue,
- (iii) followed by secondary reactions proceeding upon further rising the temperature (up to 900°C) and characterized by two different products: if vapors remain at high temperatures for a sufficient residence time they are cracked into syngas; if vapors are removed quickly from the reactor, hydrocarbons condense into the liquid phase (tar). [2,15]

The complexity of biomass pyrolysis, combined with the numerous factors that can be varied in the process, has led to the study of various pyrolysis variants as shown in Tab. 1.3. Manipulating parameters like residence time, heating rate, temperature, pressure, and reactor design it's possible to achieve specific outcomes and optimize the production of desired products.[4]

Table 1.3: Pyrolysis process variants [4]

Pyrolysis technology	Vapors residence time	Heating rate	Temperature [$^{\circ}\text{C}$]	Main products
Carbonization	Days	Very low	400	Charcoal
Conventional	5 - 30 min	Low	600	Oil, gas, char
Fast	0.5 - 5 sec	Very high	650	Bio-oil
Flash-liquid	< 1 sec	High	< 650	Bio-oil
Flash-gas	< 1 sec	High	< 650	Chemicals, gas
Vacuum	2 - 30 sec	Medium	400	Bio-oil
Hydro-pyrolysis	< 10 sec	High	< 500	Bio-oil
Methano-pyrolysis	< 10 sec	High	> 700	Chemicals

The application of pyrolysis to lignocellulosic biomass introduces an additional layer of complexity due to the remarkable diversity in the nature and composition of different biomass feedstocks. The primary components of lignocellulosic biomass—cellulose, hemicellulose, and lignin—vary significantly from one source to another. Understanding the distinct behavior and product outcomes associated with each of these macro-constituents is a crucial step in comprehending the pyrolysis process. This knowledge is indispensable for optimizing and tailoring pyrolysis to specific feedstocks, ultimately enabling more efficient and sustainable biomass conversion. [8,13]

The main biomass constituents are biopolymers. According to the literature, their primary conversion presents common characteristics and can be described by three main pathways, depending on the nature of the chemical bonds that are broken. Most frequent terms used to characterize these pathways, which are presented in figure 1.11, are char formation, depolymerization, and fragmentation. [16]

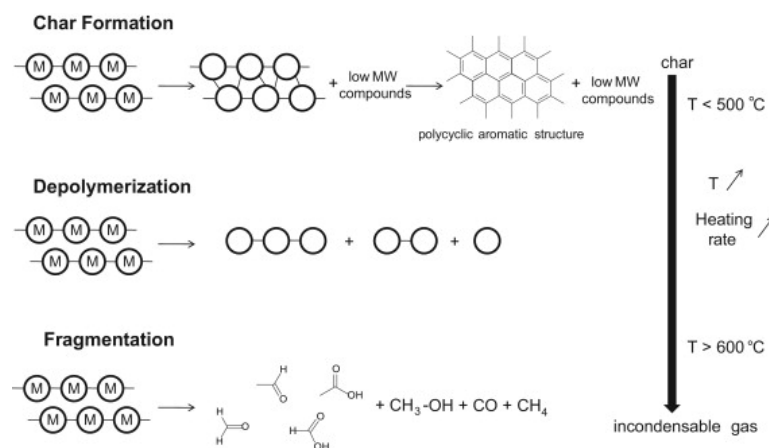


Figure 1.11: Primary mechanisms of the conversion of biomass constituents [16]

- Char formation consists in the conversion of biomass in a solid residue which presents an aromatic polycyclic structure. This pathway is generally favored by intra- and intermolecular rearrangement reactions, which result in a higher degree of reticulation and in a higher thermal stability of the residue. The main steps of this pathway are the formation of benzene rings and the combination of these rings in a polycyclic structure. All these rearrangement reactions are generally accompanied by release of water or incompressible gas.[16]
- Depolymerization consists in the breaking of the bonds between the monomer units of the polymers. After each rupture, stabilization reactions of the two new chain ends occur. Depolymerization results in a decrease in the degree of polymerization of the chains until the produced molecules become volatile. These molecules, which are condensable at ambient temperature, are most

frequently found in the liquid fraction in the form of derived-monomer, dimer or trimer.[16]

- Fragmentation consists in the cleavage of many covalent bonds of the polymer, even within the monomer units, and results in the formation of incondensable gas and of a diversity of small chain organic compounds which are condensable at ambient temperature. [16]

When the released volatile compounds are in gas phase, they can undergo secondary reactions such as cracking or recombination. Cracking reactions consist in the breaking of chemical bonds within the volatile compounds, which result in the formation of lower MW (molecular weight) molecules. Recombination (or recondensation) consists in the combination of volatile compounds to give higher MW molecules, which sometimes are no longer volatile under the temperature conditions of the reactor. [16]

Chemistry outlines of lignocellulosic biomass pyrolysis can be elucidated by examining the three primary components of biomass separately.

1.3.4.1. Lignin pyrolysis

The lignin present in wood decomposes at pyrolysis to give phenolic compounds in bio-oil. Given the variety of the chemical functions which differ in thermal stability, the main conversion step of lignin occurs over a large temperature range from 200 to 450°C, with a highest decomposition rate generally comprised between 360 and 400°C. The reactions responsible of the release of volatile compounds are mostly due to the instability of the propyl chains, of some linkages between monomer units and of the methoxy substituents of the aromatic rings. After this step, responsible of the main release of primary volatiles, a charring, which consists in the rearrangement of the char skeleton in a polycyclic aromatic structure, occurs. The volatile compounds released by these rearrangement reactions are mostly low-weight incondensable gases. Under inert atmosphere, benzene rings are very stable and their concentration within the residue tends to increase throughout the reaction. A summary of lignin pyrolysis most important reactions and products is shown in figure 1.12. [8,16,17]

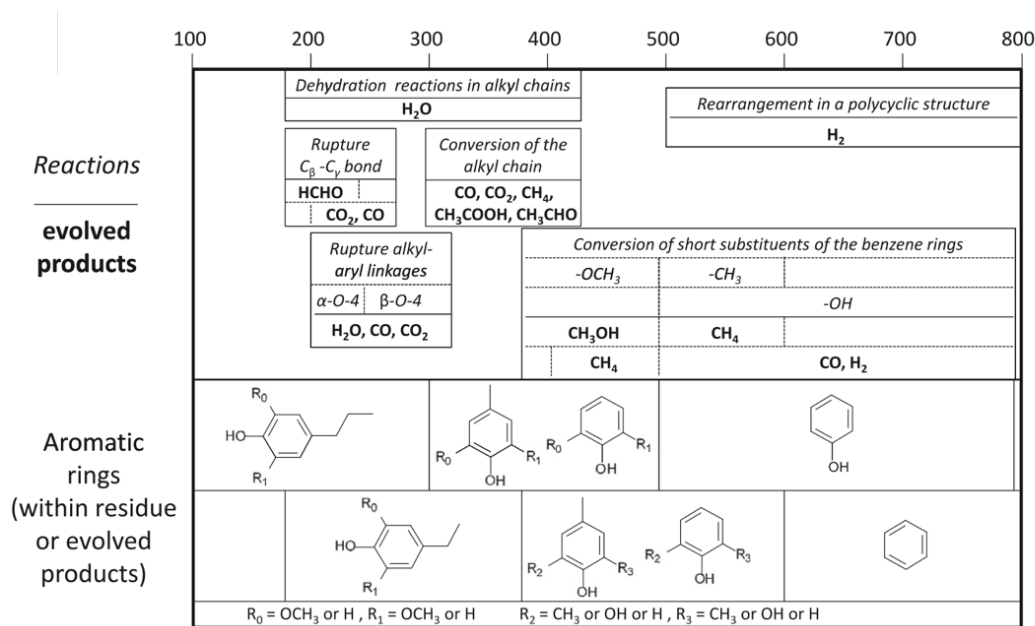


Figure 1.12: Reactions and evolution of lignin during pyrolysis [16]

1.3.4.2. Cellulose pyrolysis

Cellulose undergoes two chemical pathways at pyrolysis. The first pathway involves breaking of the polymeric chain by breaking the bonds between glucose units. This pathway leads mainly to levoglucosan. The second chemical pathway keeps the carbon chain intact and unbroken, leading mainly to aliphatic hydrocarbon chains, in addition to carbon dioxide, carbon monoxide, and water. [13]

Dehydration reactions are certainly responsible of most of the weight loss of the cellulose before 300°C. During this small mass loss, different reactions occur and can

lead to the formation of an intermediary sometimes called active cellulose or anhydrocellulose. While H₂O molecules are already released from a cellulose heated at 200°C, CO, CO₂ and organic compounds are rarely detected in the volatile phase before 280°C. [8,16,17]

The main conversion of cellulose occurs between 300 and 390°C with a highest decomposition rate generally comprised between 330 and 370°C. Depolymerization is due to the rupture of the glycosidic linkages between the monomer units and, when complete, leads to the formation of a high proportion of anhydro-oligosaccharides and anhydro-saccharides, especially of levoglucosan (1,6-anhydro-β-d-glucopyranose, C₆H₁₀O₅), whose yield can reach up to 60%, and of levoglucosenone (C₆H₆O₃). For temperatures higher than 300°C, the glycosidic bond becomes very reactive, and many reactions occur simultaneously. Cellulose depolymerization is very fast and its conversion can yield to more than 80% of volatile compounds which are mostly condensable organic compounds. [8,16,17]

The volatile fraction also contains an important amount of furans such as 5-hydroxymethylfurfural (5-HMF), 5-methylfurfural (5-MF), furfural and furfuryl alcohol. These compounds can also be considered as depolymerization products. The many reactions of depolymerization also lead to the formation of some unstable compounds containing new functions such as carbonyl and carboxyl groups. These compounds undergo dehydration or fragmentation reactions, explaining the high production of H₂O, CO, CO₂ and small chain compounds (hydroxyacetaldehyde, acetaldehyde, hydroxyacetone) on this temperature range. A summary of cellulose pyrolysis most important reactions and products is shown in figure 1.13. [8,16,17]

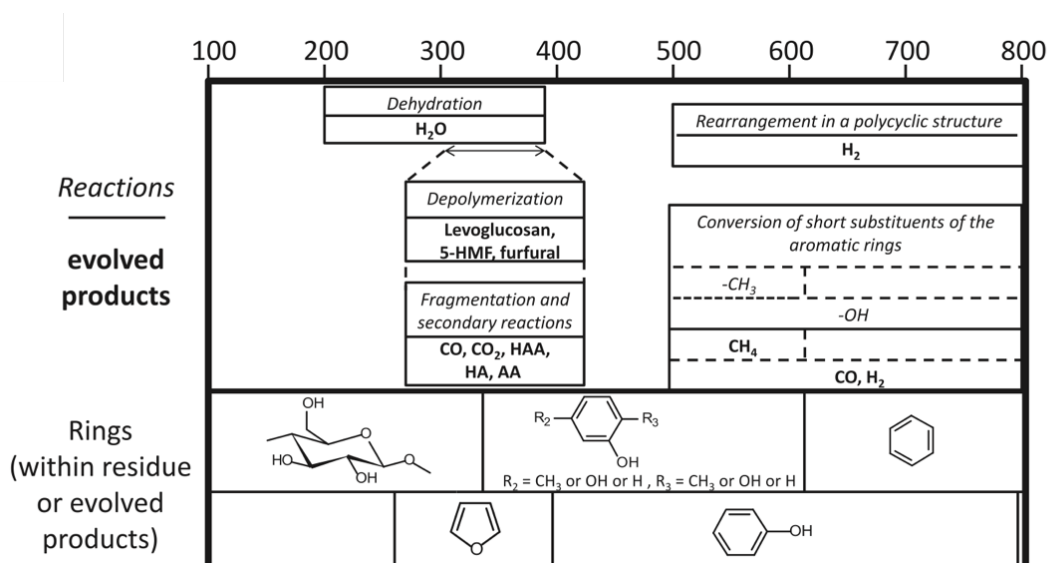


Figure 1.13: Reactions and evolution of cellulose during pyrolysis [16]

1.3.4.3. Hemicellulose pyrolysis

The hemicellulose building blocks decompose to give mainly furfurals in bio-oil. [13] Despite the variety in the composition of the hemicelluloses, analyses of these constituents show that their conversion mainly occurs in the temperature range 200–350°C. [16] The release of H₂O, characteristic of dehydration reactions within the polysaccharides, becomes significant at 200°C. At this temperature, some other chemical functions present in the substituents of the main chains are also unstable. As acetyl substituents can represent more than 10% in weight of the hemicelluloses, the fragmentation of these groups to produce acetic acid leads to significant yield of this compound. With a temperature increase to approximately 250°C, the glycosidic linkages between monomer units become very unstable and a rapid depolymerization occurs. These reactions lead to the formation of different anhydro-sugars. For example, in the pyrolysis oil obtained from the conversion of glucomannan, one can find levoglucosan, levomannosan (1,6-anhydro-β-d-mannopyranose) and levogalactosan (1,6-anhydro-α-d-galactopyranose). The pyran rings can be converted to more stable furan rings, explaining the formation of 5-hydroxymethylfurfural, 5-methylfurfural and furfural. [8,16,17]

The rapid depolymerization of the hemicelluloses causes the formation of different chemical functions and of many unstable intermediaries. These molecules undergo dehydration, fragmentation and secondary reactions which lead to the formation of significant amount of H₂O, CO₂ and CO. [8,16,17]

For temperatures higher than 35 °C, the weight loss is associated to the rearrangement of the residue during the charring process. Compared to cellulose, the char yield obtained from the hemicelluloses is higher. A summary of hemicellulose pyrolysis most important reactions and products is shown in figure 1.14. [8,16,17]

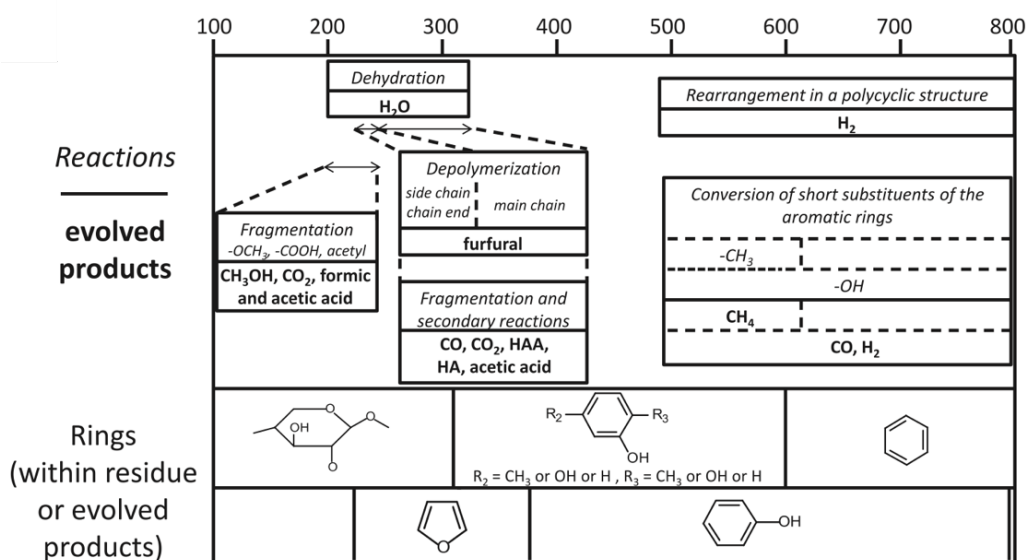


Figure 1.14: Reactions and evolution of hemicellulose during pyrolysis [16]

1.4. Experimental set-up for pyrolysis investigations

In the study of lignocellulosic biomass pyrolysis, aside from understanding the underlying chemistry, the experimental setup plays a crucial role. The choice of the setup allows for the precise control of reaction conditions, vital for optimizing the pyrolysis process to suit specific feedstocks and objectives and influence the process outcomes. Pyrolysis reactions are mainly carried out in three types of experimental set-up: thermogravimetric analyzer, fixed-bed reactor and micropyrolyzer.

1.4.1. Thermogravimetric analyzer

The thermogravimetric analyzer (Fig.1.15) is the most common instrument utilized in laboratory research to perform pyrolysis. The TGA instrument plays an important role in characterizing the thermal behavior of the biomass under investigation, giving fundamental information about its decomposition and volatilization. This state-of-the-art equipment enables precise control and measurement of the sample's weight as a function of temperature, providing invaluable insights into its thermal stability. This critical information can aid in elucidating key parameters, including the onset of pyrolysis, reaction kinetics, and the evolution of volatile and solid fractions. The main components of a thermogravimetric analyzer are a furnace and a precision balance. The furnace can heat up the sample from ambient temperature up to 1500°C to study the decomposition of the biomass over a wide range of temperatures, while the balance can detect changes in weight in the order of micrograms, giving information about the devolatilization of the sample and the temperature at which the reaction occurs. Other than giving information about mass loss the TGA returns a voltage signal which represents the endothermicity (or exothermicity) of the reaction. The sample pans of the analyzer are quite small and can accommodate only few milligrams of biomass (from 3 to 20 mg). The thermogravimetric analyzer alone cannot perform the product speciation but can be connected to a mass spectrometer to perform on-line analysis of the gaseous products and allow the withdrawal of other products for different off-line analysis. [23]

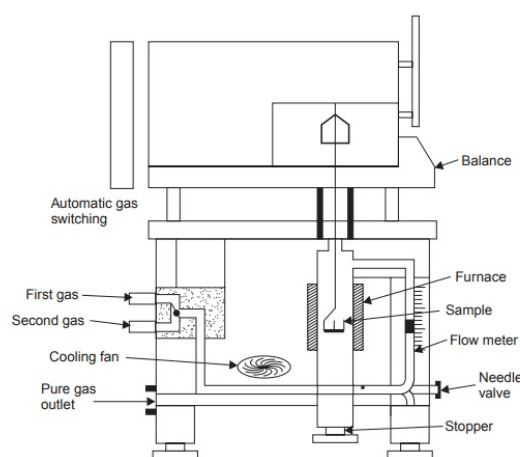


Figure 1.15: Schematic description of a thermogravimetric analyzer [23]

1.4.2. Fixed bed reactor

This kind of apparatus (Fig.1.16) usually consists of a steel tube with an internal diameter ranging from 10 to 25 mm and a length between 40 and 60 cm. The temperature is carefully controlled with thermocouples placed in different positions: inside the furnace, in contact with the fixed bed and at the outlet of the reactor. Since the furnace is pre-heated to the desired temperature and the biomass is injected when the operating conditions are reached, pyrolysis in a fixed-bed reactor can be considered almost isothermal. This set-up is the closest to the industrial one, which means that experiments reproducible on a large scale can be performed. An inert gas is always used both to eliminate the oxygen in the reactor and to transport pyrolysis products away from the heat source, avoiding secondary reactions between the products. Nitrogen or helium are the most suitable gases for this purpose and their flow rate is precisely controlled with a flow meter. Fixed-bed reactors usually do not perform online analysis and require a collection section for gaseous and liquid products at the outlet of the reactor, while the solid residue is collected from the reactor after the experiment. Although this aspect represents a complication of the experimental set up, it allows to perform a wide range of analysis on the products, such as the proximate analysis, elemental analysis, evaluation of the heating values and measurements of the surface area. [24,25]

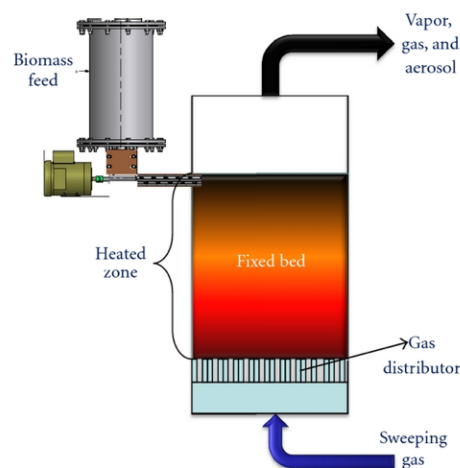


Figure 1.16: Schematic description of a fixed bed reactor for biomass pyrolysis [25]

1.4.3. Micro-pyrolizer

To achieve rapid decomposition of the macromolecules of biomass and accurate analysis of product, micro-pyrolizers can also be employed. In this setup, a small amount of biomass, typically in the microgram to milligram range, is rapidly heated, and the resulting pyrolysis products are swiftly extracted from the high-temperature zone for subsequent analysis. The maximum heating rate of micro-pyrolizers are typically over 100 °C/s to rapidly heat sample to target temperature. The retention time

of the pyrolysis vapors is typically less than 1/10 s. Pyrolysis vapors are quickly swept into coupled analytical equipment to prevent secondary reactions. [19]

Various types of micro-pyrolizers have been applied in biomass thermochemical conversion research. Based on the types of heating source, micro-pyrolizers can be classified into several types, among which micro-furnace pyrolizers, filament pyrolizers, and Curie-point pyrolizers are the most widely used.[19] Among these the first ones are the most employed due to several appreciable characteristics. Though several designs have been reported for micro-furnace pyrolizers, the most popular one is the vertical-type micro-furnace pyrolizer, the scheme of which is illustrated in figure 1.17. Samples are loaded into a sample cup or a liquid/gas syringe, and then delivered to the reaction zone. Sample cups are made from glass, quartz, or various types of metals. Electrical heating is usually adopted to heat the reaction zone, whose temperature can be controlled using temperature sensors (thermocouples or resistance thermometer devices) and feedback systems to obtain precision temperature control. Temperature can be controlled over a wide range with a fluctuation of ± 1 °C. The maximum reaction temperature is 1050 °C. To prevent the pyrolysis vapors from condensing as they leave the furnace, the interface temperature can be adjusted between 40 and 450 °C as required. Also in this kind of reactor a flow of an inert gas is necessary to perform the pyrolysis. [18,19] Pyrolysis performed in this way can be considered isothermal, resulting in a process without transport limitations. Micro-pyrolizers can also be easily coupled with online analytical instruments such as a mass spectrometer or a gas chromatograph for product speciation. [18]

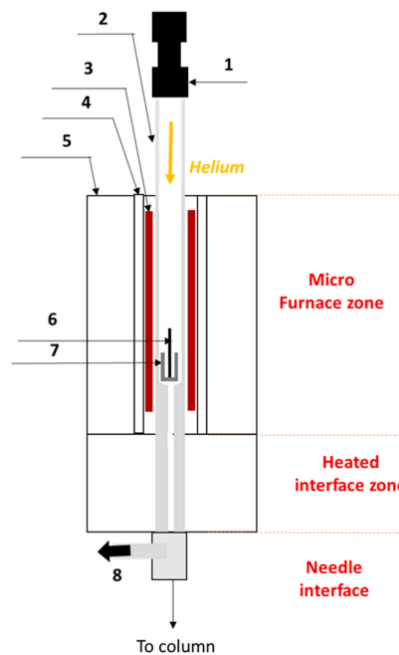


Figure 1.17: Schematic description of the pyrolizer [18]

1: sampler, 2: reactor (Quartz tube), 3: heating sleeve, 4: ceramic support, 5: Insulator, 6: stick, 7: cup, and 8: split vent.

While various setups and technologies have demonstrated their effectiveness in experimental investigations of biomass pyrolysis, such exploration still presents several challenges.

First and foremost, the pyrolysis process is subject to the influence of numerous variables, such as temperature and heating rate, making the isolation and control of individual factors a complex task. Furthermore, the inherent complexity and variability in the composition of biomass pose difficulties in establishing consistent and representative samples for experimentation. This variability extends to the product slate, making it challenging to achieve accurate quantification of yields. In addition, the collection and analysis of pyrolysis products, including bio-oil and gases, are technically demanding due to their diverse and often unstable nature. Complicating matters further, the presence of secondary reactions can impede a complete and accurate understanding of devolatilization mechanisms, making it difficult to link these mechanisms with product speciation. Lastly, scalability is a concern, as laboratory-scale experiments may not always translate directly to industrial applications, necessitating further research and development to bridge the gap. [26, 27]

Overall, experimental investigation of biomass pyrolysis poses challenges related to sample variability, process complexity and product analysis, which require careful consideration and innovative solutions.

1.5. Kinetic models for biomass pyrolysis

Kinetics are of pivotal importance for technologies and process development. They provide a fundamental understanding of how reactions or processes occur over time, allowing for an optimization of reaction conditions and leading to improved efficiency and cost-effectiveness. Moreover, accurate kinetics data are essential for designing and scaling up chemical and industrial processes both for successful process design and control. Kinetics also play a crucial role in the development of sustainable technologies, because by understanding the rate of chemical transformations, it's easier to design cleaner and more efficient processes that minimize waste and energy consumption, contributing to environmental sustainability. Therefore, one of the primary goals in biomass pyrolysis studies is to understand the kinetic mechanisms governing the process in order to optimize operating conditions and yields of the desired products in a safe and sustainable way.

The devolatilization of biomass is a complex process characterized by a multitude of chemical reactions occurring in both the gas and condensed phases. Two primary challenges in developing a kinetic model for this process stand out. First, there's the intricate task of defining the chemical structure of the reacting biomass. Second, the vast diversity in the product slate, arising from the numerous reactions during

pyrolysis. These challenges have been addressed in different ways, with several attempts documented in the existing literature. [20,21,22]

As previously introduced, the first aspect that should be considered in dealing with biomass is related to the heterogeneous nature of the material. Elemental compositions of different biomass materials are largely varying and determine its reactivity. Elemental analysis is therefore a very useful modeling tool for the characterization of biomass materials starting from basic information. Thus, biomass composition is defined in terms of a limited number of selected model or reference compounds. An elemental analysis provides a first characterization of the C/H/O ratios. [20,21]

Once the experimental analysis of biomass is available, the problem is shifted to the use of this information for the characterization of biomass in terms of a few reference species, to include in the kinetic mechanism that is used to simulate biomass pyrolysis. [20,21]

As biomass is generally composed of a mixture of cellulose, hemicellulose and lignin, reference species representative of these polymers are chosen:

- Cellulose can be characterized as its monomeric unit of glucose ($-C_6H_{10}O_5-$).
- Hemicellulose is an irregular polymer and contains monomeric units of sugars having both five- and six-membered rings. A monomeric unit having the chemical structure and composition of xylan is generally selected as hemicellulose reference component ($-C_5H_8O_4-$).
- Lignin structure is more complex and in order to describe the large variety of hardwood and softwood structures, lignin is represented by a combination of three reference species or monomeric units rich in carbon ($C_{17}H_{17}O_5$), in hydrogen ($C_{22}H_{29}O_9$), and in oxygen ($C_{20}H_{23}O_{10}$), respectively. [20,21]

On the basis of this elemental C/H/O analysis of the biomass material, a suitable combination of the reference species can then be derived. While it is possible to describe the initial biomass composition using the five reference components, the intermediate and final products exhibit a wider array of constituents, originating from a complex network of reactions.

In most devolatilization schemes, the overall kinetic scheme for biomass is obtained from the combination of the submodels for the three principal biomass pseudo components (hemicellulose, cellulose, and lignin) and, sometimes, moisture. The overall devolatilization rate is given by the summation of the individual rates for each fraction, weighted according to the percentage of respective pseudo component initially present in the original biomass material. [20,21] However, the coexistence of various biomass constituents within the same feedstock can introduce interactions that further enhance the complexity of reactions and the diversity of products to be incorporated into a kinetic model.

The mechanisms used to describe the reactive systems can therefore be categorized based on the level of approximation they introduce. In order to elucidate the process of biomass pyrolysis two types of reaction mechanisms have been developed: global and microkinetic. [20, 21, 22] The kinetic models reported in the literature for hemicellulose pyrolysis are mostly global kinetic models, which can be broadly divided into one-reaction/stage models and multi-reaction models.

The former simplifies the overall process in a single first-order reaction or two parallel reactions with different rate constants (Fig.1.18), in which gases, tars, and char are formed from biomass. This results in an easy-to-use tool but suffers from a very limited applicability. The high degree of simplification introduced allows only for qualitative predictions of the product yields, with very scarce, or no information on the product distribution. The model is able to describe the degradation rate of the starting materials and to simulate the mass loss curves. However, it is unable to predict the changes in product yields between different materials or even between the same materials under different pyrolysis conditions. [20, 21, 22]

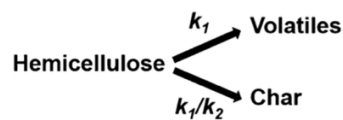


Figure 1.18: Kinetic scheme of one-reaction model of hemicellulose pyrolysis [22]

Multi-component models are more complex, as they include an attempt to characterize the feedstock composition. In this case the decomposition of biomass and the formation of products are described by a series of consecutive/parallel reactions (Fig.1.19). This model enables to address the concept that active species are formed in the initial stages of biomass pyrolysis, leading to the formation of low molecular weight products through further decomposition. Decomposition rates and conversion time for most biomass samples are predicted with reasonable accuracy, but detailed product distribution and composition are not always available. [20, 21, 22]



Figure 1.19: Kinetic scheme of multi-component model of hemicellulose pyrolysis [22]

The main characteristic of global models is that they make extensive use of lumping, by which reacting species are grouped into major products based on phase, that is, volatile compounds (bio-oil and gas), tar (bio-oil), gas, and char. A lumped kinetic analysis attempts to characterize pyrolysis reactions using a limited number of equivalent components and is only able to predict the yields of the previously defined

lumped species without any information on typical pyrolysis products and their distribution. [20, 21, 22] Overall, these global kinetic models are able to explain the experimental observations and promote an understanding of the kinetics of biomass pyrolysis. Furthermore, the use of global kinetic models for the complex pyrolysis system simplifies data collection and analysis, as well as the numerical implementation, which is attractive for many practical applications. However, the global kinetic models of biomass pyrolysis are restricted to the specific starting materials and operating conditions reported by the authors, and therefore, have very poor potential for extrapolation to other applications. Moreover, the global kinetic model cannot provide detailed information in terms of reaction pathways and resulting chemical speciation at the mechanistic level. [22]

The alternative to global models is given by microkinetic models, which describe the detailed reaction pathways and mechanisms for the decomposition of biomass (through initiation, end-chain initiation, dehydration, mid-chain dehydration, hydrolysis, etc.), the reactions of intermediates, and the formation of pyrolysis products (including glycolaldehyde, acetaldehyde, methylglyoxal, furfural, anhydro pyranoses, dianhydro-pyranoses, acetone, acetol, CO₂, CO, H₂O, char, and others). The models include more than 500 reactions, which are specified in terms of elementary steps and associated kinetic parameters. [22]

Even if there has been a recent advance in the kinetic modeling of pyrolysis further efforts are needed to obtain a full picture of thermal decomposition of biomass. Ultimately, a kinetic model that describes the complex pyrolysis reaction network at the mechanistic level would not only lead to a deeper fundamental understanding of reaction processes but could also predict the pyrolysis behavior and outcomes to guide the design of efficient pyrolytic reactors for engineering applications.

1.6. Thesis outline

Given the growing significance of biomass in the field of green and sustainable energy sources, there is an urgent need to expand our understanding of the thermochemical utilization of such feedstock. In particular, within the context of pyrolysis, in-depth studies related to primary devolatilization and product speciation stand out as critical aspects that demand thorough investigation. These studies are crucial in the development of efficient technologies for biomass conversion, and even though in recent years there has been an increasing interest, a notable deficiency in comprehensive data persists. Therefore, the primary goal of this research is to address the existing knowledge gap and contribute to the development of more efficient biomass conversion technologies.

The research presented in this thesis builds upon the groundwork laid by our research group, which has dedicated its efforts to developing an efficient and effective experimental setup for investigating pyrolysis processes. This setup, in particular, has enabled to monitor devolatilization rates and product speciation of cellulose, one of the most extensively studied components of biomass. Cellulose served as a benchmark for subsequent investigations, which were conducted throughout this experimental campaign.

The initial objectives of the research presented in this thesis were twofold: first, to utilize the pre-established experimental setup to explore previously unexamined biomass, specifically hemicelluloses. Hemicelluloses, despite being fundamental components of lignocellulosic biomass, have been comparatively neglected in the literature, with studies predominantly focusing on cellulose and lignin. Second, considering that hemicellulose is rarely found as a pure component in biomass and is usually interconnected with cellulose or other hemicelluloses, investigations have also been conducted into potential mixing effects. This allowed to better comprehend whether biomass constituents interact during the processing stages.

The first step in this exploration is to collect relevant data on devolatilization, the initial phase of biomass pyrolysis, through Thermogravimetric analysis (TGA). Enhanced comprehension of devolatilization behaviors holds potential for improving pyrolysis technologies and developing kinetic models for different feedstocks. Another aspect that is investigated is the thorough characterization of pyrolysis products through Mass Spectrometry (MS) and Gas Chromatography (GC). A comprehensive understanding of the composition of pyrolysis products is essential to optimize process conditions and maximize product yields, enabling us to tailor the output towards specific applications, such as biofuels, biochar, or specialty chemicals. In the final part of this work, a dedicated section will be allocated to results derived from a prior experimental campaign conducted by our research group in a fixed bed reactor configuration. Data from these experiments were processed, and the findings will be presented and compared to those obtained from the TGA-based campaign.

With all that said, in the upcoming chapters, a comprehensive look at our research will be provided. In chapter 2 an outline of the materials and instruments used will be presented, followed in chapter 3 by a detailed description of the experimental procedures employed in the research. Finally, an in-depth analysis of the results, accompanied by a critical discussion aimed at elucidating the significance and implications of our findings will unfold in chapters 4 to 6.

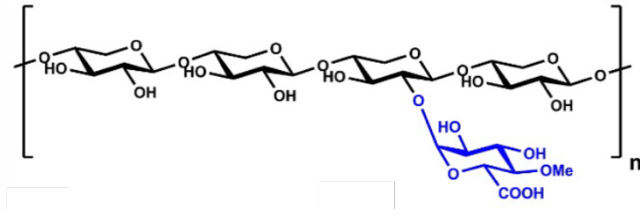


Figure 2.1: Xylan structure and aspect [28]

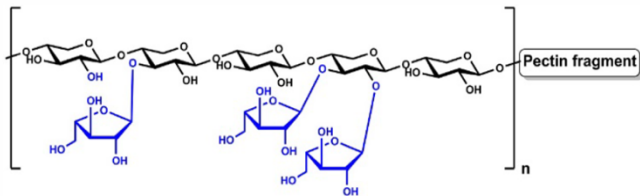


Figure 2.2: Arabinoxylan structure and aspect [28]

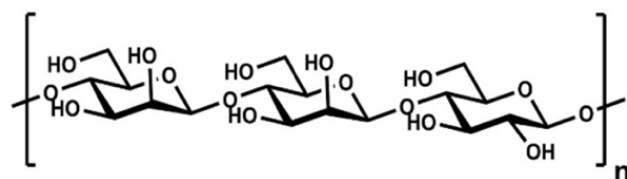


Figure 2.3: Glucomannan structure and aspect [28]

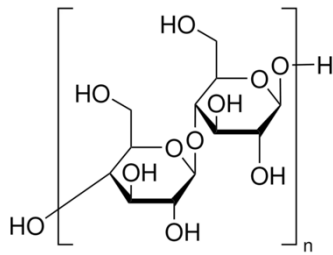


Figure 2.4: Cellulose structure and aspect [29]

2.2. TG device

The first step of this thesis work is to perform pyrolysis experiments within a thermogravimetric analyzer, specifically employing Thermogravimetric Analysis (TGA). Such technique allows to study the changes in the mass of a substance as a function of temperature (or time) in a controlled atmosphere. It is a valuable tool for characterizing the thermal stability, composition, and decomposition kinetics of a wide range of materials.

A standard thermogravimetric analyzer (Fig.2.5) includes:

- Sample Holder: Designed from materials like alumina, platinum, or quartz to securely hold samples at high temperatures.
 - Furnace: Contains a resistance heater, temperature control system, and high-temperature chamber for heating samples with precision.
 - Highly Sensitive Balance: A microbalance or analytical balance with sub-microgram sensitivity to measure sample mass changes during heating.
 - Temperature Controller: Regulates furnace temperature according to a programmed profile, ensuring precise and consistent conditions.
 - Gas Flow System: Introduces specific gases (e.g., nitrogen, air) for controlled atmospheres, preventing unwanted reactions with the sample.
 - Data Acquisition System: Records and processes real-time mass change data to generate thermogravimetric curves.
 - Dedicated Software: Controls the instrument, programs temperature profiles, and analyzes experiment data, including calculations for kinetic parameters.
- [30]

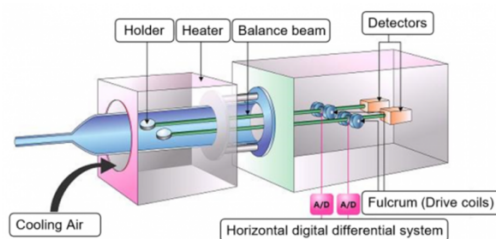


Figure 2.5: Representation of a typical TGA instrument [38]

The specific model utilized in this experiment is the Hitachi STA7300 TG-DTA, visible in figure 2.6. It boasts a temperature range extending from ambient conditions to 1500°C, with a maximum sample weight capacity of 20 mg. The instrument's dimensions are 420mm in width, 600mm in depth, and 315mm in height. [31]

This kind of equipment can be seen as consisting of two main parts: the feed section, where the desired gas is supplied to the instrument, and the reaction section, which is basically a furnace where the experiment takes place.

In the supply section, helium (He), nitrogen (N₂) and air can be provided, depending on the specific process requirements. Helium and nitrogen are stored in dedicated tanks located on external balconies adjacent to the laboratory and are delivered to the instrument through separate lines, each equipped with valves and controllers for manual operation. These valves allow precise control of the gas flow, enabling users to turn the supply on or off and adjust the flow rate as needed.

In the reaction section, an arbitrary quantity of material is carefully loaded into the sample pan, which is then positioned within the controlled environment of the oven chamber and subjected to a tailored temperature program, carefully adjusted to meet the specific requisites of the ongoing experiment. The sample pan can be made of different materials, but for our purpose ceramic pans are employed, due to their excellent thermal resistance, making them suitable for use at high temperatures, up to 1000°C. Alongside the sample pan, an empty reference pan is employed in the reaction chamber. This reference pan serves to monitor and compensate for environmental factors such as temperature fluctuations. By functioning as a control, it enables the instrument to detect and rectify any weight changes in the sample pan that are unrelated to the sample itself, thereby ensuring the precision of TGA measurements.

The system's outlet can be configured to either vent to an exhaust line or be linked to online analysis instruments, such as a mass spectrometer, for deeper analysis of gas composition.

The instrumentation is equipped with specialized software, overseeing and regulating all the crucial parameters that influence the process. It not only ensures precise control but also provides real-time data visualization. The most important parameters being monitored include the sample's weight and temperature, with continuous

measurements throughout the experiment. The primary outcome of this analysis emerges in the form of a graphical representation, where the remaining percentage of sample mass is plotted against temperature (Fig.2.7). This curve provides insights into various thermal properties of the material, including devolatilization temperature, the extent of decomposition, and the presence of multiple devolatilization steps.

Other than that, two other analyses are performed in real time, namely the DTG (Differential Thermogravimetry) and DTA (Differential Thermal Analysis).

Differential thermogravimetry displays the rate of change in the weight or mass of a sample (dm/dt) as a function of temperature. This analysis can reveal important information about the sample thermal behavior, including the temperature at which various processes or reactions, such as decomposition or volatilization, occur. The peaks or valleys in the DTG curve correspond to specific events or transitions in the material being analyzed. DTG analysis proves to be invaluable in thermal analysis as it allows for the identification of multiple devolatilization steps and enables the determination of the onset and peak temperatures of these steps. It provides a more comprehensive understanding of the thermal events taking place in the sample, compared to a standard TG curve.

The differential thermal analysis (DTA) on the other hand measures the temperature difference between the sample and a reference material as both are subjected to the same controlled temperature program. DTA can provide information about phase transitions (e.g., melting, crystallization), chemical reactions, and heat capacity changes in a sample. [30,31]



Figure 2.6: Hitachi STA7300 TG-DTA

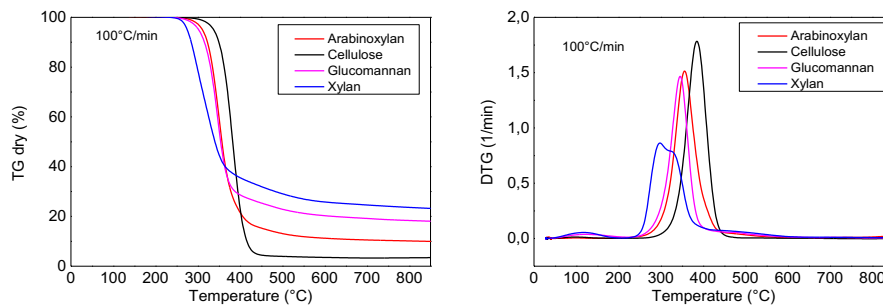


Figure 2.7: TG and DTG curves for different biomass samples

In this thesis work the TGA is used to perform pyrolysis experiments and investigate the thermal behavior of different model biomasses as will be explained in section 3.2. The biomass is carefully placed inside the sample pan and put inside the furnace. Here the temperature steadily rises in the presence of helium (He), serving as an inert gas, and in the absence of oxygen. To ensure that the samples remain free from oxygen exposure during thermal decomposition, the chamber is pre-evacuated. By analyzing the weight loss profiles and associated temperature ranges, information about biomass volatilization can be gained, gaining information for the development of kinetic mechanisms and to understand of the optimal conditions for biomass conversion.

2.3. MS device

The mass spectrometer (Fig.2.8) is an important instrument used in the course of this research to perform online analyses of the gases evolved from the pyrolysis of the biomass samples.

Mass spectrometry plays a critical role in analytical chemistry, offering invaluable insights into the molecular composition of different substances. The fundamental working principle of mass spectrometry involves the analysis of ions derived from a sample. These ions originate within a stream of neutral molecules and are subsequently sorted according to their mass-to-charge ratio (m/z). This m/z ratio directly corresponds with the mass of the subject species, and its detection yields a distinctive mass spectrum. [32] The fundamental components of a mass spectrometer, although specific configurations may vary, include:

- Ion Source: Introduces and ionizes the sample using various techniques based on sample and analyte characteristics.
- Mass Analyzer: Separates ions according to their mass-to-charge ratio (m/z), with various types available.
- Detector: Records ion abundances relative to their m/z values, selected based on analysis requirements.

- Data System: Digitizes and processes detector-generated data, converting analog signals to digital format, performing tasks like peak identification, deconvolution, and data storage.
- Vacuum System: Maintains the necessary vacuum for preventing interactions between ions and air molecules, with pumps and chambers for the ion source, mass analyzer, and detector.
- Ion Optics: Includes lenses and deflectors to focus and steer ions through the mass analyzer. [32]

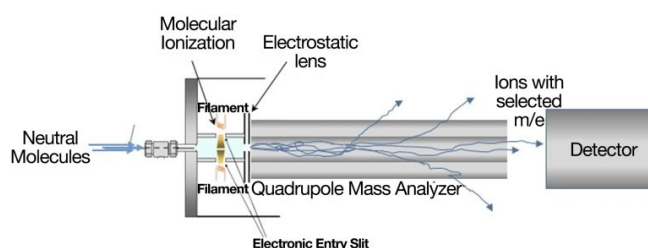


Figure 2.8: Representation of a typical MS instrument [33]

The specific mass spectrometer used in this research is an HPR-20 EGA from HIDEN Analytical, shown in figure 2.9. It is a bench top mass spectrometer configured for continuous analysis of gases and vapors from thermogravimetric analyzers (TGA). Operating to 200°C, the QIC (quartz inert capillary) flexible 2 m capillary inlet samples from 100 mbar to 2 bar gauge and provides fast response times of less than 300ms. The HPR-20 EGA system includes an external dry scroll pump which provides fast response and effective pumping for light gases. Effective pumping for light gases enables the use of helium as the carrier gas for TGA-MS studies without compromising the sample flow and response. The benefit of using helium as a carrier gas of choice for TGA-MS studies is the reduced mass spectral interference, compared to nitrogen or argon. The mass spectrometer operates under vacuum conditions, with the ionic source typically maintained at around 10^{-6} bar pressure. A pipe equipped with a needle valve allows the passage of the gas mixture and is directly connected to the outlet of the reaction section of the TG analyzer. [34]

The instrument is equipped with a complete, application specific, software package for Evolved Gas data acquisition and analysis. This software enables users to track specific mass fragments throughout experiments, facilitating the detection of particular compounds within complex mixtures and streamlining the instrument's operational processes. The data processed are normally returned in form of a mass spectrum, which is a graphical representation that provides information about the abundance of ions at different mass-to-charge ratios (m/z). However, for a more immediate and dynamic insight into the presence and behavior of specific compounds throughout the analysis, the mass spectrometer's response pertaining to a particular

ion can be plotted against time or temperature (Fig.2.10). This temporal representation offers a real-time view of the compound's presence and its evolution during the analysis. [32, 34]



Figure 2.9: HPR-20 EGA mass spectrometer from Hiden Analytical [34]

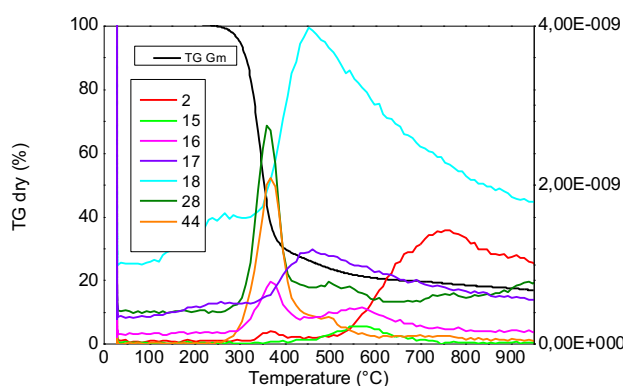


Figure 2.10: MS analysis of pyrolysis gases of glucomannan

In this thesis work, mass spectrometry has been employed to analyze the gases emitted during the pyrolysis of biomass. The analysis was conducted in real-time, with the instrument's inlet connected to the outlet of a Thermogravimetric (TG) analyzer. In particular, the mass spectrometer was utilized to monitor specific mass fragments associated with CO, CO₂, H₂O, and CH₄. This enabled the detection of these gases throughout the pyrolysis process, tracking their temporal evolution, and establishing correlations with distinct degradation processes taking place within the biomass. Ultimately, this approach facilitated the quantification of these products, shedding light on the proportion of gases generated during biomass pyrolysis. In section 3.3.1 a thorough explanation of the analytical methods employed for mass spectrometry of pyrolysis gaseous products will be provided.

2.4. GC device

The second crucial aspect of the research presented in this thesis focuses on the speciation of pyrolysis products, entailing the identification of both light and heavy products derived from biomass pyrolysis. This is accomplished through offline analysis of pyrolysis vapors and bio-oil utilizing Gas Chromatography-Mass Spectrometry with Flame Ionization Detection (GC-MS/FID) (Fig.2.11).

Gas chromatography is a widely used analytical technique in chemistry that is specifically employed to separate and analyze the various components of a mixture of gases or volatile liquids. The separation is accomplished by distributing the sample between two distinct phases: a stationary phase and a mobile phase. The mobile phase consists of a chemically inert gas like helium or nitrogen, which carries the analyte molecules through a heated column. The stationary phase can take one of the following two forms: either a solid adsorbent, referred to as gas-solid chromatography (GSC), or a liquid coated onto an inert support, known as gas-liquid chromatography (GLC). As the sample moves through the column, individual components interact differently with the stationary phase, resulting in separation. At the end of the column, there is a detector that measures the concentration of the different components as they exit the column. The data from the detector is analyzed to create a chromatogram, which is a graph showing the separation of components based on their retention times. Each peak in the chromatogram corresponds to a specific component in the sample. [35]

A Gas Chromatography-Mass Spectrometry with Flame Ionization Detection (GC-MS/FID) system comprises three essential components for comprehensive chemical compound analysis:

- Gas Chromatography (GC):
 - o Sample Injection Port: Introduces the sample.
 - o Column: Coiled tube with a stationary phase for separation.
 - o Carrier Gas: Inert gases like helium or nitrogen carry the sample.
 - o Oven: Provides precise temperature control during separation.
- Mass Spectrometer Detector (MS):
 - o Ionization Source: Ionizes sample molecules, often through electron impact.
 - o Mass Analyzer: Separates ions based on mass-to-charge ratio using various types like quadrupole or time-of-flight.
 - o Detector: Records ions' abundances, producing mass spectra for each compound.
- Flame Ionization Detector (FID):
 - o Hydrogen and Air Supplies: Mix and combust in a flame.
 - o Ionization Chamber: Combustion products produce ions.
 - o Collector Electrodes: Collect ions, generating a current proportional to the sample's organic compound concentration. [35,36]

The GC-MS/FID system enables both qualitative (via the Mass Spectrometer) and quantitative (via the Flame Ionization Detector) analysis, making it a powerful tool for chemical analysis and identification.

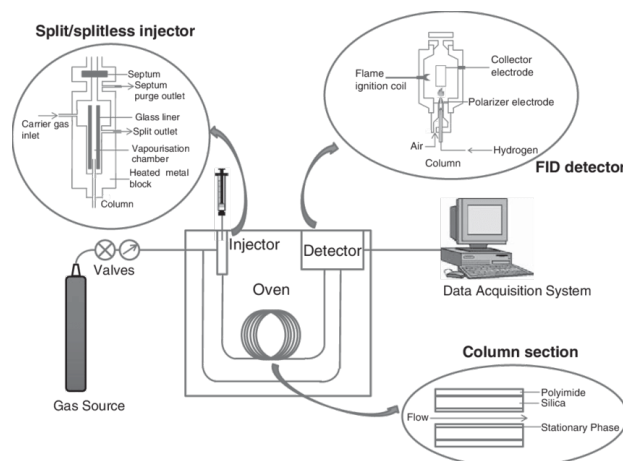


Figure 2.11: Gas Chromatograph with Flame Ionization Detection [36]

The GC instrument used during this thesis work is an Agilent 6890 Gas Chromatograph with a HP 5973 Mass Selective Detector (MSD) and can be seen in figure 2.12. It is used as an offline gas chromatograph for analysis of both gaseous and liquid mixtures. The HP 6890 Series gas chromatograph system delivers high levels of performance and features electronic pneumatics control of all gas pressures and flows. Onboard sensors automatically compensate for ambient temperature changes and barometric pressure differences to routinely achieve more accurate and reproducible results. By providing stable results, EPC reduces recalibration frequency and improves laboratory productivity. Overall thermal performance of the HP 6890 GC provides optimal chromatography including retention time repeatability, peak symmetry, and retention index accuracy, while allowing for fast GC results. The HP 6890 Plus GC is equipped with a column oven of dimensions 28 × 31 × 16 cm, which accommodates two 105 m × 0.530 mm id capillary columns. The operating temperature range is from +4 °C to 450 °C. This kind of chromatographer has a dual channel design, supporting two inlets and two detectors (MS and FID). [37]

The system is equipped with a software used to adjust column and inlet parameters including temperature, pressure, and carrier flow rates, and to select the optimal temperature ramp for the analysis. The software also allows for real time visualization of the data being processed, in order to monitor the ongoing analysis. The result of a Gas Chromatography (GC) analysis is a chromatogram (Fig.2.13-2.15), a graphical representation that shows the separation of sample components based on their retention times. Within this visual representation, each peak precisely corresponds to an individual constituent within the sample. Data coming from mass spectrometry is processed for compound identification. This involves comparing the acquired mass spectra with reference libraries or spectra from known compounds. Instead, for

quantitative analysis, the FID response signals (intensity) are used to calculate the concentration of compounds in the sample. Calibration curves, which relate signal intensity to known concentrations of standards, are used for this purpose. [35, 37]



Figure 2.12: Agilent 6890, 5973 MSD Gas Chromatography-Mass Spectrometry with Flame Ionization Detection

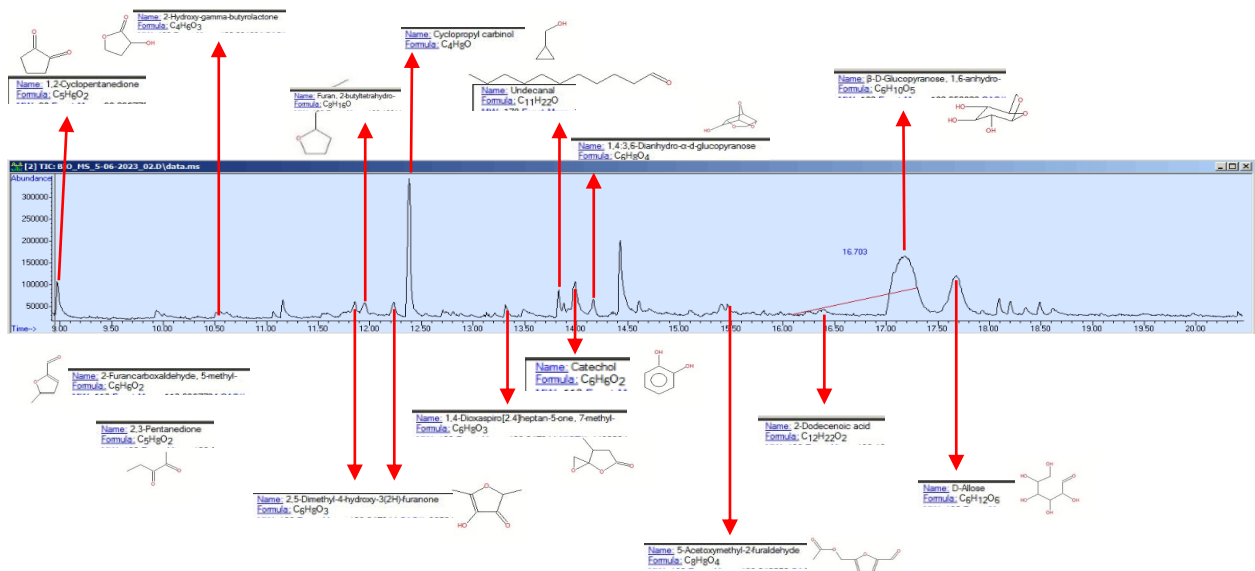


Figure 2.13: MS chromatogram of glucomannan vapors

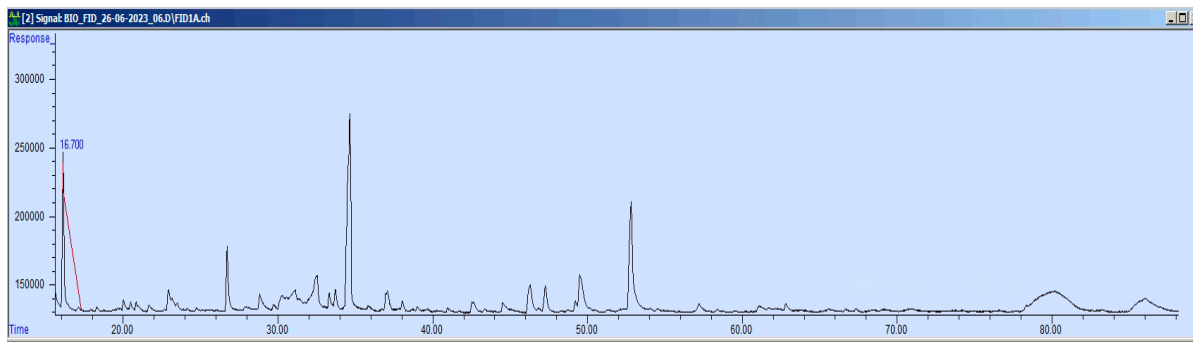


Figure 2.14: FID chromatogram of glucomannan vapors

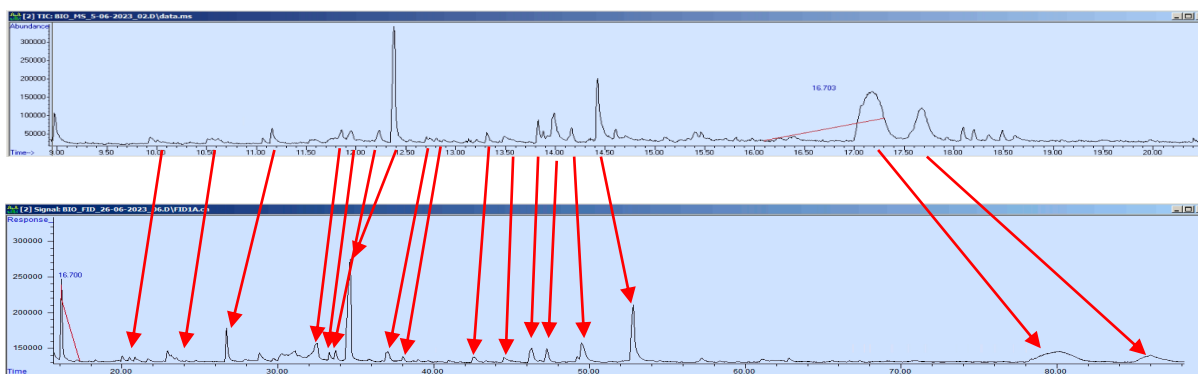


Figure 2.15: Pairing of FID and MS chromatograms for glucomannan vapors

In this thesis, gas chromatography is employed to conduct the speciation of both heavy and light products in two distinct analyses. To identify the light products, pyrolysis vapors are directly extracted from the Thermogravimetric Analyzer (TG) and subsequently injected into the Gas Chromatograph (GC) for analysis. On the other hand, the heavy products are collected in a trap situated at the TG's outlet. These heavy products are then eluted from the trap using an appropriate solvent and subsequently subjected to analysis using the GC. In this analytical process, both Mass Spectrometry (MS) and Flame Ionization Detection (FID) detectors are employed to process the data. This approach enables the attainment of both qualitative and quantitative analyses of the sample and a comprehensive speciation of the bio-oil derived from biomass pyrolysis can be accomplished. In sections 3.3.1 and 3.3.2 a comprehensive explanation of the analytical methods employed for gas chromatography of pyrolysis products will be provided.

2.5. Syringes for GC analysis of light oxygenates

To examine the vapors produced during biomass pyrolysis, it is necessary to sample them directly from a designated sampling point present in the outlet of the thermogravimetric analyzer and subsequently inject them in the gas chromatograph. This process involves using a specialized gas sampling syringe with a maximum volume of 2.5 ml. It is essential to completely fill the syringe with pyrolysis vapors to ensure an ample quantity of detectable products for analysis by either the Mass Spectrometry (MS) or Flame Ionization Detector (FID) of the gas chromatograph.

2.6. Orbo™ traps for GC analysis of heavy oxygenates

Orbo™ tubes are a valuable choice for collecting condensable pyrolysis products when performing offline gas chromatography to analyze the complex mixture produced during biomass pyrolysis. They consist in glass tubes containing two beds of the same selective adsorbent, with a layer of glass wool to separate them. The first bed is bigger and captures the majority of the products, while the second is used as an additional small reserve bed.

Throughout the experiments three types of traps have been tested:

- An Orbo™ 32 – Large charcoal tubes (Fig.2.16), characterized by an active charcoal adsorbent.



Figure 2.16: Orbo™ 32 – Large charcoal tubes [29]

- An Orbo™ 23 – 2-HMP on Amberlite® XAD®-2 (20/40) with sorbent capacities of 120/60 mg (Fig.2.17).

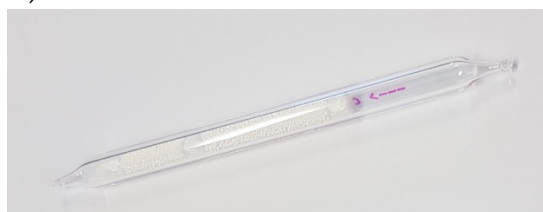


Figure 2.17: Orbo™ 23 – 2-HMP on Amberlite® XAD®-2 (20/40) [29]

- An Orbo™ 609 sorbent, specifically Amberlite® XAD®-2 (20/50) with sorbent capacities of 400/200 mg (Fig.2.18).

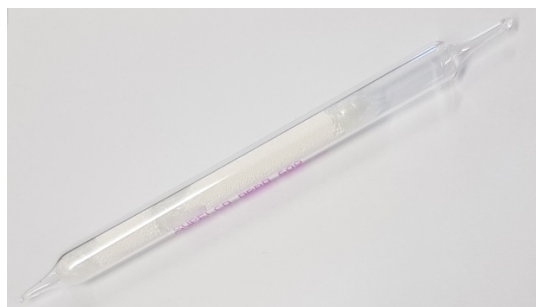


Figure 2.18: Orbo™ 609 Amberlite® XAD®-2 (20/50) sorbent [29]

3 Tuning of experimental procedures

All the experiments were held on the 1st floor of the laboratory in B18 building in Politecnico di Milano La Masa Campus. To perform the pyrolysis investigations described in this thesis, a specialized experimental configuration is employed. This experimental setup, depicted in figure 3.1, was initially developed and utilized at Politecnico di Milano for cellulose research. The novel approach presented in this work is to adapt such configuration to the exploration of a broader range of biomass sources, including hemicelluloses. This class of biomass components presents several differences if compared to cellulose, such as a more complex decomposition pathway under pyrolytic conditions and a different product slate. These aspects certainly pose challenges which need a careful investigation.

The utilized experimental setup enables the acquisition of data relevant to the kinetics of biomass devolatilization, while also conducting analysis of the resulting product range:

- The system employs first of all a thermogravimetric (TG) analyzer for the execution of pyrolysis experiments, allowing for precise monitoring of mass loss under variable heating rates, maintaining control over temperature conditions, and effectively suppressing secondary gas-phase reactions.
- Then, diverse analytical techniques and sampling procedures are used to perform product speciation:
 - o online mass spectrometry for gases (i.e., CO, CO₂, CH₄) and water identification,
 - o sorbent traps (Orbo™) for offline gas chromatography coupled with flame ionization detection (FID) and mass spectrometry (MS) to measure heavy oxygenates (C₆+),
 - o as well as point vapor collection for immediate analysis of light oxygenates (C₁–C₅ products) through GC/FID-MS.

Speciation protocols will allow then to identify and individually quantify all the components present in the sample.

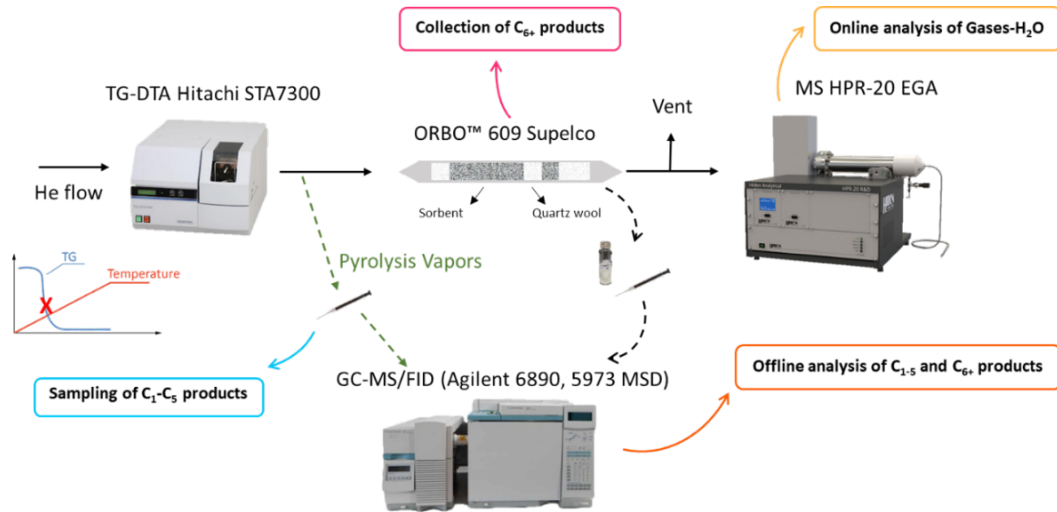


Figure 3.1: TGA-based setup for biomass pyrolysis tests with complete product speciation

3.1. Calibration for quantitative analysis

Calibrating instruments before embarking on an experimental campaign is of fundamental importance. It serves as the foundation for accurate and reliable scientific research, as it ensures that the measurements taken during the experiment are not only precise but also accurate. Calibration is a crucial step with the aim of achieving not just qualitative but also quantitative results. Without proper calibration of instrumentation, accurate quantification of products becomes impossible, underscoring the significance of this process in obtaining reliable and precise analytical outcomes. Calibrated instruments moreover provide a baseline for accurate measurements and also facilitate the comparison of results across different experiments, settings, and laboratories, enhancing the reproducibility and robustness of scientific findings.

- The TG analyzer requires a calibration of the internal mass flow controller for each gas flowing in the instrument, to obtain a relation between the nominal flow rate imposed from the TG software and the real flow rate determined by the characteristics of the gas.
- The Mass Spectrometer needs individual calibrations for every gas to be analyzed. This calibration process is used to compute a specific response factor for each gas species, which is crucial for accurately quantifying the products.
- In the Gas Chromatograph the FID sensor must be calibrated injecting a known quantity of a certain species and calculating its response factor, that will be then used as a reference during the quantification process of all other species.

All the calibration processes are carried out following a procedure that will be precisely described in the following paragraphs.

3.1.1. Mass flow controller calibration

The thermogravimetric analyzer utilized for acquiring kinetic data regarding biomass devolatilization necessitates an oxygen-free operating environment. To achieve this, the instrument relies on a continuous supply of inert gas. Throughout the entirety of the experimental campaign, helium served as the chosen inert gas.

Helium mass flow rate is set from the TGA software depending on the need of the experiments. Since the internal controller of the instrument is calibrated with nitrogen, it is necessary to manually compute the relation between the nominal flow rate defined in the software and the real one that flows through the instrument for helium.

The following procedure was used to calibrate the flow controller for helium:

- The nominal flow rate was set from the TGA software, ranging from $25 \frac{Nml}{min}$ to $250 \frac{Nml}{min}$.
- The imposed flow rate was gradually increased with a step of $25 \frac{Nml}{min}$, to cover significant values of flow rate in the whole range defined in the previous step. An exception is made for values in the middle of the scale: a flow rate of $120 \frac{Nml}{min}$ was used instead of $125 \frac{Nml}{min}$ because it was a specific value utilized in different experiments.
- The real flow rate was measured in a bubble flowmeter with a chronometer (sensitivity 0.01 s); an average of five measurements was considered.

Knowing the volume in ml filled by the gas, the time required at the imposed flow rate to fill this volume (expressed in seconds) and the room temperature during the measurements (expressed in Celsius), it is possible to compute the actual flow rate with the following formula (Eq.3.1):

$$F_i = \frac{V_f - V_i}{t} * 60 * \frac{273.15}{273.15 + T} \quad (3.1)$$

Where F_i [ml/s] is the real flow rate, V_f [ml] is the final volume occupied by the gas, V_i [ml] is the initial volume (always set equal to zero), t [s] is the time and T [°C] is the temperature.

The data collected were used to build a linear regression curve, as shown in figure 3.2. This curve is described by equation 3.2, where F_i is the actual flow rate and x is the nominal flow rate. The slope and y-intercept (m and q , respectively) were derived from the linear relationship and adopted as parameters to calculate the nominal flow rate to set as input parameter for the following experiments:

$$F_i = m * x + q \quad (3.2)$$

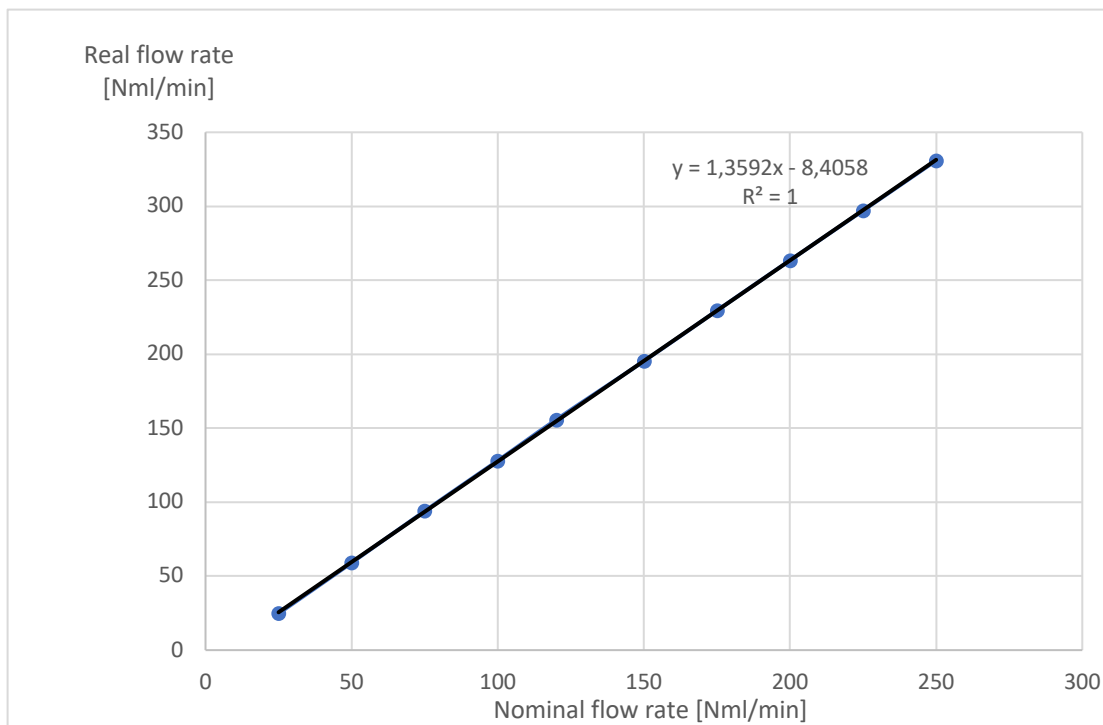


Figure 3.2: Calibration curve for helium

3.1.2. Mass spectrometer calibration

The analysis of pyrolysis gaseous products requires the use of an on-line MS. The spectrometer is able to determine and quantify the molecules produced by the reactions that occur upstream the instrument, but returns a signal expressed in mbar that requires some manipulation to make it significant.

In particular, a response factor for every gas of interest should be calculated in order to convert the raw signal of the spectrometer to a meaningful quantity (Fig.3.3). Such response factor is defined by the following equation (Eq. 3.3):

$$Y_i = f_i * (\text{Raw signal}_i - \text{Raw signal}_{i,0}) \quad (3.3)$$

Where Y_i is the molar fraction of the i -species; f_i is the response factor of the i -species; raw signal $_i$ and raw signal $_{i,0}$ are the values in mbar returned by the instrument respectively at a known concentration and in absence of the i -species.

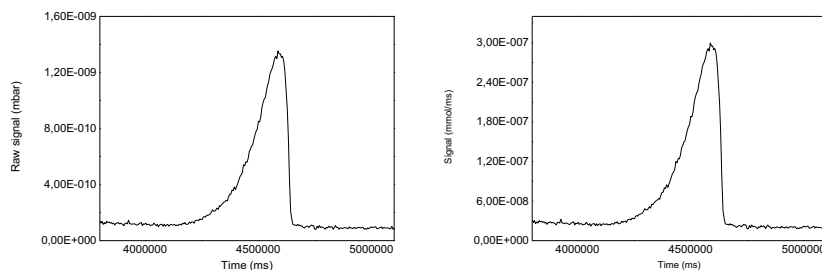
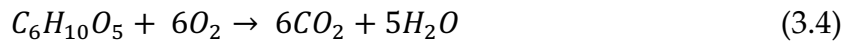


Figure 3.3: Conversion of raw data from mass spectrometer using the response factor

By letting a gas of known composition flow through the mass spectrometer it is therefore possible to calculate the response factor for that specific compound and to use this result in the quantification of gases coming from biomass pyrolysis reactions.

This simple procedure has been adopted for the calibration of CO₂ signal, which is supplied for this purpose from cylinders where its concentration is known. For the sake of simplicity, it has been assumed that CO, methane and methanol are characterized by the same response factor of carbon dioxide. Its value is reported in table 3.1.

Calculating the response factor for water, requires instead a slightly more complicated procedure, as it cannot be supplied in gaseous form, from a tank with known composition. In this case a cellulose sample is burned in the TG analyzer, whose outlet is connected to the inlet of the mass spectrometer. As cellulose is burned in air, it releases water together with other combustion products according to equation 3.4:



Knowing the initial mass of cellulose (m_{cell}) and its molar mass ($MW_{cell} = 162 \text{ g/mol}$), it is possible to compute the initial moles of biomass (x_{cell}) from equation 3.5:

$$x_{cell} = m_{cell} * MW_{cell} \quad (3.5)$$

Simply following the stoichiometry of the oxidation reaction, it is then possible to calculate the expected moles of water produced (exp_{H_2O}) from equation 3.6:

$$exp_{H_2O} = 5 * x_{cell} \quad (3.6)$$

Once the expected moles are calculated, the real quantity of water obtained from cellulose combustion can be calculated by plotting the raw signal obtained from the mass spectrometer as a function of time and by computing the area of the peak to obtain its integral production. The response factor can then be found thanks to equation 3.7:

$$f_{H_2O} = \frac{exp_{H_2O}}{x_{H_2O} * Air \ flow} \quad (3.7)$$

The response factor calculated with such protocol is reported in table 3.1.

A similar approach to that used with water can also be applied to determine the CO₂ response factor. This alternative method can be used to eliminate the need for external tanks and to check the accuracy of the factor previously computed. In this case a sample of calcium carbonate (CaCO₃) is thermally decomposed in the TG analyzer,

whose outlet is connected to the inlet of the mass spectrometer, resulting in the production of CO₂ as follows (Eq.3.8):



Again, knowing the initial mass of calcium carbonate (m_{cell}) and its molar mass ($MW_{\text{CaCO}_3} = 100 \text{ g/mol}$), it is possible to compute the initial moles of biomass (x_{CaCO_3}) and the expected moles of CO₂ produced (exp_{CO_2}).

$$x_{\text{CaCO}_3} = m_{\text{CaCO}_3} * MW_{\text{CaCO}_3} \quad (3.9)$$

$$\text{exp}_{\text{H}_2\text{O}} = 5 * x_{\text{cell}} \quad (3.10)$$

The real quantity of CO₂ obtained from CaCO₃ decomposition can be then calculated by computing the area of the peak related to carbon dioxide obtained from the mass spectrometer. The response factor can then be found thanks to equation 3.11:

$$f_{\text{CO}_2} = \frac{\text{exp}_{\text{CO}_2}}{x_{\text{CO}_2} * \text{Air flow}} \quad (3.11)$$

The response factor calculated with such protocol is reported in the following table (Tab.3.1), and, as it can be seen, is comparable to the one calculated with the alternative method:

Table 3.1: Calibration factors for species in mass spectrometer

Species	Formula	fi
Carbon dioxide from external tank	CO ₂	1.30E+06
Carbon dioxide from CaCO ₃	CO ₂	1.30E+06
Carbon monoxide	CO	1.30E+06
Methane	CH ₄	1.30E+06
Methanol	CH ₃ OH	1.30E+06
Water	H ₂ O	1.60E+06

3.1.3. Gas chromatograph calibration

The quantification of the pyrolysis condensable products, trapped in the sorbent tubes previously cited, relies on the off-line GC analysis performed with the FID detector.

This instrument generates a graphical representation of the outcomes known as a gas chromatogram, where each peak corresponds to a specific chemical species. Both the height and width of the peak provide valuable information regarding the concentration and total quantity of the product.

To ensure accurate quantification, the pyrolysis products are eluted in a solution referred to as the 'mother solution' before undergoing analysis in the GC. This solution contains acetone and a predetermined quantity of fluoronaphtalene, serving as an internal standard for reference purposes (Tab.3.2).

Table 3.2: Mother solution

Mother solution	
Acetone (ml)	250
F-org (μL)	10

The results obtained from gas chromatography are initially presented as GC Area, derived from the integration of the peaks corresponding to individual compounds. To enhance their practical significance, these values are further transformed into meaningful quantities, specifically measured in millimoles (mmol) of products, using equation 3.12:

$$\frac{M_i}{V_{FNapht}} = f_i * \frac{A_i}{A_{F-org}} \quad (3.12)$$

M_i represents the moles (mmol) of the i -species, V_{F-org} is the volume (μL) of the internal standard contained in the washing solution, f_i is the response factor for the i species, A_i is the area of the i species and A_{F-org} is the area of the internal standard in the washing solution, both obtained from the gas chromatogram.

In order to properly apply this formula, one would need to calculate the response factor for every species which is expected to be a product of biomass pyrolysis, however that would require too great of an effort. For this reason, a single species has been chosen as the reference product of biomass pyrolysis, being it the most abundant and easily detectable in most analysis. The product of choice is levoglucosan (LVG) and it has been assumed that the value calculated for its response factor is similar to the value for the other species.

Adopting a calibration solution, with known quantity of levoglucosan dissolved in the mother solution, it is possible to compute the response factor exploiting the inverse formula derived from equation 3.12. A combination of different calibration solutions, showed in table 3.3, has been used to produce an average value that is representative of the operating conditions. Moreover, to ensure reproducibility of the results all the solutions have been tested three times.

Table 3.3: Response factors for different calibration solutions

Response factors for different calibration solutions					
LVG (mg)	Mother solution (ml)	Total F-org (μL)	LVG / F-org (mg/ μL)	LVG / F-org (mmol/ μL)	f_i
4.4	50	2	2.2	0.0137	0.0320
5.3	50	2	2.65	0.0164	0.0351
9.8	5	0.2	49	0.3041	0.0306
10.4	5	0.2	52	0.3227	0.0288
20.1	5	0.2	100.5	0.6237	0.0276
23	5	0.2	115	0.7137	0.0348
29.6	5	0.2	148	0.9185	0.0360
30	5	0.2	150	0.9309	0.0315

The final response factor for LVG, computed as an average between all the values of f_i is $f_i = 0.0326$.

3.2. Devolatilization kinetics

This thesis employs a systematic approach to investigate biomass pyrolysis, commencing with an in-depth analysis of devolatilization kinetics through thermogravimetric analysis. The goal is to gain insights into the devolatilization of biomass across a range of different samples. This investigation aims to explore the impact of crucial pyrolysis process parameters and evaluate the potential presence of mixing effects. The ultimate goal is to elucidate the fundamental mechanisms involved in pyrolysis and generate pertinent data for the development of kinetic models.

To achieve this, a series of experiments were conducted using a TG analyzer on both pure components and mixtures, enabling the examination of the sample's thermal behavior and the plotting of mass loss curves.

The following samples have been studied during this campaign:

- Cellulose
- Xylan
- Glucomannan
- Arabinoxylan
- Xylan & Cellulose
- Xylan & Glucomannan
- Xylan & Arabinoxylan
- Xylan & Cellulose & Arabinoxylan & Glucomannan

3.2.1. Before the experiment

Before each experiment, a standardized procedure was diligently followed:

1. Initial helium line check: The helium line, extending down to the building's basement, was first inspected. The valve was ensured to be open, and the line's pressure was verified to be at the correct level. If the pressure deviated from the target value of 1 bar, necessary adjustments were made using the appropriate pressure reducer.
2. Sample pan preparation: The sample pan within the TG analyzer was carefully extracted from the instrument using tweezers. Subsequently, any residual solids from the prior experiment were removed from the pan using a paper towel and compressed air. The cleaned pan was then reinserted into the instrument.
3. Taring the TG balance: To accurately measure biomass weight loss, the TG balance was tared, setting the empty pan's initial weight to zero.
4. Biomass loading: After instrument calibration, the pan was removed, loaded with the chosen biomass, and weighed once more.

For a sample comprising a mixture of various biomasses, additional steps were necessary:

5. First Biomass Storage: After weighing the first biomass, it is removed from the sample pan and placed in a folded weighing paper.
6. Taring the TG Balance Again: The TG balance is tared once more, preparing it for the next component of the mixture.
7. Mixing and Combining Components: The second component is weighed, removed from the pan, and then meticulously blended with the first component to achieve a homogeneous mixture.
8. Weighing the Final Mixture: The well-mixed biomass mixture is transferred to the pan on the tared balance and weighed once more.

This procedure facilitates the individual measurement of each biomass component to determine the fractions present in the final mixture. Additionally, it allows for the calculation of the total sample weight and helps assess the biomass lost during the transfer steps, typically amounting to approximately 10% of the biomass.

3.2.2. Biomass pyrolysis in the TG analyzer

After loading the biomass into the TG analyzer, the experiment's input parameters can be adjusted using dedicated software. Specifically, the temperature profile and the types of gases flowing in the oven need to be chosen to simulate typical pyrolysis conditions.

The experiment comprises three distinct steps, each with specific operating conditions:

- I. An initial 40-minute phase at ambient temperature, with a helium (He) flow rate of 229 ml/min. This step helps clear the system of any residual gases from previous tests and eliminates oxygen in the furnace.
- II. A phase with a gradual temperature increase from ambient to 950°C, maintaining the He flow rate at 229 ml/min. This step serves to evaporate moisture from the biomass and perform the pyrolysis process.
- III. A final 10-minute phase at a steady 950°C temperature, with air flowing at 229 ml/min. This stage is designed to burn any condensed products that could obstruct the system and remove any char residues from the sample pan.

The temperature ramp rate in the second step can be adjusted to different values. Each biomass sample was tested at three distinct temperature ramp rates: 100°C/min, 20°C/min, and 3°C/min.

3.2.3. Data processing

The TG software provides both a graphical representation of the experiment's results, plotting the TG (weight loss) and DTG (derivative of the TG) curves against the temperature and an Excel file with all the data acquired during the test (time, temperature, TG and DTG). The TG and DTG signals provided by the software are presented as cumulative and expressed respectively in [μg] and [$\mu\text{g}/\text{min}$], which means that the results from different tests cannot be compared without some manipulation. The main modifications to apply are:

- Convert the TG [μg] in TG [%]
- Convert the DTG [$\mu\text{g}/\text{min}$] in DTG [1/min]
- Neglect the initial evaporation step, removing the moisture from the total mass and working in dry basis, in order to focus just on the pyrolysis process.

To refine the data the following calculations have been performed:

- Given the cumulative loss of mass (TG [μg]), it was possible to compute the remaining fraction of the total mass (TG [%]) at each time step.

$$TG [\%] = \frac{\text{Sample weight} + \text{cumulative loss}}{\text{Sample weight}} \quad (3.13)$$

- The dry mass [%] was determined through graphical identification of the end of the evaporation phase on the TG curve (Fig.3.4). The total dry mass [mg] was then computed by multiplying the sample weight by the dry mass percentage.

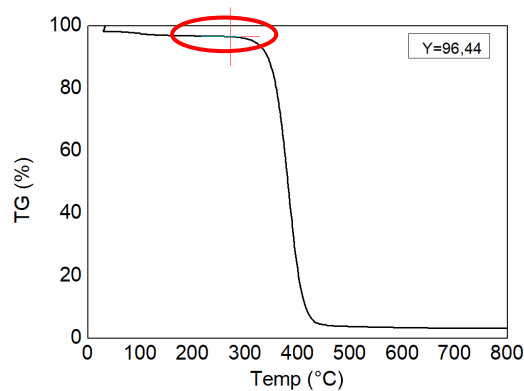


Figure 3.4: TG curve with dry mass definition

- The moisture was then calculated as the difference between the sample weight [mg] and the dry mass [mg]. A summary of moisture percentages of the different biomass analyzed is reported in table 3.4.

Table 3.4: Moisture (%) of different biomasses

Species	Moisture [%]
Cellulose	3,4
Arabinoxylan	9,25
Glucomannan	6,8
Xylan	12,4

- Using the cumulative loss of mass (TG [μg]) and the quantity of moisture, it was possible to compute the cumulative loss of dry mass (TG_{dry} [μg]) at each time step:

$$TG_{dry} [\mu\text{g}] = \text{cumulative loss} + \text{moisture} \quad (3.14)$$

- Given the cumulative loss of dry mass (TG_{dry} [μg]) and the total dry mass, it was possible to compute the remaining fraction of the total dry mass at each time step:

$$TG_{dry} [\%] = \frac{\text{Total dry mass} + \text{cumulative loss of dry mass}}{\text{Total dry mass}} \quad (3.15)$$

- Lastly, the derivative of the cumulative loss of mass (DTG [$\mu\text{g}/\text{min}$]) was utilized to calculate the normalized DTG [1/min], dividing the cumulative loss by the sample weight in μg .

Once TG_{dry} [%] and normalized DTG [1/min] are established, they can be plotted against temperature, offering a visual representation of the sample's behavior. This enables comparisons with other samples, highlighting both similarities and differences between them. In this way single biomasses could be compared with each other, analyzing aspects such as:

- Moisture content.
- Temperature at which devolatilization occurs.
- Number of steps of devolatilization.
- Solid residue.

3.3. Speciation of pyrolysis products

The second crucial aspect of the research presented in this thesis regards product speciation. An extensive investigation was conducted to perform a qualitative and quantitative analysis of pyrolysis products, with the goal of identifying all the species present in both the gas and condensed phases. To achieve this objective, various methods were employed, encompassing both online and offline analyses. Specifically, a mass spectrometer was connected to the outlet of the thermogravimetric analyzer to quantify gaseous products such as CO, CO₂, H₂O, and CH₄. Simultaneously, an offline gas chromatograph was used to quantify light compounds (ketones, acids, C5 and C6 sugars, alcohols, furan derivatives, and cyclo-oxygenates) and heavy oxygenates (primarily C6 sugars) in separate analyses.

Consequently, for the speciation of the biomass sample, three distinct experimental protocols and data processing methods were developed, providing a comprehensive analysis of the pyrolysis products. In the subsequent paragraphs a comprehensive explanation of these protocols will be provided.

Speciation of pyrolysis products was carried out for the following feedstocks:

- Xylan
- Glucomannan
- Xylan & Glucomannan
- Xylan & Cellulose

3.3.1. Speciation of pyrolysis gases and heavy oxygenates

Gas analysis and pyrolysis heavy product trapping are performed within the same experiment, whereas vapor sampling requires a separate run. The reason for this distinction is that the sorbent tubes employed for product trapping effectively capture all the species generated during the pyrolysis process, allowing only gases to pass through. Consequently, these gases can be detected by the mass spectrometer without interference from other species that should have been retained by the trap. Furthermore, the introduction of heavy species into the mass spectrometer could potentially cause problems for the delicate detection instruments. Therefore, it is advantageous to intercept and halt these heavy species beforehand to ensure the smooth operation of the instrumentation. Another crucial reason for this separation lies in the distinct carrier gas flowrate requirements during pyrolysis for the analysis of light and heavy oxygenates. Combining these analyses into a single experiment would be impractical due to the incompatible conditions needed for each case.

3.3.1.1. Before the experiment

The biomass pyrolysis process is once again conducted within the TG analyzer, following the same preparation procedure described in paragraph 3.2.1. Additional preparation steps are then necessary to perform product analysis.

For the online gas analysis, the primary task involves the careful connection of the TG's outlet to the mass spectrometer's inlet, ensuring a secure, leak-free connection. Additionally, the software should be configured for data collection by selecting the ions corresponding to the species of interest that need to be quantified.

For the offline analysis of heavy products using the gas chromatograph (GC), the following preparation steps are essential:

1. First, ensure that the helium (He) and hydrogen (H₂) gas lines are open.
2. Next, the GC column used for analysis (either MS or FID) should be cleaned. Acetone is employed as cleaning agent prior to liquid analysis.

Heavier products are collected in an Orbo™ sorbent trap before analysis, necessitating additional setup preparations:

1. Carefully open the Orbo™ sorbent tubes by cutting the glass ends.
2. Connect one or two sorbent tubes in series directly to the outlet of the TG analyzer using a hose equipped with a screw for instrument connection and a gasket to prevent leaks.
3. If two sorbent tubes are employed, connect them to each other with a small rubber hose.
4. Wrap each connection point, where potential leaks may occur, with Teflon tape for added security.

As previously mentioned, gas analysis and heavy product collection take place within the same experiment. Therefore, when preparing the setup, it is crucial to first connect the outlet of the TG to the Orbo™ trap and then link the outlet of the Orbo™ trap to the inlet of the mass spectrometer.

3.3.1.2. Biomass pyrolysis in the TG analyzer with gas and heavy oxygenates speciation

The experiment is divided into four distinct steps, similar to the ones used for the kinetic investigation campaign:

- I. A forty-minute period under steady conditions at ambient temperature, with a helium flow rate of 229 ml/min. At the beginning of the analysis, the mass spectrometer signals for each gas under study may not accurately represent the experiment's initial conditions due to line impurities. The forty minutes allocated to this first step are crucial for cleaning the lines and achieving a stable and realistic condition.

- II. A constant temperature increase at a rate of 100°C/min, starting from ambient temperature and reaching 950°C, with a helium flow rate of 229ml/min. During step two, pyrolysis occurs. Given that the outlet of the TG is connected to the sorbent tubes, heavy products are retained, while gases are allowed to pass through undisturbed and enter the mass spectrometer for analysis. In this case, a high inert gas flow rate is necessary to ensure rapid transportation of all products into the Orbo™ tubes, preventing condensation before they reach the collection section.
- III. A forty-minute period under steady conditions at 950°C with helium flowing at 229 ml/min is executed. These extra minutes in a steady state are required for manually disconnecting the sorbent tubes and the MS line from the TG analyzer to prevent air to flow into the instruments, altering the analysis results.
- IV. Finally, a ten-minute duration under steady conditions at 950°C with an air flow of 229 ml/min is employed to burn any condensed products that might obstruct the TG lines and eliminate any char residues from the sample pan.

During this speciation experiment, the following gases are analyzed in the MS, by selecting the corresponding ions in the software: methane ($m/z = 15$), water ($m/z = 16, 17, 18$), carbon monoxide ($m/z = 28$), methanol ($m/z = 32$), carbon dioxide ($m/z = 28, 44$); in addition to these single species, a bar scan analysis is performed, where the instrument searches for all the m/z fragments in a given range (m/z between 0 and 150). Thanks to this scan it is possible to detect any species that has passed through the trap at the outlet of the TG, both providing information on the possible presence of additional gases that were not considered in the previous list, as well as prove the efficiency of the sorbent tube to trap all the desired organic species.

When disconnected from the TGA outlet, the Orbo™ is disassembled from the Teflon and from the hose used for connections, and its contents are carefully transferred into a vial. The vial contents are washed with a 10 mL solution comprising acetone and an internal standard utilized as a reference in the subsequent GC analysis. It is crucial to precisely measure the quantity of the "mother solution" used in each vial, as it serves as the key parameter for quantification purposes.

Once the pyrolysis products have been eluted from the sorbent phase, allowing for accurate identification and quantification, the vial's contents can be sampled using a liquid-specific syringe and subsequently injected into either of the two GC columns for analysis.

The analytical method employed in the gas chromatograph comprises the following steps:

- I. Five minutes in steady conditions at 40°C.
- II. Constant increase of the temperature from 40°C to 110°C with a ramp of 10°C/min.
- III. Constant increase of the temperature from 110°C to 300°C with a ramp of 12°C/min.
- IV. Thirteen minutes in steady conditions at 300°C.

At lower temperatures, the analysis primarily detects lighter compounds, while rising the temperature, the focus shifts towards identifying heavier products characterized by longer retention times. This is because an increase in the temperature corresponds to a decrease of the volatility of the products, which require more time to travel through the GC column.

For the purpose of this analysis, the emphasis is placed on quantifying the heavy products retained in the Orbo™ tubes. Therefore, only the products detected during the second and third steps are considered for quantification. Compounds detected at later retention times are also typically omitted from consideration, as they often do not represent pyrolysis products but rather contaminants or impurities.

Since the content of the vial can be used for both the analysis in the GC-MS and GC-FID detectors, a single sample and a single run in the TG is sufficient for a complete liquid quantification.

3.3.1.3. Data processing of gaseous products

The mass spectrometer software offers two key outputs for analyzing the gas evolution during the reaction: a graphical representation displaying the concentration of each species in millibars plotted against time, providing a visual trend, and an Excel file containing a numerical summary of the results.

To quantify the gaseous products, the following steps are necessary:

1. Input the numerical data for each species into a dedicated graphical software, Origin.
2. Generate plots for each product's temporal evolution, with time on the x-axis in milliseconds and signal intensity on the y-axis in millibars (Fig.3.5).
3. Utilize a specific software function to compute the integral area under each chart between two designated points, representing the reaction's beginning and end.

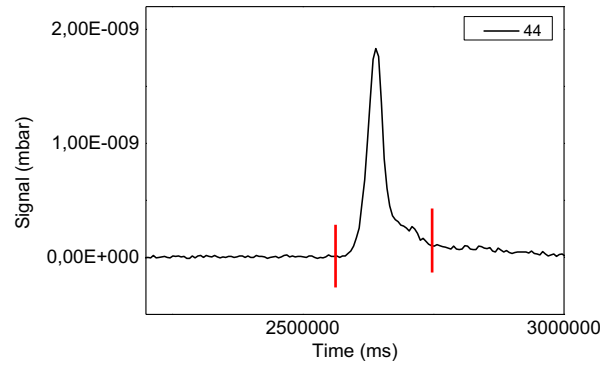


Figure 3.5: Example of the trend of CO₂ (m/z=44) plotted to compute the integral area

4. Given the volumetric helium flow rate (V_{He}) in terms of [NmL/min], convert this value in molar flow rate [mmol/ms]:

$$\dot{m}_{He} = \frac{V_{He}}{60 \cdot 1000 \cdot 22.4} \quad (3.16)$$

5. Knowing the helium molar flow rate used during the experiment (\dot{m}_{He}), the response factor determined during the calibration phase for each species (f_i) and the integral areas computed in the previous step for each species (A_i), calculate the mass [mg] of each produced species using the following formula:

$$m_i = MW_i \cdot A_i \cdot f_i \cdot \dot{m}_{He} \quad (3.17)$$

6. Compute the initial mass of biomass used during the pyrolysis reaction on a dry basis following the same procedure used during the kinetic investigation campaign (see paragraph 3.2.3.)
7. Calculate the mass yield (m_{y_i}) for each gaseous species on the total dry mass used for the experiment:

$$m_{y_i} = \frac{m_i}{m_{dry}} \cdot 100 \quad (3.18)$$

By employing this approach, it is possible to quantify methane, water, carbon monoxide, methanol, carbon dioxide, and the total gas production, expressing the results both in terms of milligrams and mass yield for each sample under analysis.

This methodology facilitates the comparison of different biomasses based on the quantities of gases produced during the pyrolysis process.

3.3.1.4. Data processing of heavy products

The analysis of heavy products relies on two distinct outputs from the same instrument: the chromatogram and mass spectra from the GC-MS (Fig.3.6-3.7) and the chromatogram obtained through the GC-FID. The first one can be easily analyzed through the GC software: by simply double-clicking on each peak, an online library opens, and the software automatically generates a list of potential species corresponding to the peak. Each compound in the list is assigned a specific probability value, and only species exceeding a predetermined probability threshold are taken into consideration. In addition to the name of the detected species, it is also possible to identify their chemical formula and their molecular weight, that will be useful for the quantification.

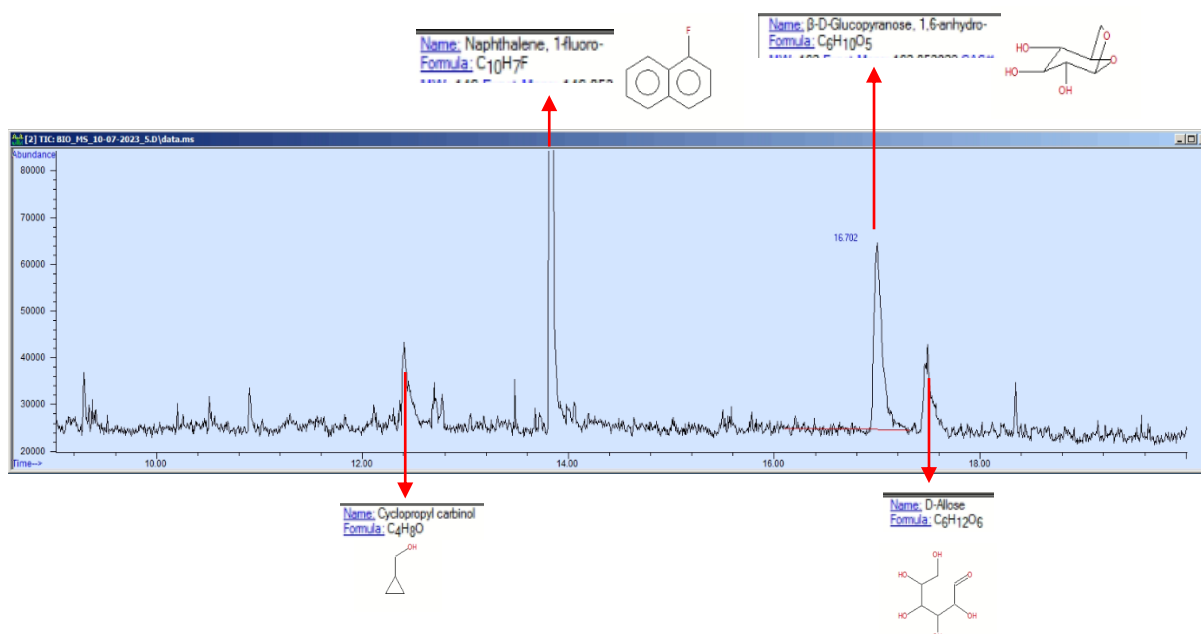


Figure 3.6: Example of a GC-MS output where significant species have been detected using the online library provided by the analysis software

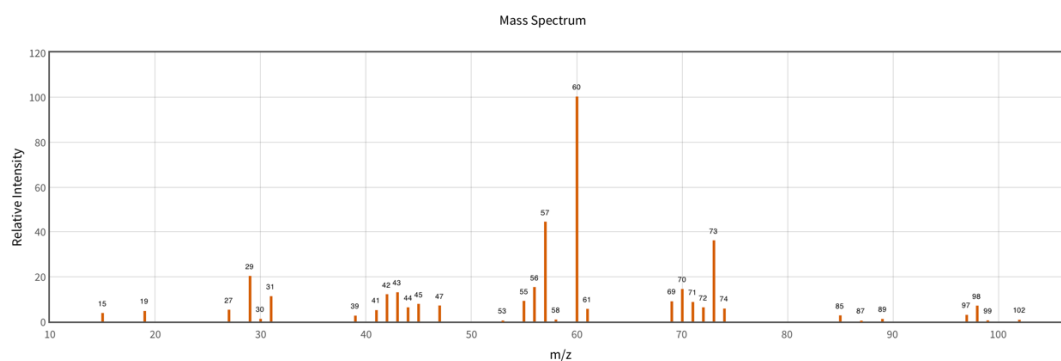


Figure 3.7: Example of mass spectrum for levoglucosan which can be associated to the corresponding peak on the GC-MS chromatogram

Once the product identification and qualitative analysis of species in the sample are complete, the next step involves examining the GC-FID chromatogram. While this chart resembles the one obtained with the MS detector, it represents a fundamentally different type of data. Therefore, the software is unable to directly link the peaks to specific chemical species.

Due to this distinction, the initial task during product analysis is to establish a connection between the two graphs, leveraging their similarities. The outcome of this coupling process is illustrated in figure 3.8.

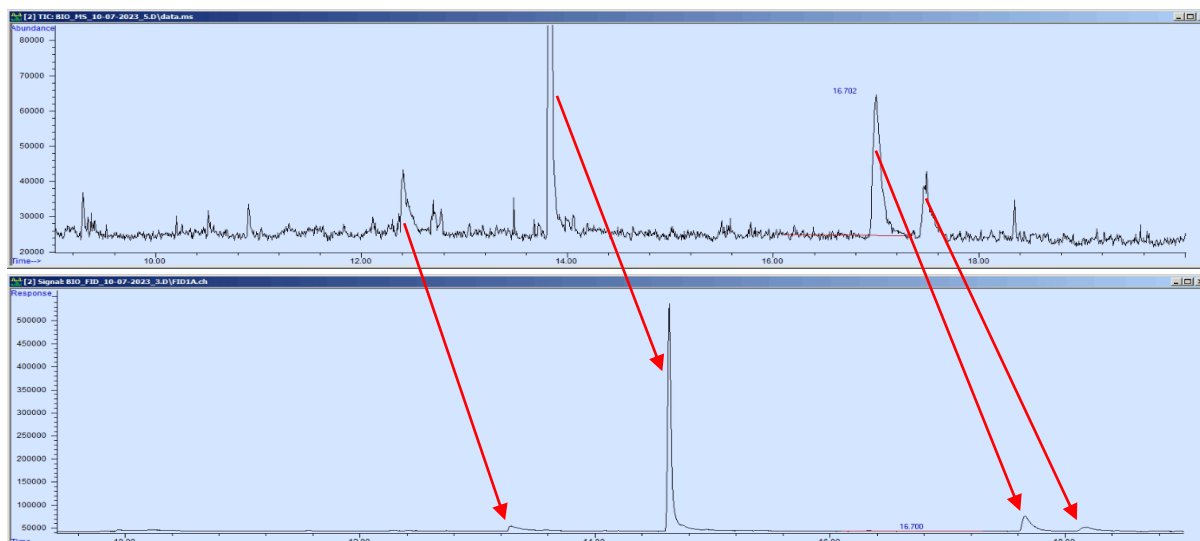


Figure 3.8: Example of coupling between GC-MS and GC-FID chromatograms

Once that each peak of the chromatogram has been coupled, it is possible to proceed with the quantification. All the manipulations of the data performed during this process are based on the same formula utilized during the calibration of the GC and the definition of the response factor; the aim of the calculations is to determine the millimoles of each species M_i :

$$\frac{M_i}{V_{F-org}} = f_{LVG} * \frac{A_i}{A_{F-org}} \quad (3.19)$$

In order to use this formula, it is necessary to know the response factor for levoglucosan (f_{LVG}), previously calculated in the calibration step, the quantity of internal standard (V_{F-org}) present in the vial which has been analyzed, and the integral areas of the peaks for each pyrolysis product identified in the chromatogram (A_i), as well as that of fluoronaphtalene (A_{F-org}).

In order to complete the quantification process, it is therefore necessary to follow these steps:

- Manually integrate the peaks in the GC-FID chromatogram through the GC software, as shown in figure 3.9: each red line defines the start and end points of the integration. The software itself provides the value of each area (Tab. 3.5).

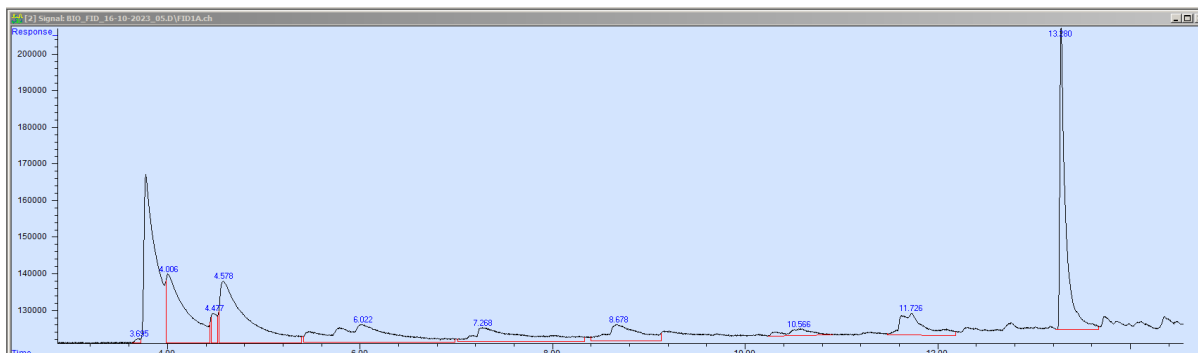


Figure 3.9: Example of the integration performed by the GC-FID

Table 3.5: Example of the numerical output of the GC software.

Peak #	Ret Time	Area
1	8.656	1483836
2	9.886	175377
3	10.341	765907
4	13.362	846585
5	14.077	98697
6	14.633	6904138
7	15.436	324544
8	16.326	258316
9	17.638	1421505
10	18.133	790798
11	19.269	540993

- Couple the area provided by the software to the species previously identified through the GC-MS library and to their molecular weight (MW_i).
- Calculate the quantity of internal standard contained in the analyzed vial (V_{F-org}), as a proportion between the quantities of acetone (V_{ac_sol}) and internal standard (V_{F-org_sol}) utilized during the preparation of the mother solution, and the quantity of solution in the vial (V_{MS}):

$$V_{F-org} = \frac{V_{F-org_sol} * V_{MS}}{V_{ac_sol}} \quad (3.20)$$

- Calculate the millimoles (mol_i) of each species following:

$$mol_i = V_{F-org} * f_{LVG} * \frac{A_i}{A_{LVG}} \quad (3.21)$$

- Determine the mass of each product, expressed in milligrams, as the product between the millimoles of the i -species (mol_i) and its molecular weight (MW_i):

$$m_i = mol_i * MW_i \quad (3.22)$$

- Finally, determine the percentage of mass yield of every product (m_{y_i}) simply as the ratio between the mass of the i -species (m_i) and the total initial mass, defined on a dry basis (m_{dry}):

$$m_{y_i} = \frac{m_i}{m_{dry}} * 100 \quad (3.23)$$

The sum of the percentage mass yield corresponds to the total amount of heavy products obtained during the pyrolysis reaction. Typically, in this context, heavy products are defined as compounds with retention times greater than the internal standard. Consequently, when lighter compounds are identified, they are often excluded from this category and instead quantified as part of the vapor products. The final result of the quantification process is illustrated in table 3.6.

Table 3.6: Example of the quantification's results: in green the species considered as heavy products

Peak #	Ret Time	Species	MW	Area	mmol i	mg	mass yield [%]
1	8.656	Furan methanol	98	1483836	0.0027	0.266	2.61
2	9.886	Dioxane	144	175377	0.0003	0.046	0.45
3	10.341	Methyl furanone	98	765907	0.0014	0.137	1.35
4	13.362	Cyclopropyl carbinol	72	846585	0.0015	0.111	1.09
5	14.077	Levoglucosenone	126	98697	0.0002	0.023	0.22
6	14.633	Fluoronaphtalene	-	6904138	0.0126	-	-
7	15.436	???	162	324544	0.0006	0.096	0.94
8	16.326	???	162	258316	0.0005	0.077	0.75
9	17.638	Levoglucosan	162	1421505	0.0026	0.421	4.13
10	18.133	D-allose	180	790798	0.0014	0.260	2.56
11	19.269	???	180	540993	0.0010	0.178	1.75
						Tot	10.13

At this stage, comparative analysis can be performed for samples consisting of individual biomasses. Such an analysis involves the comparison of the species produced, encompassing both qualitative and quantitative aspects.

3.3.2. Speciation of pyrolysis light oxygenates

As previously stated, analysis and speciation of pyrolysis vapors require a separate experiment. This separation is primarily attributed to the divergent operating conditions required, which are incompatible with those employed for gases and heavier products.

3.3.2.1. Before the experiment

The procedure described in paragraph 3.2.1 is followed for the preparation of the TG analyzer, where the pyrolysis process takes place. Additional preparation steps are then necessary to perform the offline analysis of light oxygenates employing gas chromatography:

1. First, ensure that the helium (He) and hydrogen (H₂) gas lines are open.
2. Next, the GC column used for analysis (either MS or FID) should be cleaned. When analyzing vapors, ambient air is injected to cleanse the instrument.

For vapor analysis in the gas chromatograph, the samples are withdrawn directly from a sampling point located in the TG outlet line and are promptly injected into the GC for analysis, so no further preparation is necessary.

3.3.2.2. Biomass pyrolysis in the TG analyzer with light oxygenates speciation

Pyrolysis takes place in three different steps similarly to what already seen, where the only difference stands in the helium flow rate:

- I. Forty minutes in steady conditions at ambient temperature, with an He flow rate of 229 ml/min.
- II. Constant increase of the temperature with a temperature ramp of 100°C/min from ambient to 950°C with the He flow rate equal to 22.9 ml/min. A high heating ramp is employed to obtain a pulse of products while a low inert gas flow rate is used because a higher value would cause an excessive dilution of the products, making the GC analysis difficult.
- III. Ten minutes in steady conditions at 950°C with air flowing at 229 ml/min.

In step two, pyrolysis vapors are extracted using a syringe specifically designed for gas sampling. These vapors are withdrawn from the collection point located at the TG furnace outlet and are subsequently injected into the gas chromatograph. Each analysis is limited to a maximum volume of 2.5 mL, which aligns with the syringe's maximum capacity.

The vapor collection phase represents the most critical phase, given the rapid completion of pyrolysis within a short time frame. It is crucial to pinpoint the optimal sampling moment during which to capture the highest possible number of pyrolysis products. This optimal moment can be determined by analyzing the outcomes of the devolatilization investigation. Typically, the pyrolysis process exhibits its peak vapor production concurrent with the maximum derivative thermogravimetry (DTG) value. This peak can be associated with either a specific temperature or a particular mass loss threshold, both of which can serve as reference points for the precise timing of product withdrawal.

Upon the collection and injection of vapors into either of the two gas chromatograph columns (MS or FID), the analysis can proceed according to the following steps:

- I. An initial five-minute phase under steady conditions at 40°C.
- II. A continuous temperature increase from 40°C to 110°C with a ramp rate of 10°C/min. GC-FID vapors analysis for glucomannan is the only exception, with a ramp of 1°C/min from 40°C to 300°C.

- III. A subsequent constant temperature increase from 110°C to 300°C with a ramp rate of 12°C/min, except for GC-FID vapor analysis of glucomannan, where the unique ramp rate of 1°C/min is again applied.
- IV. A final thirteen-minute phase conducted under steady conditions at 300°C. The maximum temperature limit of 300°C is dictated by both technical instrument constraints and the threshold for detecting species devolatilization.

The first step is specifically designed to detect the lightest and most volatile products, often visible only during vapor analysis. The second and third steps are designed to identify heavier products, requiring higher temperatures and longer retention times to traverse the entire GC column. It's noteworthy that the heavier species found in the vapors often overlap with those present in the liquid analyses, serving as a valuable common reference point between vapor and liquid speciation, useful for the subsequent data processing. The last step is primarily intended for very heavy compounds, typically excluded from product quantification due to their non-representative nature of pyrolysis products and their characterization as impurities.

Given that a comprehensive vapor analysis necessitates the utilization of both MS and FID detectors, it is necessary to replicate the same experimental procedure described above for the same sample at least twice, once for each GC column.

3.3.2.3. Data processing of vapors

The analysis of vapors follows a similar conceptual framework to that of heavy products. In this context, the GC-MS detector is utilized for species identification within the sample, while the GC-FID is employed for their quantification. The practical steps necessary to complete the quantification process are analogous, with only minor distinctions due to the absence of an internal standard in the injected vapor mixture.

The millimoles of the different compounds are determined with a formula similar to that employed for the GC calibration and the liquids quantification. In this case, fluoronaphtalene is replaced with a generic reference (M_{ref} and A_{ref}) selected from common species found in both vapors and heavy products.

$$\frac{mol_i}{M_{Ref_vap}} = \frac{A_i}{A_{Ref}} \quad (3.24)$$

The choice of the reference species becomes therefore a crucial point in vapor quantification. A sensible choice would be a species that is clearly detectable in both vapor and heavy product analysis, that is representative of the pyrolysis products of the specific biomass analyzed and that it is not subjected to condensation before the sampling point.

Once that the reference has been chosen, the quantification can proceed as follows:

- Manually integrate the peaks in the chromatogram through the GC software; the software itself provides the value of each area.
- Couple the area provided by the software to the species identified in the mass spectrum and to their molecular weight (MW_i).
- Compute the initial dry mass of the experiment conducted for vapor (m_{dry_vap}) quantification, following the same procedure presented in the previous paragraphs.
- Given the millimoles of the reference species (M_{ref_liq}) determined in the heavy products quantification, compute the millimoles of the same species in the vapors (M_{ref_vap}) via a simple proportion:

$$M_{Ref_vap} = \frac{M_{Ref_liq} * m_{dry_vap}}{m_{dry_liq}} \quad (3.25)$$

- Calculate the millimoles (M_i) of each species using:

$$M_i = M_{Ref_vap} * \frac{A_i}{A_{Ref}} \quad (3.26)$$

- Determine the mass of each product, expressed in milligrams, as the product between the millimoles of the i-species (M_i) and its molecular weight (MW_i):

$$m_i = M_i * MW_i \quad (3.27)$$

- Finally, determine the percentage of mass yield of every product (m_{y_i}) simply as the ratio between the mass of the i-species (m_i) and the total initial mass of the vapor experiment, defined on a dry basis (m_{dry_vap}):

$$m_{y_i} = \frac{m_i}{m_{dry_vap}} * 100 \quad (3.28)$$

The sum of the percentage mass yield represents the total vapor production during the pyrolysis process. It's essential to note that all common species identified in both heavy products and vapors, including the chosen reference for vapor quantification, are quantified only once. Typically, lighter products are quantified with the vapors, while products with higher retention times are quantified with the heavy products.

The final outcome of the quantification process is a table similar to the one previously displayed for heavy products (Tab.3.6). Once again, comparative analyses can be conducted for individual biomass types, including aspects such as the number and range of species produced.

3.3.3. Char quantification

The final component required to conclude the quantification process and achieve mass balance closure is the determination of solid residue. This can be graphically assessed by plotting the TG_{dry} [%] data acquired during the kinetic investigation campaign. As the temperature reaches approximately 650°C to 800°C , biomass pyrolysis is completed, leaving behind char and ashes as the remnants of the initial biomass. The specific value corresponding to the solid residue can be observed in figure 3.10, reported as an example of data collected just before the onset of air combustion.

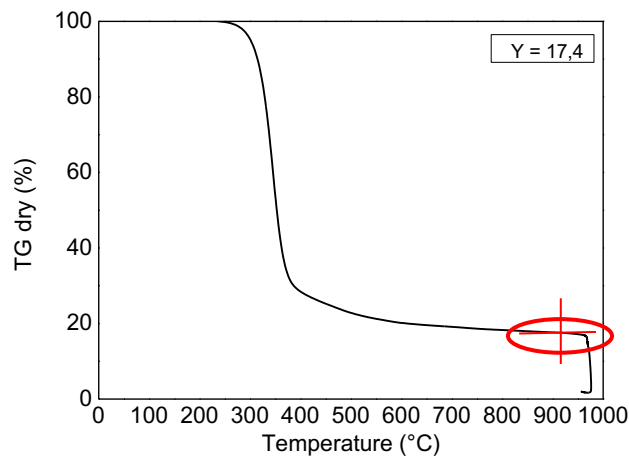


Figure 3.10: Example of the graphical char quantification

3.3.4. Final quantification

The objective of the speciation campaign is to investigate the species generated during the pyrolysis of various biomass sources and to quantitatively assess the resulting products in terms of mass yields. To achieve this goal, all results pertaining to gases, vapors, heavy products, and solid residue need to be consolidated into a final, comprehensive balance.

This final balance is categorized as follows:

- Gas: this category includes methane, carbon monoxide and carbon dioxide.
- Bio-oil: this set of products is composed by the methanol and water quantified with the gas, and all products quantified both with heavy species and vapors.
- Solid residue.

Vapors and liquid products are categorized together since, in combination with water, they collectively form bio-oil, a significant product resulting from biomass pyrolysis. However, it's crucial to distinguish water from the organic phase during quantification to obtain a comprehensive understanding of bio-oil's composition.

3.4. Pyrolysis of mixtures

Another pivotal aspect of this thesis involves analyzing the behavior of biomass mixtures under pyrolytic conditions. Specifically, it is of crucial importance to understand whether individual components exhibit additive behavior when combined in the same sample or if mixing effects are present.

To address this, data from experiments featuring pure compounds were combined to deduce an expected behavior for the mixture by assuming additive properties. The desired quantities were thus calculated as weighted averages, according to equation 3.29. This theoretical model was then compared to data obtained from experiments involving actual mixtures for a comprehensive analysis.

This approach has been applied to all types of results obtained for single components such as TG and DTG curves and pyrolysis products mass yields.

$$A_{mix} = A_1 * w_1 + A_2 * w_2 \quad (3.29)$$

Where A_{mix} is the value of the calculated property for the theoretical mixture, A_1 and A_2 are the experimental values of the properties of the individual components 1 and 2, and w_1 and w_2 are the weight fraction of components 1 and 2 present in the actual mixture.

3.5. Optimization of GC analysis

The gas chromatograph produces a graphical representation of the analysis results, where each species is depicted on a chart. The x-axis corresponds to the retention time, and the y-axis represents the intensity of each peak. The height of each peak is directly proportional to the concentration of the species in the solution, and it is ideal to have well-separated, distinct peaks to achieve a clear chromatogram.

However, if the GC's operational parameters are not set correctly, particularly when the temperature ramp used to separate the stationary and mobile phases is too steep, it can lead to species with similar retention times not being adequately separated. As a consequence, their corresponding peaks may appear partially overlapped. This issue impacts both the MS and FID detectors, making it challenging to define and quantify different species accurately.

To address this, preliminary experiments were conducted to optimize the operating conditions. This tuning phase employs a trial-and-error approach. Initially, products resulting from the pyrolysis of each biomass are analyzed with the fastest temperature ramp. If the results are not satisfactory, the ramp is adjusted to slower rates. Three different ramp settings have been employed (10°C/min, 5°C/min, and 1°C/min) to determine the optimal working conditions, and the results are detailed in table 3.7.

Table 3.7: Temperature ramp used in the GC analysis of different biomass samples

		Glucomannan	
Detector	Vapor	Liquid	
<i>GC-MS</i>	10°C/min	10°C/min	
<i>GC-FID</i>	1°C/min	10°C/min	

		Xylan	
Detector	Vapor	Liquid	
<i>GC-MS</i>	10°C/min	10°C/min	
<i>GC-FID</i>	10°C/min	10°C/min	

		Xylan & Glucomannan	
Detector	Vapor	Liquid	
<i>GC-MS</i>	10°C/min	10°C/min	
<i>GC-FID</i>	10°C/min	10°C/min	

		Xylan & Cellulose	
Detector	Vapor	Liquid	
<i>GC-MS</i>	10°C/min	10°C/min	
<i>GC-FID</i>	10°C/min	10°C/min	

It is evident that the majority of the analyses can be effectively executed using the fastest temperature ramp. Adhering to this constraint is essential since unnecessarily slowing down the temperature ramp can result in a reduced number of detectable species by the instrument and less pronounced, less intense peaks in the chromatogram.

For illustrative purposes, figures 3.11, 3.12, 3.13, and 3.14 depict examples of the outcomes of the optimization process for the analysis of glucomannan. These figures serve to highlight the distinctions between favorable and unsuitable operating conditions.

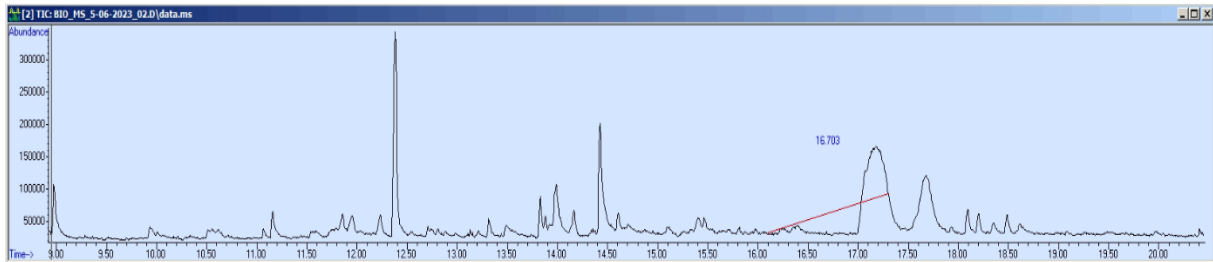


Figure 3.11: GC-MS at 10°C/min for glucomannan: ideal situation

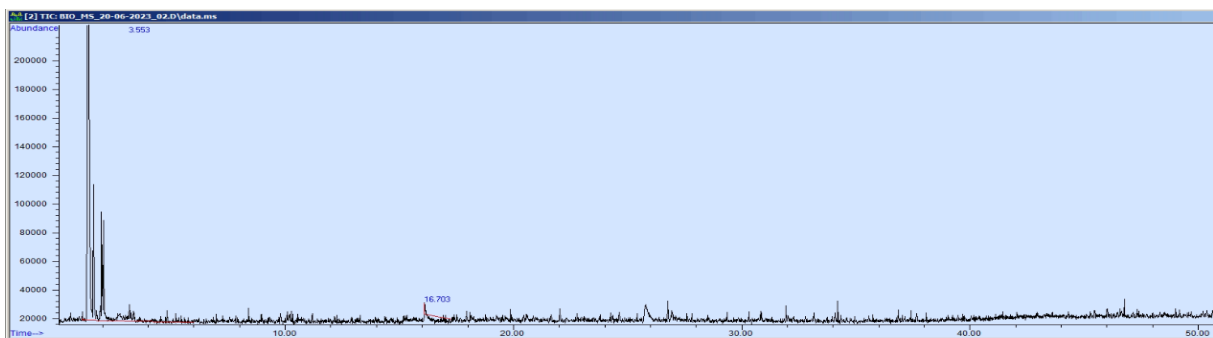


Figure 3.12: GC-MS at 5°C/min for glucomannan: peaks are too low and less species are detected.

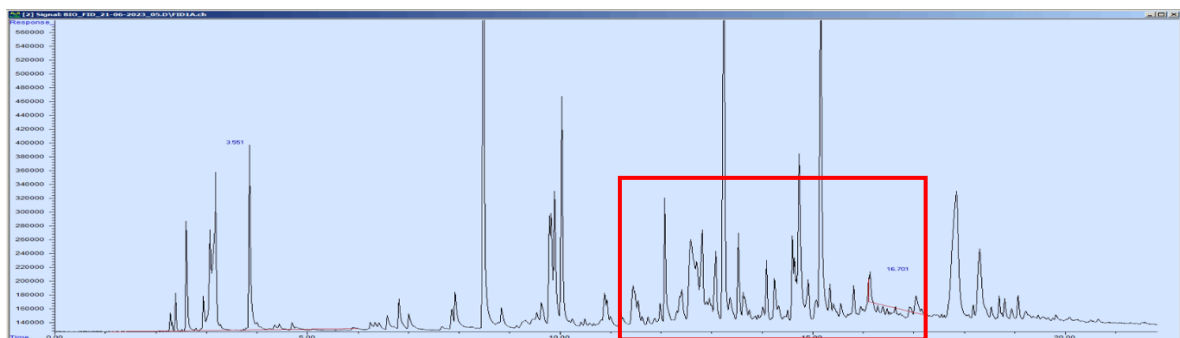


Figure 3.13: GC-FID at 10°C/min for glucomannan: peaks in the selected area are not well separated.

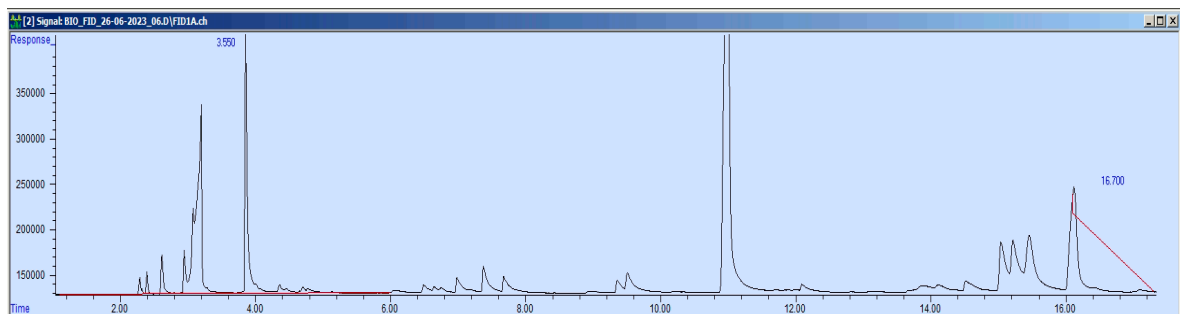


Figure 3.14: GC-FID at 1°C/min for glucomannan: ideal situation

3.6. Choice of Orbo™ trap for heavy oxygenates analysis

Throughout the experiments three types of traps have been tested and one has been selected as the appropriate one.

The first model of sorbent used was Orbo™ 32 – Large charcoal tubes, characterized by an active charcoal adsorbent. The problem in this case was that the pyrolysis products interacted too strongly with the sorbent and the use of mild organic solvents, such as acetone, was not able to desorb them. Even worse, the internal standard specifically put in the solvent to perform the quantification of the products, was itself adsorbed by active charcoal and was not seen in any of the analysis performed (Fig.3.15).

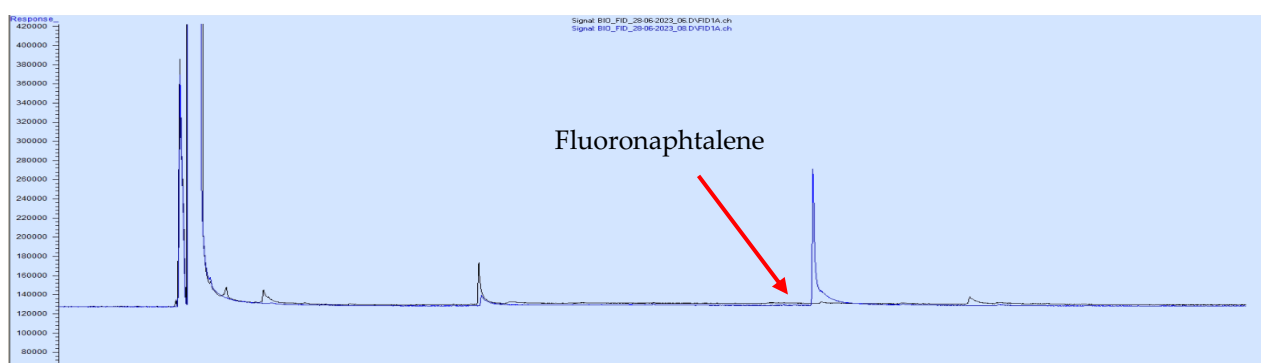


Figure 3.15: GC-FID Chromatogram using Orbo™ 32 – Large charcoal tubes

In blue: chromatogram of the “mother solution” (250 ml of acetone with 10 µl of fluoronaphtalene as internal standard indicated by the red arrow), in black: chromatogram of bio-oil collected using Orbo™ 32 – Large charcoal tubes showing no products and no internal standard.

The second model of sorbent was Orbo™ 23 – 2-HMP on Amberlite® XAD®-2 (20/40) with sorbent capacities of 120/60 mg . The problem in this case was that the adsorbent material was reactive with pyrolysis products. This model in fact, contains Hydroxymethyl piperidine, which is a N-containing molecule able to react with organic products. The resulting chromatogram, visible in figure 3.16, is a sequence of N-containing products that cannot be matched with the original precursor.

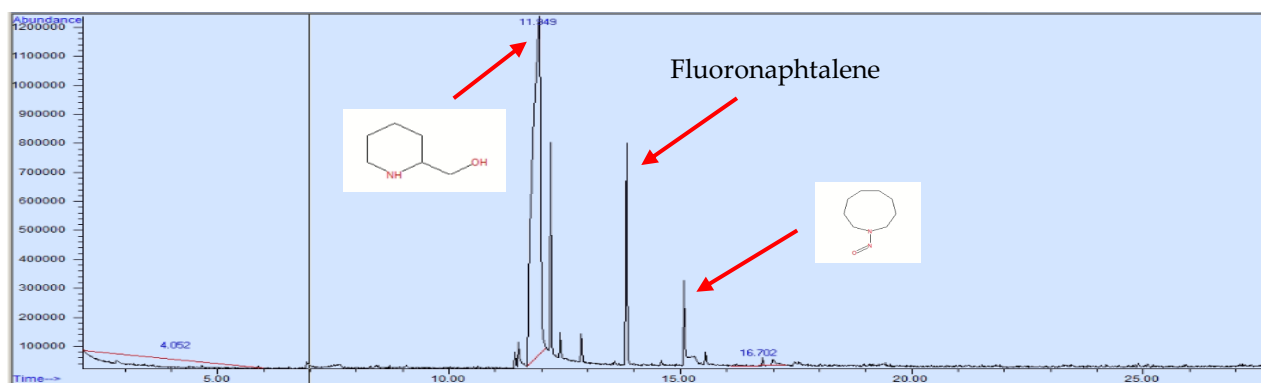


Figure 3.16: GC-FID Chromatogram using Orbo™ 23 – 2-HMP on Amberlite® XAD®-2 (20/40) tubes

Chromatogram of bio-oil collected using Orbo™ 23 – 2-HMP on Amberlite® XAD®-2 (20/40) tubes showing N-containing products.

The third model used was the Orbo™ 609 sorbent, specifically Amberlite® XAD®-2 (20/50) with sorbent capacities of 400/200 mg. This sorbent bed has demonstrated exceptional efficiency in trapping condensable products from pyrolysis vapors, making it the optimal choice for offline analysis. Furthermore, the organic compounds are readily released upon washing the trap with acetone. In figure 3.17 a chromatogram for bio-oil collected by Orbo™ 609 sorbent is shown, showing pyrolysis products of glucomannan.

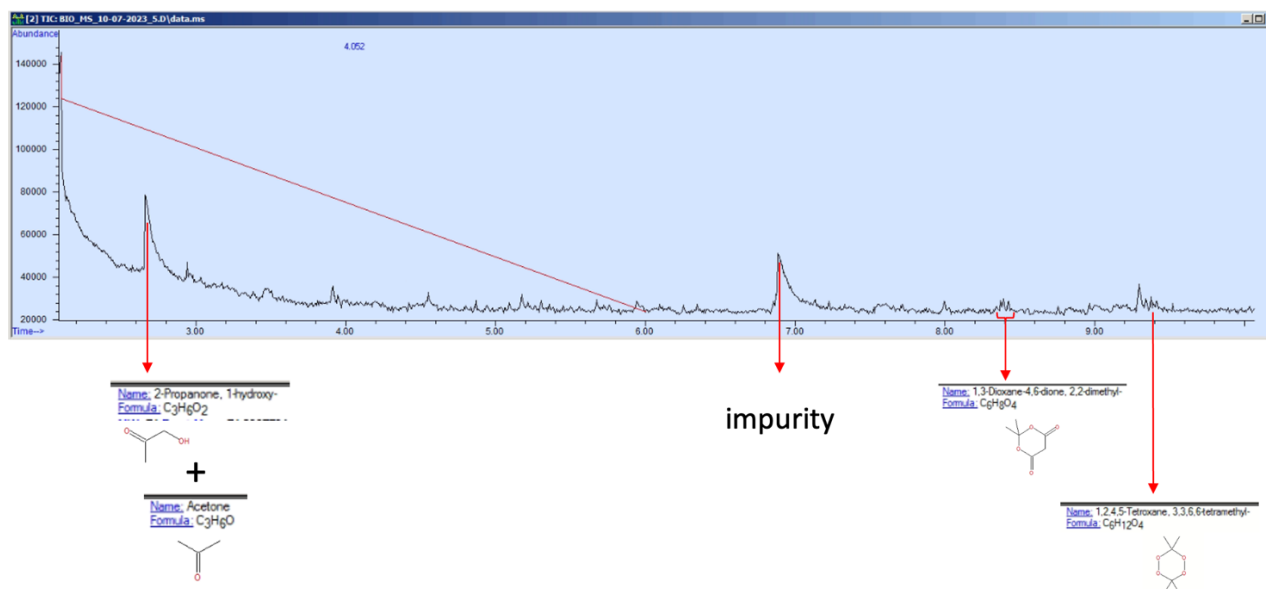


Figure 3.17: GC-FID Chromatogram using Orbo™ 609 Amberlite® XAD®-2 (20/50) tubes

3.7. NTNU campaign

Some of the work done in this thesis relies on data coming from an experimental campaign carried out during a PhD doctoral program at NTNU (Norwegian University of Science and Technology) in Trondheim. Experimental data were then processed and analyzed in this thesis work.

3.7.1. NTNU setup

In this study, a laboratory-scale vertical reactor with a fixed bed configuration is employed. The reactor is constructed using a tubular stainless-steel design, featuring a 22 mm inner diameter. External heating is achieved using an electric oven, and precise temperature control is maintained through direct contact with the reactor's outer surface by a K-thermocouple. To enhance heat transfer, the reactor is enclosed within a copper housing.

The setup includes a separate cold zone located above the furnace, where biomass is stored and injected into the reactor under an inert atmosphere at the appropriate time. The biomass is contained within a stainless-steel wire (inner diameter: 15 mm) situated between two layers of quartz wool. For analysis, the products are collected at the reactor outlet, utilizing a glass condenser and a gas bag. Due to the limitations of this reactor type in providing real-time analysis, the following instruments are integrated into the setup: Agilent gas chromatograph, equipped with Molesieve 5A and Porapak Q columns, which includes two detectors (TCD and FID) for analyzing the gaseous mixture stored in the gas bag; GC-MS instrument (Agilent 7820A, 5977E MSD) for species identification and GC-FID (Agilent 7820A) for species quantification of the condensed phase; a volumetric titrator provided by Mettler Toledo (V20S) for the assessment of the water content of the bio-oil through Karl-Fischer titration.

3.7.2. NTNU procedure

During the experimental campaign, samples comprising 0.5 grams of cellulose, xylan, or glucomannan powders were used. The fixed bed reactor previously described, was heated to the desired temperature of either 500°C or 550°C. Following this, the furnace underwent a one-hour stabilization period. Once this phase was completed, the biomass sample stored in the wire within the cold zone was introduced into the reactor and placed in the central area of the furnace.

During both the pre-heating and pyrolysis phases, a continuous flow of nitrogen (N₂) at a rate of 166 NmL/min was maintained and carefully controlled via a Bronkhorst mass flow controller.

The actual pyrolysis reaction in each experiment typically lasted 8.5 minutes, which proved sufficient to convert the entire biomass within the reactor.

Volatile substances generated during the pyrolysis phase were directed into a glass condenser, efficiently cooled to -17°C with a water and ethylene glycol mixture.

In the condenser, condensable species were collected, while gaseous products were stored in a gas bag. After each experiment, both the gas bag and the condenser were disconnected.

Additionally, to prevent the combustion of char, a continuous flow of nitrogen (N₂) at a rate of 10 NmL/min was maintained within the reactor during the cooling phase.

The composition of the gaseous mixture stored in the gas bag was analyzed using an Agilent gas chromatograph, equipped with Molesieve 5A and Porapak Q columns, and featuring two detectors (TCD, FID). The integral mass yield of each gas product, such as CO, CO₂, CH₄, and light hydrocarbons, was determined using nitrogen as an internal standard.

The condenser was cleaned using tetrahydrofuran (THF) to extract the bio-oil collected during the experiment. A known quantity of dichloromethane (DCM) was added as an internal standard for subsequent GC analyses. The composition of the mixture was then analyzed using a GC-MS instrument (Agilent 7820A, 5977E MSD) for species identification and a GC-FID (Agilent 7820A) for species quantification.

The water content of the bio-oil was assessed through Karl-Fischer titration, utilizing a volumetric titrator provided by Mettler Toledo (V20S).

By combining these composition analyses with a weighing protocol involving measurements taken before and after each experiment, it was possible to determine the integral mass yield of the bio-oil and each individual condensable product. Furthermore, the amount of solid residue was quantified by accurately measuring the weight of the wire mesh before and after the experiment.

The subsequent chapter will present and discuss the results derived from the detailed investigation explained, leading to a thorough discussion and to the formulation of conclusions.

4 Investigation on hemicellulose pyrolysis

As already mentioned, the aim of this thesis is to gain deeper insights on biomass pyrolysis, a crucial process in the pursuit of sustainable energy and biofuel production. In particular, our focus has been directed towards hemicelluloses, a group of biomass constituents that, despite their significance, have remained relatively unexplored in the existing literature. Hemicelluloses are omnipresent companions of cellulose and lignin in biomass, and understanding their behavior is essential for comprehensive insights into biomass pyrolysis.

Our research journey consists of two main points: the investigation of devolatilization behavior and the meticulous speciation of the products derived from this complex process. Devolatilization, the initial and decisive step in biomass pyrolysis, is the process by which volatile compounds are released from the biomass matrix. As a result of this thermal decomposition a diverse array of compounds is produced. By digging into a detailed examination of devolatilization trends and speciation of products, it is possible to optimize pyrolysis processes and maximize the potential utilization of biomass resources.

In terms of methodology, as detailed in the preceding chapter, our research employed a Thermogravimetric Analyzer (TG) for the examination of biomass devolatilization and an online Mass Spectrometer (MS) in conjunction with offline Gas Chromatography (GC) to conduct an in-depth analysis of the speciation of pyrolysis products. Moreover, data coming from a series of experiments performed in a fixed bed reactor configuration were processed and included in this thesis.

In this chapter, we present the outcome of our experimental investigations, offering a comprehensive view of our findings in relation to hemicellulose pyrolysis. The results will encompass a range of key data. We will illustrate Thermogravimetric (TG) and Derivative Thermogravimetric (DTG) curves for various biomasses, which will offer insights into critical aspects of the pyrolysis process, including the initiation temperature, the number of steps in the process, and the amount of residual solid material left behind. In addition, we will offer an overview of primary pyrolysis product categories, such as gases, bio-oil, and char. Furthermore, we will delve deeper into the bio-oil fraction, providing specific insights that reveal both distinctions and commonalities among the analyzed samples.

4.1. Effect of carrier flowrate and sample mass on TG curves

One of the primary objectives of this thesis is to shed light on the devolatilization process of biomass. Such insights represent a valuable tool in developing a robust kinetic mechanism capable of comprehensively describing the intricate array of reactions occurring during this critical phase of pyrolysis. As previously mentioned, the devolatilization experiments are conducted within a thermogravimetric analyzer (TGA), an instrument well-suited for kinetic investigations, as evidenced in the existing literature. Nevertheless, to ensure the reliability of our data, tests have been conducted to rule out the impact of certain operational parameters and ensure the dependency of TG curves only on the heating rate, enhancing the value of these results for the development of kinetic models.

Two are the parameters on which the analysis has been conducted: the mass of the loaded sample and the flowrate of the carrier gas. These parameters are critical in optimizing the experimental conditions for accurate and meaningful results.

4.1.1. Carrier flow rate influence

Examining the influence of carrier gas flow rate is a crucial step, as throughout our work various flow rates were employed for specific experimental reasons.

In figure 4.1, the thermogravimetric curves for glucomannan, xylan and arabinoxylan samples tested at different carrier gas (helium) flow rates are shown. The x-axis represents temperature, while the y-axis displays the percentage of remaining mass (calculated on a dry basis as explained in paragraph 3.2.3). All samples were subjected to a rapid heating rate of 100°C/min.

Examining the graphs, it becomes evident that the mass loss curves of xylan and glucomannan are nearly identical, indicating that the influence of helium flow rate on the conducted pyrolysis experiments can be effectively disregarded. As further evidence of this, the percentage error of solid residue for the various samples has been calculated through equation 4.1 and the results included in table 4.1. All the solid residue values have been collected at 700°C. Once again, the exceptionally low difference presented for glucomannan and xylan in the table affirm that there are no discernible differences between the experiments, effectively eliminating any concerns related to the impact of the carrier gas flow rate on TG curves.

In the case of arabinoxylan however, a distinct pattern emerges. In the initial part of the curves, from 200°C to 400°C, when the initial phase of pyrolysis takes place, no discernible distinctions emerge. However, at higher temperatures, disparities on solid residue become evident among the experiments, with percentage difference from the mean value ranging from 9% to 41%, as visible in table 4.1. According to the available

data, it is not possible to define a specific trend of the solid residue, since it is impossible to find a direct correlation between the carrier flow rate and the residue. As a matter of fact, the intermediate value of the carrier flow rate corresponds to the lowest solid residue. These anomalies suggest that both the carrier flowrate and the variability in the arabinoxylan behavior have an influence over the solid residue.

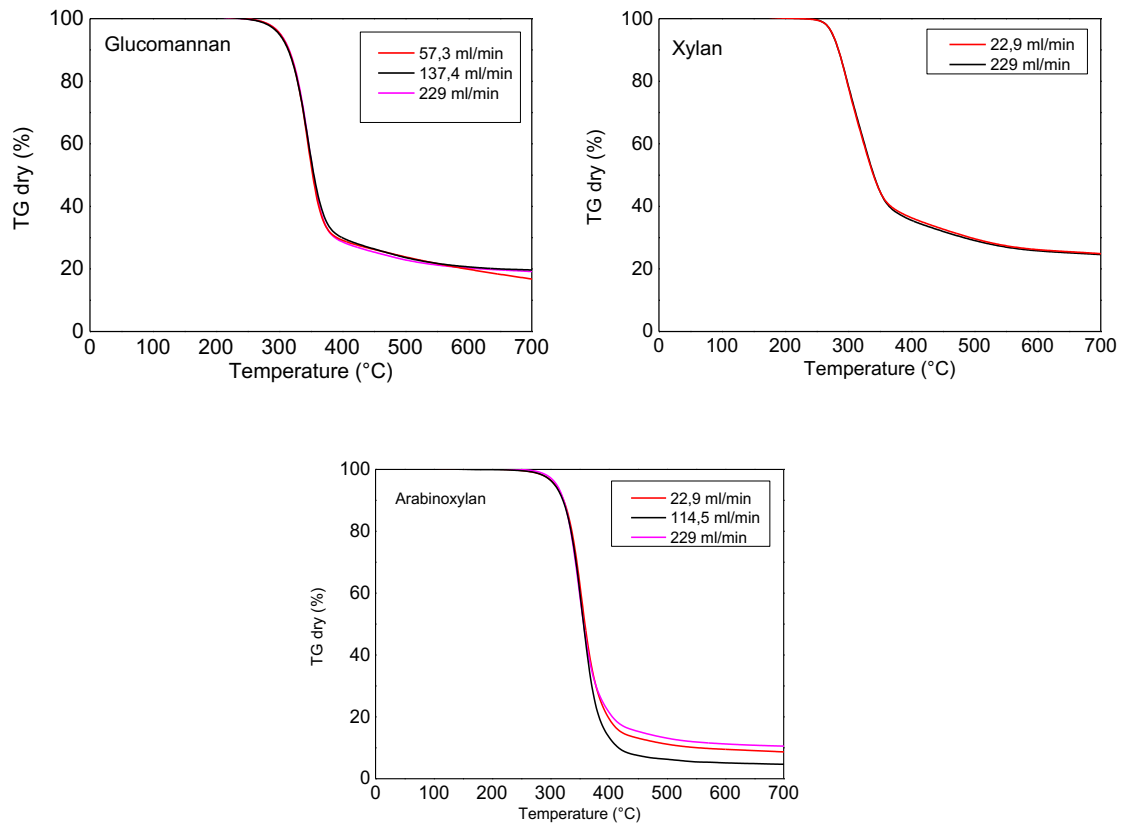


Figure 4.1: TG curves for glucomannan, xylan and arabinoxylan, under a heating rate of 100°C/min and with different carrier gas flowrate

Table 4.1: Solid residue for samples subjected to different carrier flowrates

	Solid residue glucomannan [%]				Solid residue xylan [%]		
	57.3 ml/min	137.4 ml/min	229 ml/min	Average	22.9 ml/min	229 ml/min	Average
	17.3	19.6	19.2	18.7	23.5	23.5	23.5
% error	7.5	4.8	2.7		0	0	

	Solid residue arabinoxylan [%]			
	22.9 ml/min	114.5 ml/min	229 ml/min	Average
	8.8	4.7	10.7	8.1
% error	9.1	41.7	32.6	

$$\% \text{ error} = \left| \frac{\text{solid residue} - \text{average}}{\text{mean value}} * 100 \right| \quad (4.1)$$

4.1.2. Mass influence

While the maximum load capacity in the TG sample pan is relatively restricted, we also conducted experiments using varying sample masses to evaluate whether this parameter influences devolatilization curves.

In Figure 4.2, the mass loss curves for glucomannan, xylan and arabinoxylan samples of differing mass are depicted. Once again, a heating rate of 100°C/min was maintained.

Also in this case the devolatilization process of xylan and glucomannan displayed no discernible influence, as evidenced by the overlapping curves for the different experiments.

However, arabinoxylan showed once again a different behavior, in all similar to the one described before. In fact, one parameter that appears to be affected by the mass loaded in the pan is the solid residue. In particular, higher biomass loads result in higher solid residue values. Table 4.2 provides a summary of the percentage error for solid residue for the various samples, revealing noticeable differences for arabinoxylan.

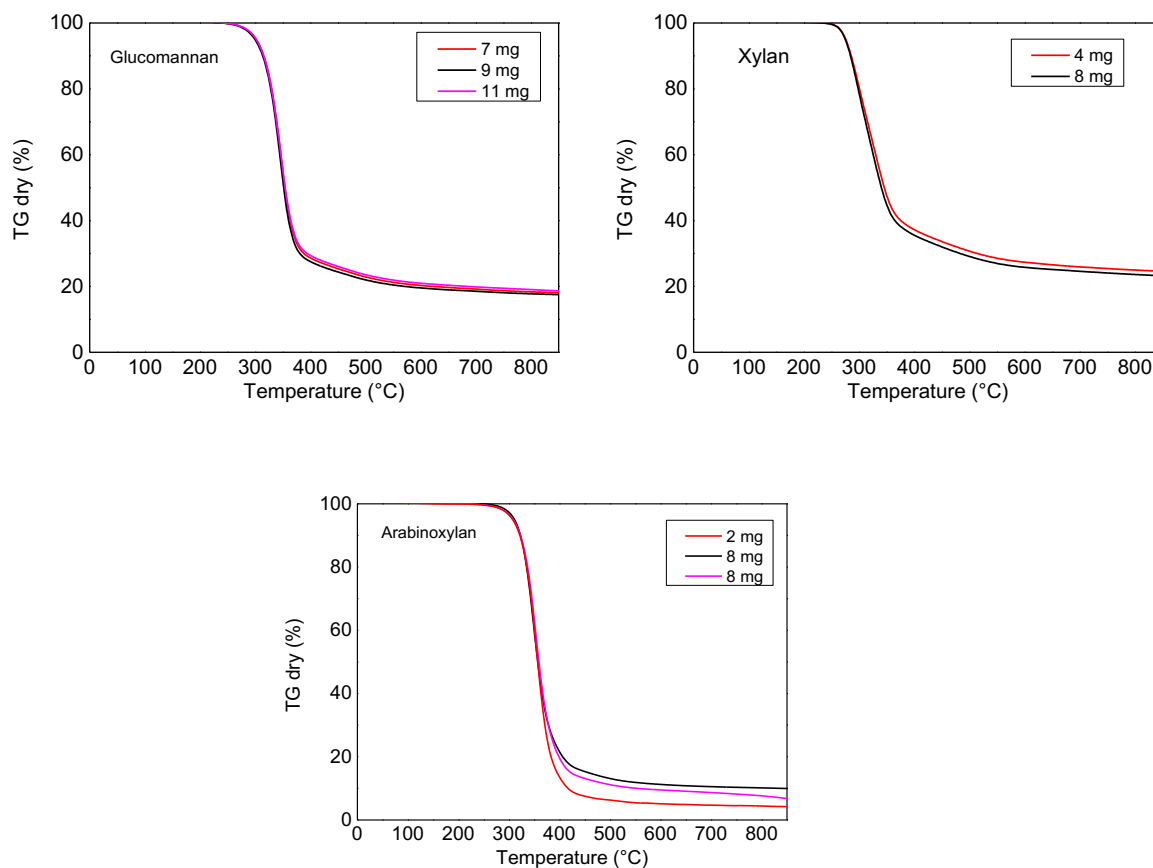


Figure 4.2: TG curves for glucomannan, xylan and arabinoxylan under a heating rate of 100°C/min, 229ml/min of helium flowrate and with different mass values

Table 4.2: Solid residue for samples of different mass

	Solid residue glucomannan [%]				Solid residue xylan [%]			Solid residue arabinoxylan [%]			
	7 mg	9 mg	11 mg	Average	4 mg	8 mg	Average	2 mg	8 mg	8 mg	Average
	18.1	17.7	18.8	18.2	25.1	23.6	24.35	4.2	10	9.6	7.93
% error	0.5	2.7	3.3		3.1	3.1		47.1	26.1	21.0	

4.2. Devolatilization trends

In this section, we will present our findings related to the devolatilization of hemicellulose.

Our research aims to investigate the thermal behavior of the chosen biomass samples during devolatilization. To achieve this, we employed a Thermogravimetric Analyzer and followed the experimental procedures described section 3.2. We utilized two primary outputs to analyze the behavior of different biomass samples: the weight loss curve (TG curve) and the derivative weight loss curve (DTG curve).

In Figure 4.3 TG and DTG curves for various hemicelluloses analyzed as pure components, including xylan, glucomannan, and arabinoxylan, are presented. Additionally, curves for cellulose are included for reference, as it has been previously studied within our research group.

On the x-axis, the temperature is plotted, while the y-axis displays the remaining percentage of the sample's mass (calculated on a dry basis) for the TG curves, and the rate of mass loss (normalized to the sample's initial mass) for the DTG curves.

The profiles of devolatilization during heating in an inert atmosphere reveal distinct characteristics among the polysaccharides. Overall, as evident from the TG curves, mass loss occurs within a similar temperature range for all hemicelluloses, typically falling between approximately 200–400°C. However, as indicated by the DTG curves, this process involves varying steps and peak temperatures for each hemicellulose.

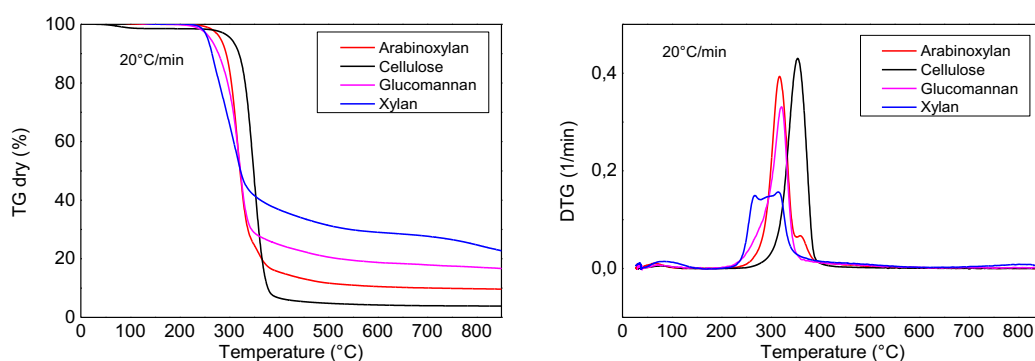


Figure 4.3: TG (left) and DTG (right) curves for the different hemicellulose samples analyzed with a heating rate of 20°C/min

The weight loss curves on the left side of figure 4.3 reveal that the pyrolysis of hemicelluloses commences at lower temperatures than that of cellulose. In this sequence, we observe xylan, glucomannan, and arabinoxylan. Additionally, hemicellulose pyrolysis yields a higher quantity of solid residue compared to cellulose.

Interestingly, this leads to a reverse order of solid residue production, with arabinoxylan having the least, followed by glucomannan and xylan.

Another crucial observation pertains to the multi-step nature of hemicellulose devolatilization. This is evident in the TG curves, where changes in slope indicate distinct decomposition stages. The DTG curves offer an even clearer depiction, with each peak representing a specific event in the devolatilization process. Notably, cellulose exhibits a single, well-defined, and high peak at 353°C, indicating that its devolatilization occurs in one stage within a narrow temperature range. A similar behavior is seen in glucomannan, which features a unique peak at a lower temperature than cellulose (at 320°C), however with a secondary contribution at 270°C, as evident from the change in the slope. In contrast, arabinoxylan and xylan display more intricate profiles. Arabinoxylan exhibits an initial peak similar to that of glucomannan, but also presents a smaller peak at 360°C. Xylan, on the other hand, shows two peaks of comparable height, one at 265°C and another at 315°C.

The disparities in decomposition profiles between hemicelluloses and cellulose can largely be attributed to the inherently irregular structure of the former. Cellulose features a relatively uniform composition, with linear chains that pack into a semi-crystalline structure. While this arrangement requires a higher devolatilization temperature, it also results in a distinct and narrow decomposition peak. On the other hand, hemicelluloses exhibit an amorphous structure characterized by branched chains comprising a variety of monomers and lateral substituents. This structural diversity facilitates the onset of devolatilization reactions but simultaneously complicates the decomposition pathway, due to the multitude of bonds that must be broken.

It is worth noting that literature on hemicellulose pyrolysis often takes xylan as a representative species of this biomass compound class. However, hemicellulose is a diverse group encompassing numerous compounds. Consequently, solely relying on xylan as a representative is limiting. Figure 4.3 clearly demonstrates that each hemicellulose exhibits a distinct behavior under pyrolytic conditions that cannot be simply generalized to xylan behavior. Therefore, a comprehensive exploration of the thermal behavior of different hemicelluloses is essential. The inherent variety and complexity of the hemicellulose pyrolysis process undoubtedly underscore the need for further research to gain a comprehensive understanding of it.

4.2.1. Investigation on heating rate

In the field of hemicellulose pyrolysis, understanding the influence of heating rate has emerged as a pivotal aspect of research. The rate at which biomass is heated during pyrolysis can significantly impact the reaction kinetics, product distribution, and ultimately the efficiency of energy conversion processes. Thus, investigating the effect of heating rate on hemicellulose pyrolysis is not only scientifically intriguing but also

holds substantial practical implications. To study this aspect, we performed pyrolysis experiments in the TGA varying the heating rate.

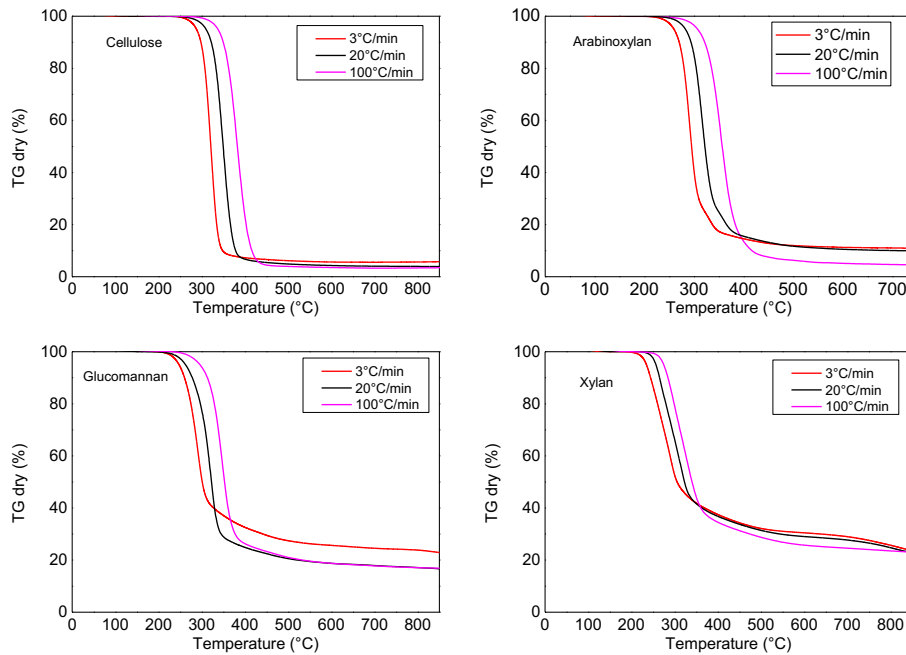


Figure 4.4: Mass loss curves for cellulose, arabinoxylan, glucomannan and xylan at varying heating rate

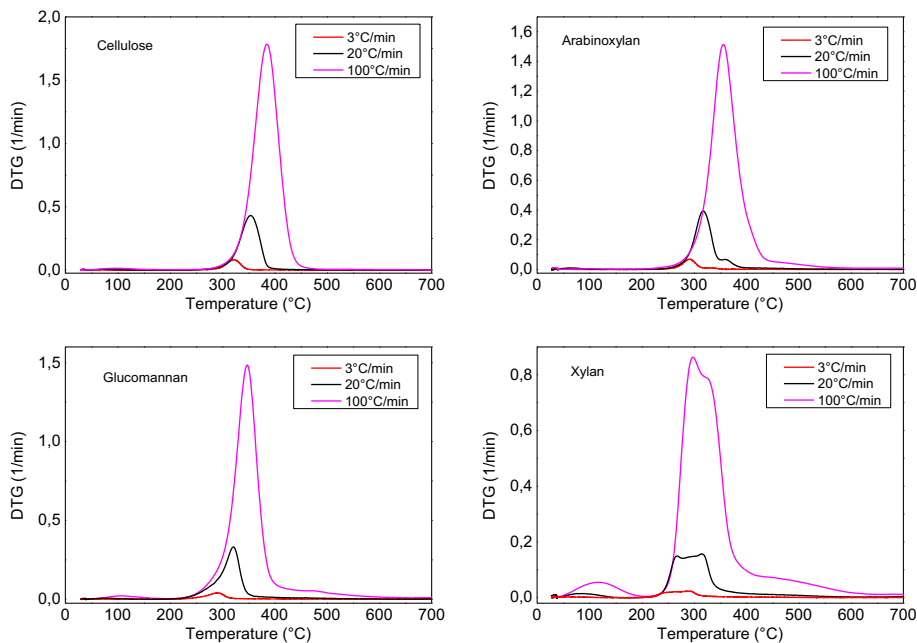


Figure 4.5: DTG curves for cellulose, arabinoxylan, glucomannan and xylan at varying heating rate

In figure 4.4, the mass loss curves collected at varying heating rates for xylan, glucomannan, arabinoxylan, and cellulose are illustrated. Again, the x-axis depicts temperature, while the y-axis shows the remaining mass percentage. In this case, we conducted the experiments using three different heating rates ($3^{\circ}\text{C}/\text{min}$, $20^{\circ}\text{C}/\text{min}$, $100^{\circ}\text{C}/\text{min}$) to explore the influence of this parameter on the devolatilization process.

The results reveal a consistent trend across all hemicelluloses and cellulose samples. Specifically, we observed that as the heating rate increased, the onset temperature for the devolatilization process shifted towards higher values. Consequently, the mass loss event representing biomass devolatilization moved to the right in the graph. Furthermore, a higher heating rate corresponded to a reduced solid residue, as evidenced in the latter part of the curves. The remaining mass percentage at the end of the curves, representing the solid residue of the process, was lower for experiments conducted at higher heating rates.

This trend is largely attributed to the dynamic nature of the experiment in the TG, whose duration varies significantly with the heating rate. This can be clearly seen in figure 4.6, where TG curves for xylan are plotted as a function of time, rather than temperature.

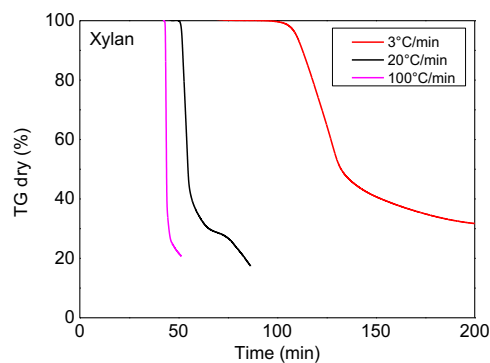


Figure 4.6: TG curves for xylan plotted as a function of time

Employing lower heating rates thus offers the advantage of a more rapid initiation of the pyrolysis process, but it simultaneously results in higher solid residue values. Furthermore, lower heating rates provide an additional benefit in terms of analytical insights. They enable a more distinct differentiation of the stages within the devolatilization process of a specific biomass, enhancing the clarity of the process's observation.

This clarity becomes evident when examining figure 4.5, where peaks in the DTG (Derivative Thermogravimetry) curves become more pronounced in experiments employing lower heating rates, thus enabling an easier identification of the different pyrolysis steps.

4.3. Speciation of pyrolysis products

Another crucial aspect in comprehending and characterizing the pyrolysis process of hemicellulose is to achieve a thorough product speciation. Pyrolysis products can be categorized into three primary fractions: bio-oil, gases, and char. Gaining insights into the yields and distribution of pyrolysis products within these categories is pivotal for process understanding and optimization.

This section will present the results of the speciation campaign. Given the intricate and diverse distribution of products, a comprehensive array of experimental setups and procedures, as elaborated in sections 3.3, has been employed to achieve a complete speciation. The results will thus encompass a combination of outputs derived from various analysis, such as online mass spectrometry and offline gas chromatography.

Initially, we will provide a broad overview of pyrolysis products coming from a single biomass, categorizing them into the broader possible groups: char, bio-oil (further subdivided into the organic phase and water), and gases. These results will be expressed in terms of integral mass yields, facilitating rapid data visualization and enabling comparisons with other samples.

Subsequently, our focus will turn to bio-oil, as it constitutes the most significant category of products, with potential applications in sustainable energy and chemistry. In this context, we will differentiate products based on the number of carbon atoms or class of organic compounds. This approach will yield deeper insights into product distribution and the devolatilization mechanisms of specific biomass sources.

This speciation protocol has been applied in this context to glucomannan and xylan.

4.3.1. Glucomannan

In figure 4.7, the pyrolysis products of glucomannan are depicted. The solid residue remaining in the sample pan of the thermogravimetric analyzer accounts for a mass yield of 19%. The bio-oil component comprises 62% of the total products, with 45.9% attributed to organic species and an additional 16.1% composed of water. Pyrolysis gases constitute 12.6% of the overall products.

It is noteworthy that despite the complexity of the system an impressive value for the total mass balance has been achieved, registering at 93.7% instead of the expected 100%. This small discrepancy could be attributed to various technical challenges encountered during the speciation experiments, such as condensation of products before the sampling point, potential leakages in the lines and analytical issues.

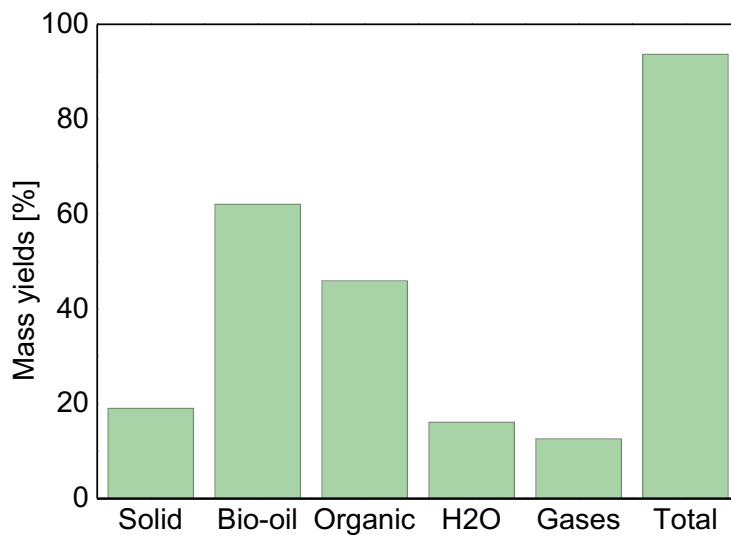


Figure 4.7: Glucomannan main pyrolysis products

The primary category of pyrolysis products is bio-oil. This encompasses an organic phase, rich in both light and heavy oxygenates generated during the pyrolysis process, along with water. Figure 4.8 illustrates the speciation of glucomannan bio-oil, wherein species identified in both vapor and liquid analyses are categorized based on their functional groups. Notably, the mass yield of water is 16.1%, while other noteworthy constituents include anhydrosugars (17.7%), cyclo oxygenates (8.9%), and furan derivatives (14.6%).

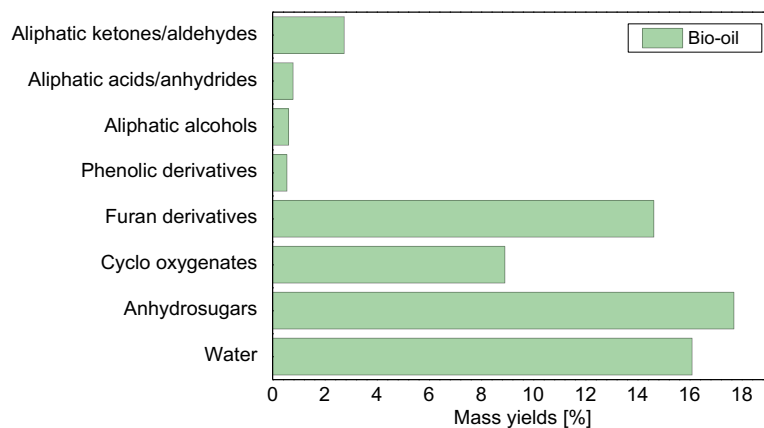


Figure 4.8: Glucomannan bio-oil speciation

Additionally, the organic products derived from both pyrolysis vapors and liquids can be further classified based on the number of carbon atoms present in each species. Figure 4.9 presents the classification of glucomannan organic phase according to this criterion. As it is evident, the pyrolysis of this specific biomass predominantly produces C6 (26.8%) and C5 (10.2%) products. The release of these monomeric units is reflected by the presence in the organic phase of species such as levoglucosan and furans, as detailed in table 4.3.

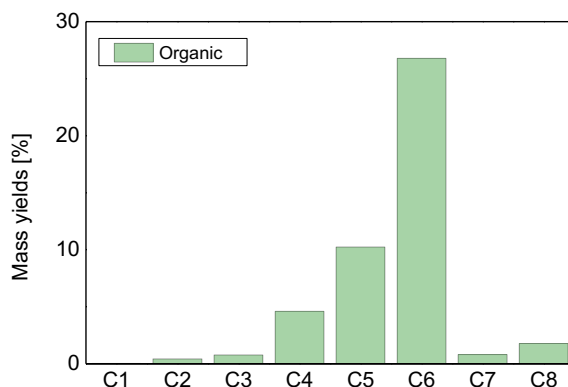


Figure 4.9: Glucomannan organic phase speciation

Finally, a focus can be placed on the gases produced by glucomannan pyrolysis, which are shown in figure 4.10. CO and CO₂ constitute the majority of the products, with a mass yield of 4.62 % and 7.7 % respectively. Traces on methane and methanol were also observed.

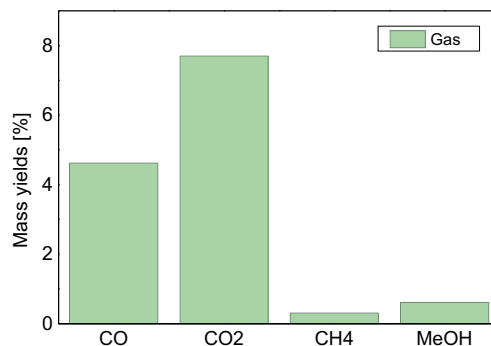


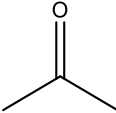

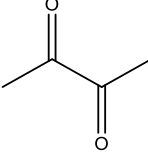
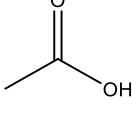
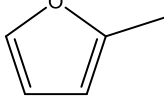
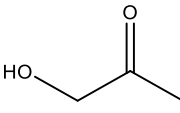
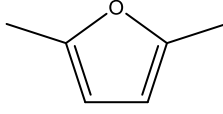
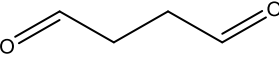
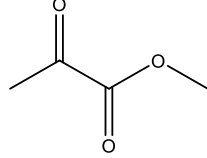
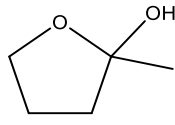
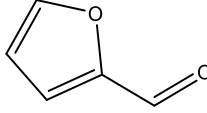
Figure 4.10: Glucomannan gas speciation

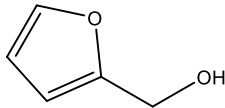
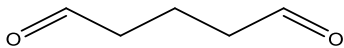
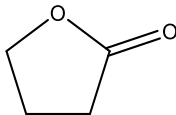
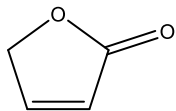
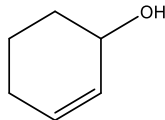
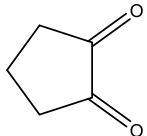
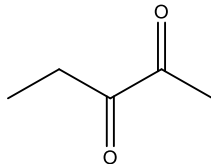
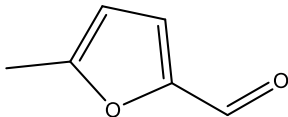
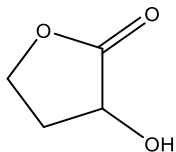
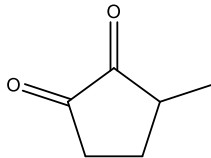
It is crucial to underscore that the achievement of a comprehensive balance has been realized through meticulous characterization of pyrolysis products at the level of individual species. Especially for the organic fraction of bio-oil such characterization poses significant challenges. As depicted in figures 4.8 and 4.9, the species identified within both pyrolysis vapors and heavy products span a wide spectrum of classes, encompassing diverse functional groups and varying numbers of carbon atoms.

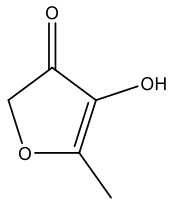
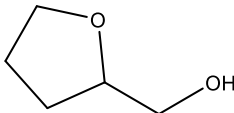
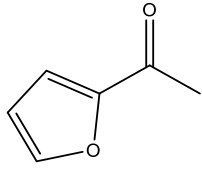
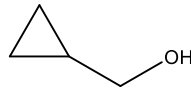
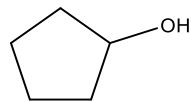
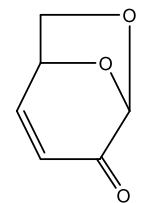
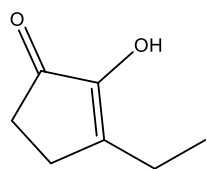
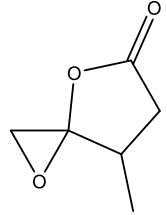
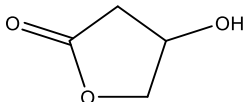
It is important to note that within each family of compounds, numerous distinct species exist. The identification and quantification of these species demanded substantial effort. As exemplified in table 4.3, a detailed list of individual species identified in glucomannan pyrolysis vapors is presented encompassing a total of 40 different species.

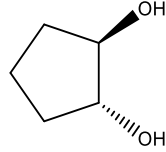
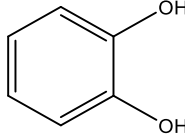
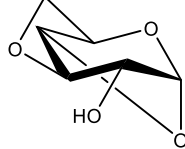
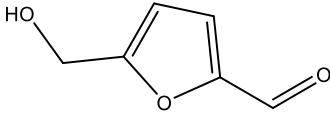
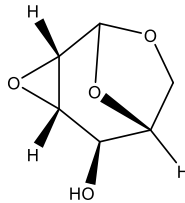
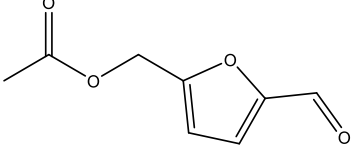
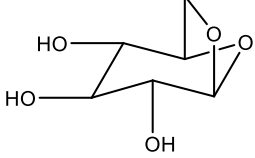
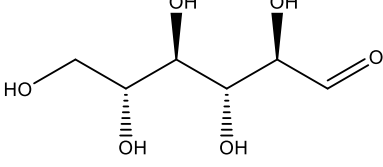
Table 4.3: Glucomannan pyrolysis vapors products

Species in glucomannan vapors		
SPECIES	FORMULA	STRUCTURE
Formaldehyde	CH ₂ O	
Acetaldehyde	C ₂ H ₄ O	

Acetone	C_3H_6O	
Furan	C_4H_4O	
2,3 butanedione	$C_4H_6O_2$	
Acetic acid	$C_2H_4O_2$	
Furan, 2-methyl	C_5H_6O	
2-propanone, 1-hydroxy	$C_3H_6O_2$	
Furan, 2,5-dimethyl	C_6H_8O	
Succindialdehyde	$C_4H_6O_2$	
Propanoic acid, 2-oxo-, methyl ester	$C_4H_6O_3$	
2-Furanol, tetrahydro-2-methyl-	$C_5H_{10}O_2$	
Furfural	$C_5H_4O_2$	

2-furanmethanol	$C_5H_6O_2$	
Glutaraldehyde	$C_5H_8O_2$	
Butyrolactone	$C_4H_6O_2$	
2(5H)-Furanone	$C_4H_4O_2$	
2-Cyclohexen-1-ol	$C_6H_{10}O$	
1,2-Cyclopentanedione	$C_5H_6O_2$	
2,3-Pentanedione	$C_5H_8O_2$	
2-Furancarboxaldehyde, 5-methyl	$C_6H_6O_2$	
2-Hydroxy-gamma-butyrolactone	$C_4H_6O_3$	
1,2-Cyclopentanedione, 3-methyl	$C_6H_8O_2$	

2,5-Dimethyl-4-hydroxy-3(2H)-furanone	$C_6H_8O_3$	
2-Furanmethanol, tetrahydro-	$C_5H_{10}O_2$	
Ethanone, 1-(2-furanyl)-	$C_6H_6O_2$	
Cyclopropyl carbinol	C_4H_8O	
Cyclopentanol	$C_5H_{10}O$	
Levoglucosenone	$C_6H_6O_3$	
2-Cyclopenten-1-one, 3-ethyl-2-hydroxy-	$C_7H_{10}O_2$	
1,4-Dioxaspiro[2,4]heptan-5-one, 7-methyl	$C_6H_8O_3$	
2(3H)-Furanone, dihydro-4-hydroxy-	$C_4H_6O_3$	

1,2-Cyclopentanediol, trans-	$C_5H_{10}O_2$	
Catechol	$C_6H_6O_2$	
1,4:3,6-Dianhydro- α -d-glucopyranose	$C_6H_8O_4$	
5-Hydroxymethylfurfural	$C_6H_6O_3$	
2,3-Anhydro-d-mannosan	$C_6H_8O_4$	
5-acetoxymethyl-2-furaldehyde	$C_8H_8O_4$	
Beta-D-Glucopyranose, 1,6-anhydro	$C_6H_{12}O_6$	
D_allose	$C_6H_{12}O_6$	

To ensure the repeatability of our data, the same experiments were conducted multiple times. Consequently, the reported outcomes represent the mean calculated from several iterations of the experiment. In order to assess the reliability and precision of the data obtained in this study from such measures, a brief analysis of experimental

error was undertaken. In particular, to quantify the variability within the dataset, the standard deviation was computed following equation 4.2. The inclusion of standard deviation calculations serves as a crucial component in elucidating the robustness of our findings, providing insights into the experimental uncertainties associated with our measurements.

$$\sigma = \sqrt{\frac{\sum_{i=1}^N (x_i - \mu)^2}{N}} \quad (4.2)$$

The standard deviation for specific components from glucomannan speciation is presented in figure 4.11 and table 4.4. Remarkably, the calculated standard deviation values are relatively low, underscoring the robustness of our data. This finding attests to the consistency and precision achieved in our experimental procedures.

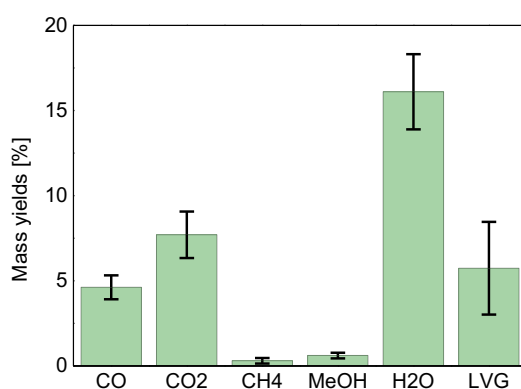


Figure 4.11: Visual representation of standard deviation for glucomannan pyrolysis products

Table 4.4: Standard deviation for glucomannan pyrolysis products

	Glucomannan products mass yield [%]					
	Experiment 1	Experiment 2	Experiment 3	Experiment 4	Media	St dev
CO	3.1	4.1	3.3	4.6	3.8	0.7
CO₂	10.4	7.5	8.9	7.7	8.6	1.4
CH₄	0.6	0.6	0.4	0.3	0.5	0.2
MeOH	-	0.4	-	0.6	0.5	0.2
H₂O	19.5	15.8	20.0	16.1	17.8	2.2
LVG	4.3	4.1	4.7	9.8	5.7	2.7

4.3.2. Xylan

The same protocol applied to glucomannan was applied also to xylan and the same outcomes will be reported in the following.

In figure 4.12, the pyrolysis products of xylan are illustrated, divided in their main categories. The residual solid in the thermogravimetric analyzer sample pan represents 25.2% of the initial mass. Within the total products, bio-oil constitutes 39.1%, of which 12.9% is organic compounds, and an additional 26.2% is water. Pyrolysis gases make up 30.5% of the product mix.

Again, the overall mass balance does not reach the anticipated 100%, stopping instead at 94.7%. This deviation may once again be attributed to various technical challenges encountered during the speciation experiments, as explained in the previous case.

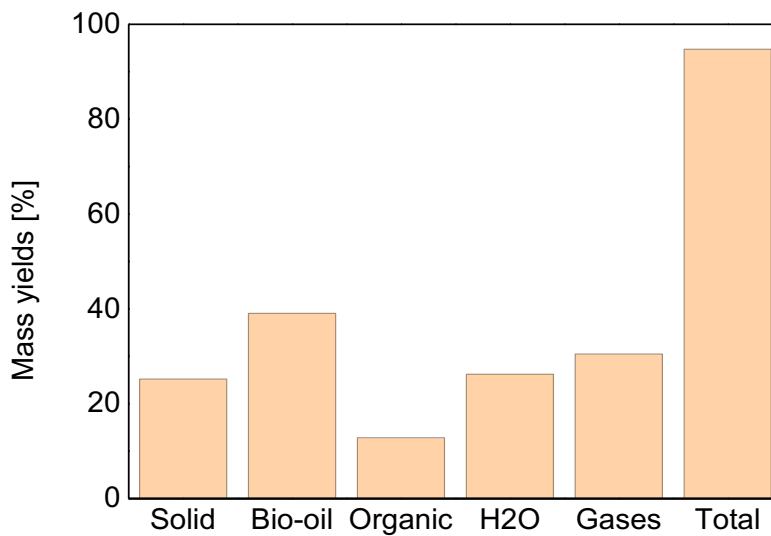


Figure 4.12: Xylan main pyrolysis products

Figure 4.13 illustrates the speciation of xylan bio-oil, the principal category of pyrolysis products, which includes an organic phase and water. The light and heavy oxygenates which constitute the organic phase are categorized in this case based on their functional groups. From the reported outcomes we can deduce that water constitutes 26.2% of the bio-oil, while other remarkable constituents are mainly included in the aliphatic ketones and aldehydes (4.3%) categories.

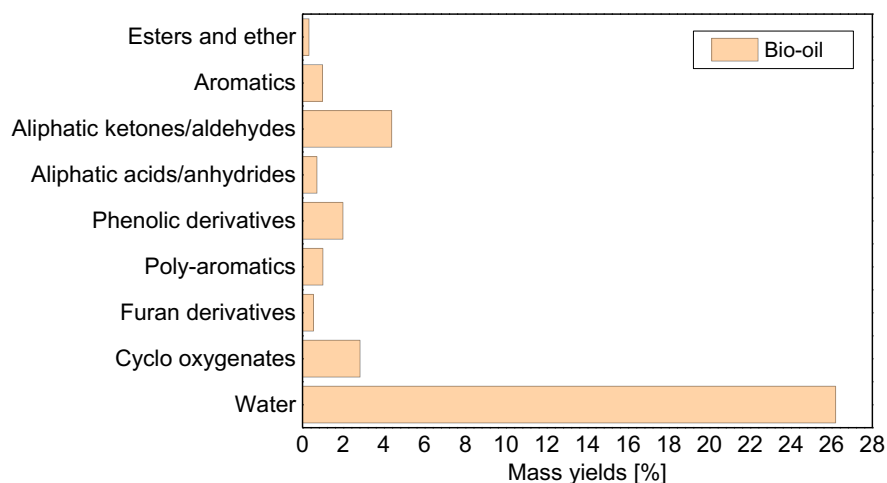


Figure 4.13: Xylan bio-oil speciation

To have a different visualization of the organic products derived from both pyrolysis vapors and liquids, they can be grouped based on the number of carbon atoms present in each species. Figure 4.14 presents this different classification of xylan organic phase. In this case, pyrolysis predominantly produces C5 (2.4%), but also comparable quantities of C2, C4, C7 and C8 products (2-2.3% of mass yields), differently from what happened with glucomannan.

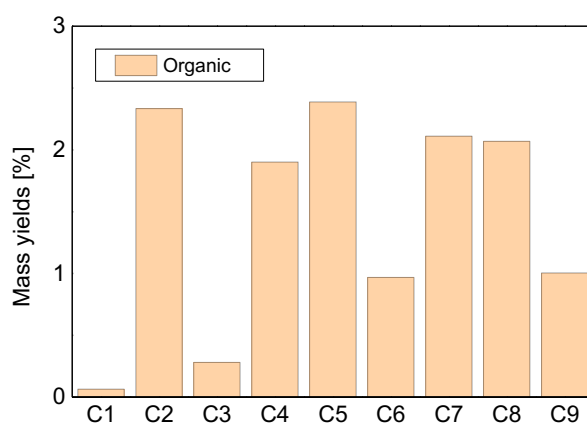


Figure 4.14: Xylan organic phase speciation

Finally, a speciation of the gaseous products of xylan pyrolysis is shown in figure 4.15. CO and CO₂ constitute the majority of the products, with a mass yield of 9.0% and 20.2% respectively.

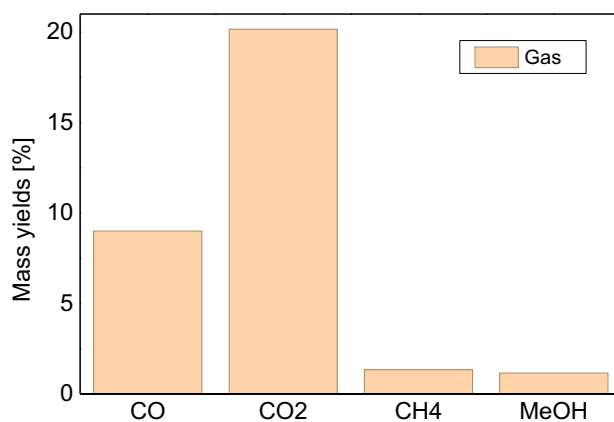
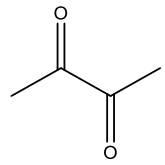
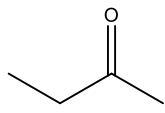
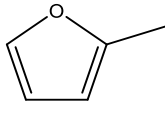
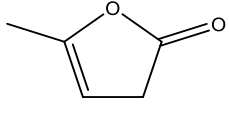
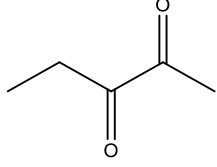
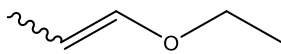
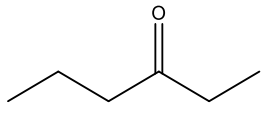
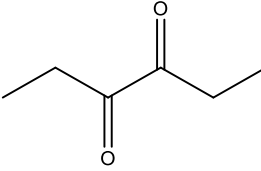
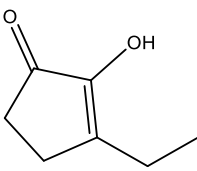
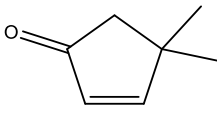
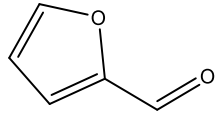


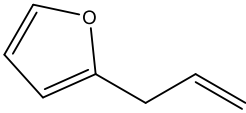
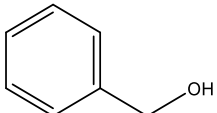
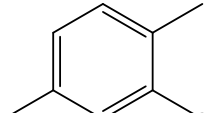
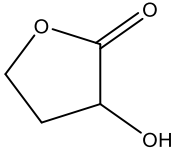
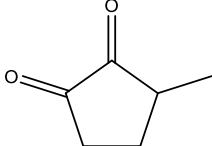
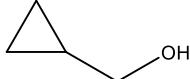
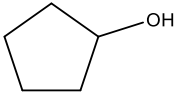
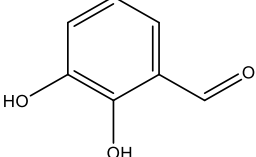
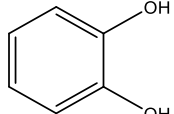
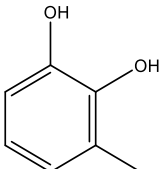
Figure 4.15: Xylan gas speciation

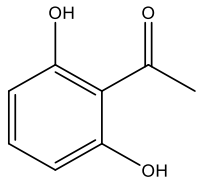
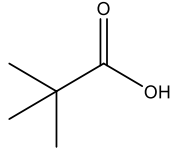
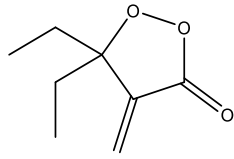
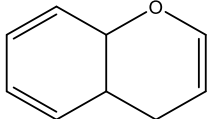
Table 4.5 provides list of products (29) identified during xylan vapors analysis, serving as a noteworthy example to illustrate the diverse array of species present in the organic phase of the bio-oil of this particular hemicellulose.

Table 4.5: Xylan pyrolysis vapors products

Species in xylan vapors		
SPECIES	FORMULA	STRUCTURE
Formaldehyde	CH ₂ O	
Acetaldehyde	C ₂ H ₄ O	
Acetone	C ₃ H ₆ O	
Furan	C ₄ H ₄ O	

2,3 butanedione	$C_4H_6O_2$	
2-butanone	C_4H_8O	
Furan, 2-methyl-	C_5H_6O	
2(3H)-Furanone, 5-methyl-	$C_5H_6O_2$	
2,3 pentanedione	$C_5H_8O_2$	
Ethyl-1-propenyl ether	$C_5H_{10}O$	
3-Hexanone	$C_6H_{12}O$	
3,4-Hexanedione	$C_6H_{10}O_2$	
2-Cyclopenten-1-one, 3,4-dimethyl-	$C_7H_{10}O_2$	
4,4-Dimethyl-2-cyclopenten-1-one	$C_7H_{10}O$	
Furfural	$C_5H_4O_2$	

Furan, 2-(2-propenyl)-	C_7H_8O	
Benzyl alcohol	C_7H_8O	
Phenol, 2,5-dimethyl-	$C_8H_{10}O$	
2-Hydroxy-gamma-butyrolactone	$C_4H_6O_3$	
1,2-Cyclopentanedione, 3-methyl-	$C_6H_8O_2$	
Cyclo propyl carbinol	C_4H_8O	
Cyclopentanol	$C_5H_{10}O$	
2,3-Dihydroxybenzaldehyde	$C_7H_6O_3$	
Catechol	$C_6H_6O_2$	
1,2-Benzenediol, 3-methyl-	$C_7H_8O_2$	

Resorcinol, 2-acetyl-	$C_8H_8O_3$	
Propanoic acid, 2,2-dimethyl-	$C_5H_{10}O_2$	
1,2-Dioxolan-3-one, 5,5-diethyl-4-methylene-	$C_8H_{12}O_3$	
Benzopyran	C_9H_8O	

In order to assess the reliability and precision of the dataset obtained from this biomass a brief analysis of uncertainties was performed also in the case of xylan. Once again, the standard deviation was computed to gain insights into the variability of the results and to prove the robustness of our findings.

The standard deviation for specific components from xylan speciation is presented in figure 4.16 and table 4.6. Notably, the calculated standard deviation values are higher than for glucomannan, but still remaining at acceptable levels.

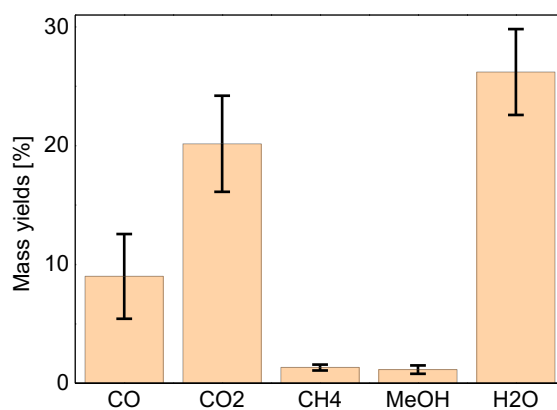


Figure 4.16: Visual representation of standard deviation for xylan pyrolysis products

Table 4.6: Standard deviation for xylan pyrolysis products

	Xylan				
	Experiment 1	Experiment 2	Experiment 3	Media	St dev
CO	3.9	2.1	9.0	5.0	3.6
CO₂	13.9	12.6	20.2	15.6	4.0
CH₄	0.8	1.1	1.3	1.1	0.3
MeOH	0.7	-	1.2	0.9	0.4
H₂O	19.2	21.1	26.2	22.2	3.6
LVG	6.4	-	-	3.2	4.5

4.3.3. Comparison between Glucomannan and Xylan

To consolidate the findings of this section, a comparative analysis between the two examined hemicelluloses is provided below:

- Figure 4.17 illustrates the overall mass balance for glucomannan and xylan. Glucomannan demonstrates a higher mass yield for bio-oil, particularly in the organic phase, while xylan exhibits a higher value of gas yield and solid residue.
- In figure 4.18, the bio-oil from the two biomasses is compared: xylan exhibits a greater water mass yield, while glucomannan proves richer in both light and heavy oxygenates. Another important difference is that on one side glucomannan is rich in anhydrosugar and on the other side xylan do not yield any of them.
- Figure 4.19 compares the organic phase, revealing consistently higher mass yields for glucomannan, with the exception of C2 species.
- Finally, in figure 4.20, gaseous products are scrutinized, indicating that xylan yields a higher amount of CO₂.

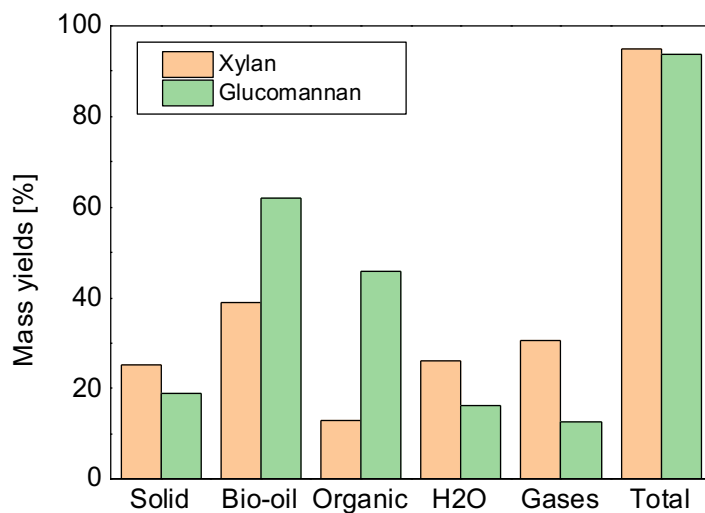


Figure 4.17: Glucomannan and xylan pyrolysis products comparison

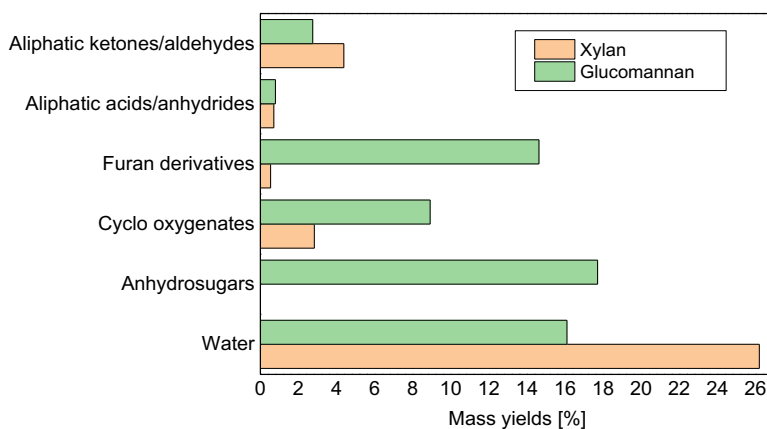


Figure 4.18: Glucomannan and xylan bio-oil comparison

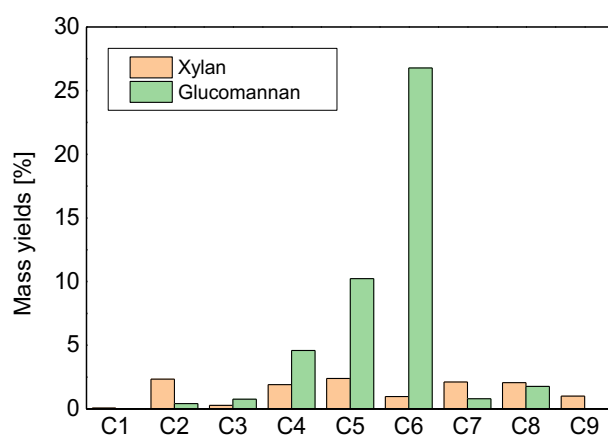


Figure 4.19: Glucomannan and xylan organic phase comparison

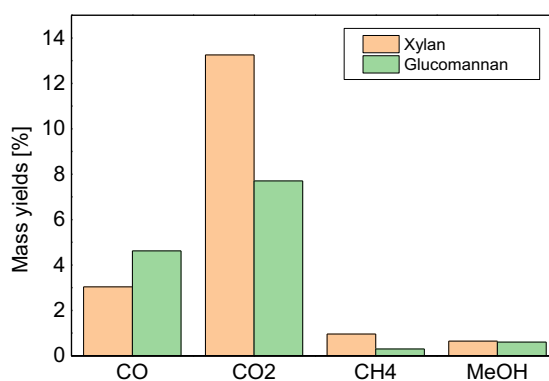


Figure 4.20: Glucomannan and xylan gases comparison

5 Biomass mixtures pyrolysis

An additional pivotal aspect explored within this thesis is the examination of biomass mixtures. In natural sources in fact, hemicelluloses are never found as pure components but coexist with other constituents such as different hemicelluloses, cellulose, and lignin. Consequently, investigating the pyrolytic behavior of these mixtures is important to elucidate possible interaction as well as synergistic effects between various components in the sample.

The presented results are organized into two sections: devolatilization investigation and speciation investigation. This distinction allows for a comprehensive exploration of potential mixing effects on both the pyrolysis kinetics of biomass and the subsequent distribution of products.

5.1. Mixtures devolatilization

In this section, we present the results of the mixture devolatilization analysis. To gain comprehensive insights into this process, we employed two primary outcomes from thermogravimetric analysis (TGA): TG and DTG curves.

The TG curve presents temperature on the x-axis and the percentage of remaining mass on the y-axis, while the DTG curve illustrates the rate of mass loss normalized against the initial sample mass as a function of temperature. These outputs serve to elucidate various thermal properties of the sample, including devolatilization temperature, the extent of decomposition, and the potential existence of multiple devolatilization steps.

The mixtures studied include:

- Xylan and Cellulose binary mixture (50:50 wt%)
- Xylan and Glucomannan binary mixture (50:50 wt%)
- Xylan and Arabinoxylan binary mixture (50:50 wt%)
- Xylan, Cellulose, Glucomannan, and Arabinoxylan quaternary mixture (25:25:25:25 wt%)

Xylan was chosen as a common component across all mixtures, serving both as a reference and aligning with established literature practices where xylan is often considered representative of hemicelluloses. In the case of cellulose previous experimental results were used.

Experimental data obtained from samples composed of mixtures were compared with theoretical expectations calculated from individual biomass devolatilization data. The theoretical behavior of mixtures was computed under the assumption of fully additive behavior, wherein each biomass in the mixture contributes independently to the overall behavior. Theoretical mixture TG and DTG curves were therefore derived by averaging the curves of the individual components, according to their weight fraction in the mixture, using equation 5.1. Subsequently, these theoretical mixture curves were compared with the experimental data from mixture samples, facilitating an investigation into the potential presence of mixing effects.

$$TG_{theo} = TG_i * w_i + TG_j * w_j \quad (5.1)$$

In figures 5.1, 5.2 and 5.3 we present TG and DTG curves for the xylan and cellulose mixture. Dashed lines represent data for xylan and cellulose as pure components in both graphs. Theoretical mixture data, computed as the average between the individual components, is also plotted. Experiments were conducted using three different heating ramps (3°C/min, 20°C/min, and 100°C/min), mirroring the experimental conditions used to analyze single biomasses. This consistent methodology allows for a meaningful comparison of the mixture's behavior under different thermal conditions.

Upon analyzing figure 5.1, which depicts data from experiments performed at 3°C/min, the comparison between the real mixture and the expected behavior reveals no notable distinctions in both TG and DTG curves. The same trend can be observed also in figure 5.2, where the intermediate heating rate (20°C/min) was employed. This well evidences the additive behavior of the real mixture, as it closely converges with that of the theoretical mixtures, approaching an almost superimposable alignment of curves.

Figure 5.3 instead depicts TG and DTG curves at 100°C/min. Even if in general a good adherence to the expected behavior can still be observed, some differences are also noticeable. Specifically, the TG curve for the real mixture appears shifted to the right in its initial phase, meaning that the pyrolysis process has a slightly higher onset temperature. Moreover, it is evident that the experimental mixture yields less solid residue than expected. This trend is further elucidated by the DTG curve, where the first devolatilization peak is suppressed in the real mixture if compared to the theoretical mixture. This subdued peak, which represents xylan contribution to the devolatilization, contrasts with the anticipated behavior. Moreover, the peak associated with cellulose devolatilization is anticipated and shifted to lower temperatures. This behavior reflects the difficult temperature control experienced at high heating rate due to the short duration of the experiment. Moreover, the problem is exacerbated by cellulose presence, due to the high endothermicity of its pyrolysis.

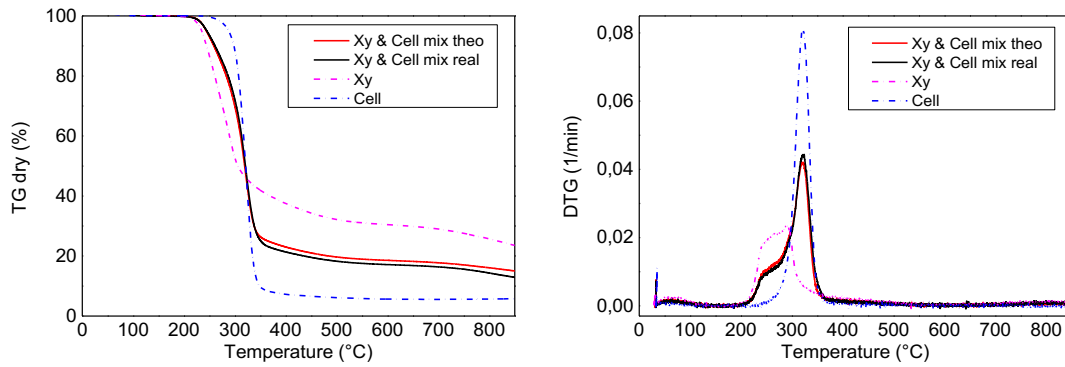


Figure 5.1: Xylan and cellulose mixture pyrolysis with a heating ramp of 3°C/min

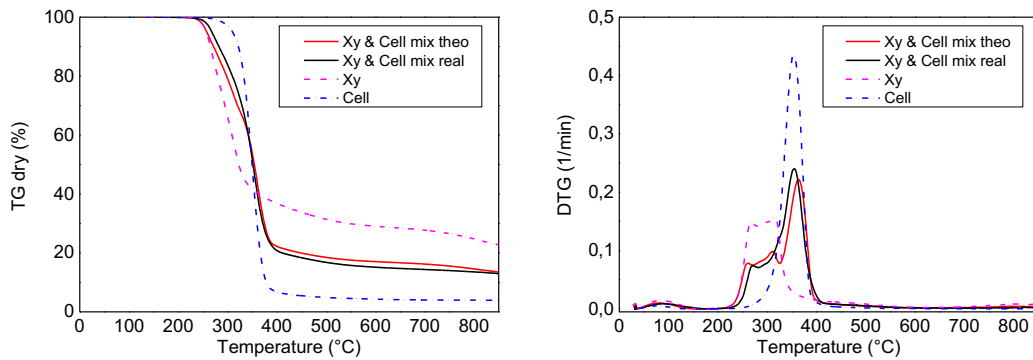


Figure 5.2: Xylan and cellulose mixture pyrolysis with a heating ramp of 20°C/min

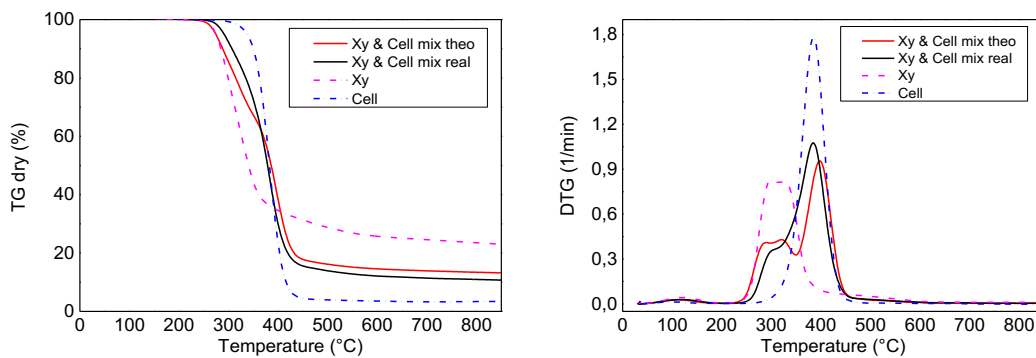


Figure 5.3: Xylan and cellulose mixture pyrolysis with a heating ramp of 100°C/min

In figures 5.4, 5.5, and 5.6, we depict the thermogravimetric (TG) and derivative thermogravimetric (DTG) curves for the xylan and glucomannan mixture. Dashed lines on the graphs represent data coming from the devolatilization of pure components. Theoretical mixture data, always derived as the average of the individual components, is also included. To ensure a comprehensive analysis, experiments were again conducted using three distinct heating ramps ($3^{\circ}\text{C}/\text{min}$, $20^{\circ}\text{C}/\text{min}$, and $100^{\circ}\text{C}/\text{min}$), aligning with the conditions employed for the analysis of individual biomasses.

As a general trend experimental mixtures measurements matched those evaluated considering a fully additive behavior. This evidence becomes clearer with the decrease in the heating rate, when temperature control is improved and DTG curves are more definite.

A distinctive feature that emerges in the TG curve at intermediate heating ramp ($20^{\circ}\text{C}/\text{min}$), depicted in figure 5.5 is that the experimental mixture yields a slightly higher amount of solid residue than expected. Instead at $100^{\circ}\text{C}/\text{min}$ (figure 5.6) a subtle suppression of xylan devolatilization peak in the DTG curve can be observed.

However, it is crucial to emphasize that, the observed differences between experimental and theoretical data for the xylan and glucomannan mixture are minimal, and could be due to experimental errors, for example in the weighting phase. It can be therefore said that the experimental findings align closely with the calculated expectations.

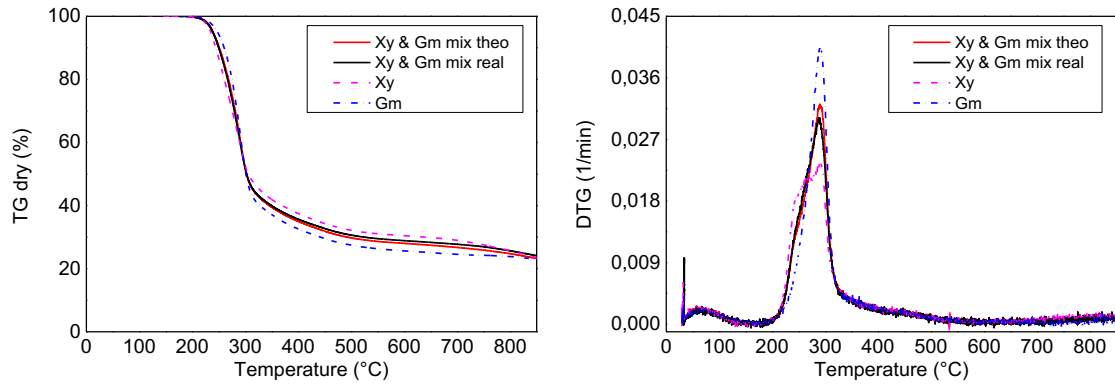


Figure 5.4: Xylan and glucomannan mixture pyrolysis with a heating ramp of 3°C/min

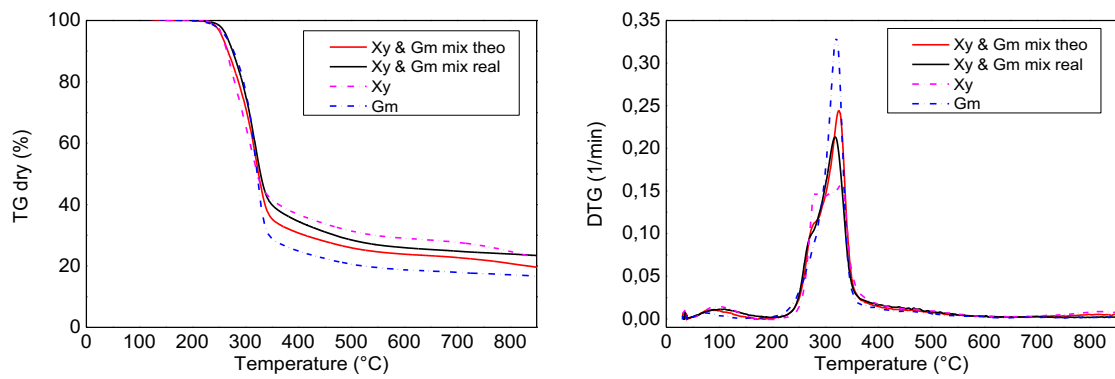


Figure 5.5: Xylan and glucomannan mixture pyrolysis with a heating ramp of 20°C/min

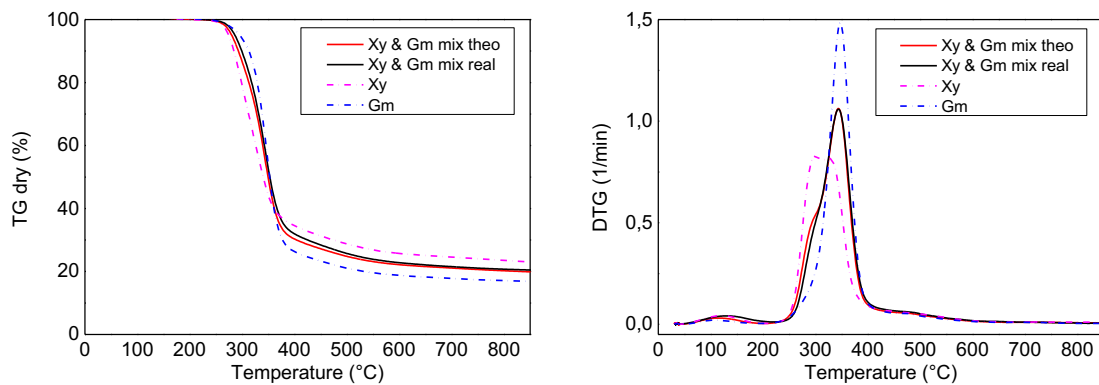


Figure 5.6: Xylan and glucomannan mixture pyrolysis with a heating ramp of 100°C/min

In figures 5.7, 5.8, and 5.9, the thermogravimetric (TG) and derivative thermogravimetric (DTG) curves for the xylan and arabinoxylan mixture are reported. Once again devolatilization of pure components is represented by dashed lines and theoretical mixture data, average of the individual components, is also included. Three distinct heating ramps ($3^{\circ}\text{C}/\text{min}$, $20^{\circ}\text{C}/\text{min}$, and $100^{\circ}\text{C}/\text{min}$) were employed to align the experiments with the conditions used for individual biomasses.

Broadly the behavior of the xylan and arabinoxylan experimental mixture exhibits a close resemblance to the theoretical mixture. This similarity is underscored by the consistent alignment of TG and DG curves across all cases, with discernible differences being relatively minimal. Mirroring the trend observed in prior scenarios curves at the slower rate ($3^{\circ}\text{C}/\text{min}$), as illustrated in figure 5.7, become superimposable due to a better control of the experiment given by the imposed conditions.

Notably, a subtle suppression of the xylan contribution is observed, as reflected in the DTG curves. Additionally, there is a slight upward shift in the onset temperature of the pyrolysis process. However, it is important to highlight that the peak temperature of arabinoxylan devolatilization in the mixture is well-preserved. Regarding the solid residue, a clear trend is not evident. At the higher heating ramp ($100^{\circ}\text{C}/\text{min}$), the experimental mixture exhibits higher solid residue than expected, while at $20^{\circ}\text{C}/\text{min}$, the trend is reversed. However, being these differences practically negligible, they could once again be ascribed to experimental errors.

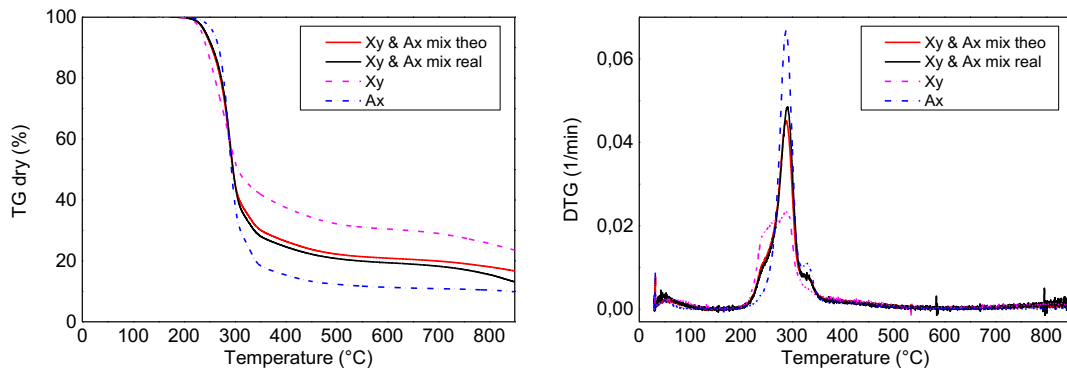


Figure 5.7: Xylan and arabinoxylan mixture pyrolysis with a heating ramp of 3°C/min

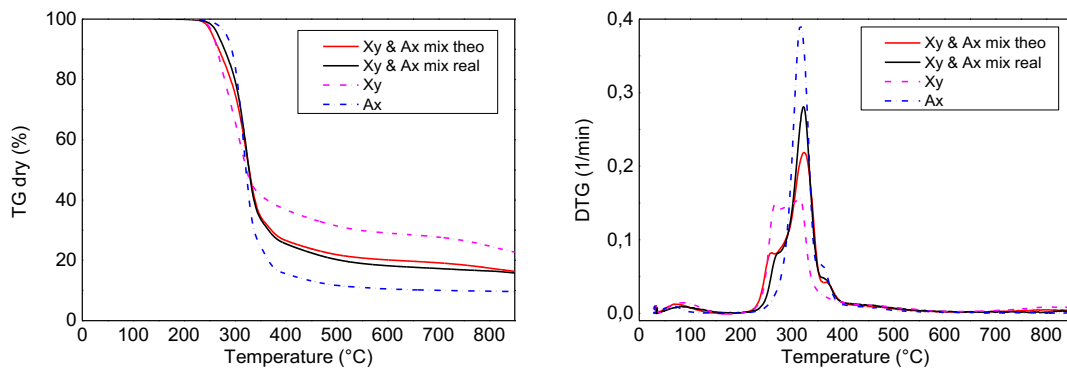


Figure 5.8: Xylan and arabinoxylan mixture pyrolysis with a heating ramp of 20°C/min

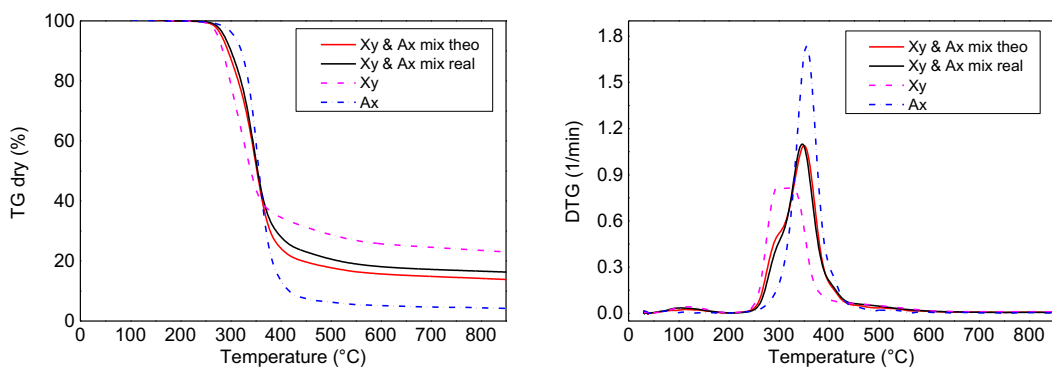


Figure 5.9: Xylan and arabinoxylan mixture pyrolysis with a heating ramp of 100°C/min

Finally, in figures 5.10, 5.11, and 5.12, the thermogravimetric (TG) and derivative thermogravimetric (DTG) curves for a mixture comprising all four analyzed biomasses (xylan, cellulose, glucomannan and arabinoxylan) are reported. In this instance, for the sake of clarity, curves representing the devolatilization of the single components are omitted. Therefore, only curves for the theoretical and experimental mixtures are included. As usual, three distinct heating ramps ($3^{\circ}\text{C}/\text{min}$, $20^{\circ}\text{C}/\text{min}$, and $100^{\circ}\text{C}/\text{min}$) were employed to align the experiments with the conditions used for individual biomasses.

Upon closer examination, it becomes evident that, once again, reducing the heating rate results in a diminished gap between actual and expected outcomes and at $3^{\circ}\text{C}/\text{min}$ TG and DTG curves perfectly overlap. Notably, the variances are most pronounced at higher heating rates, particularly at $100^{\circ}\text{C}/\text{min}$. In such instances, the thermogravimetric curves reveal a departure, showing a higher onset temperature for the process and a substantially higher solid residue in the actual mixture compared to the expected values. Additionally, the derivative thermogravimetric curves unveil a convergence of the individual biomass contributions present in the theoretical curve. In the experimental mixture, these contributions are subdued, manifesting as a singular prominent peak that encompasses the combined effects of all individual biomasses. By decreasing the heating rate such contributions become more pronounced, aligning with the calculated curve.

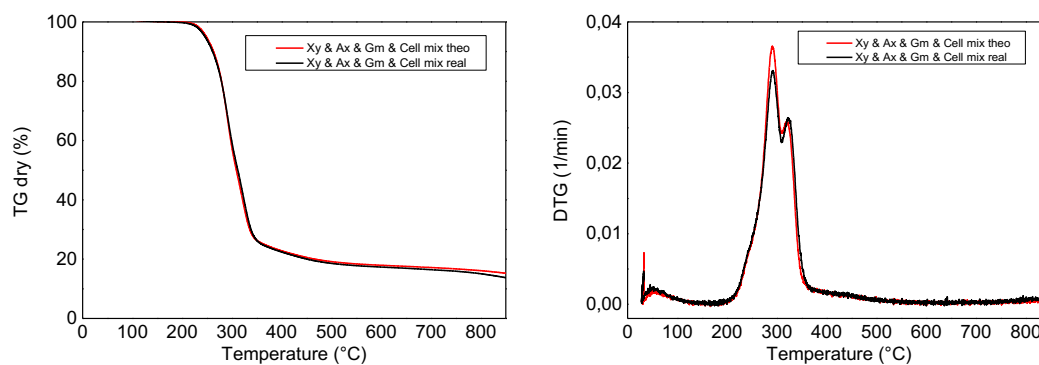


Figure 5.10: Xylan, arabinoxylan, glucomannan and cellulose mixture pyrolysis with a heating ramp of 3°C/min

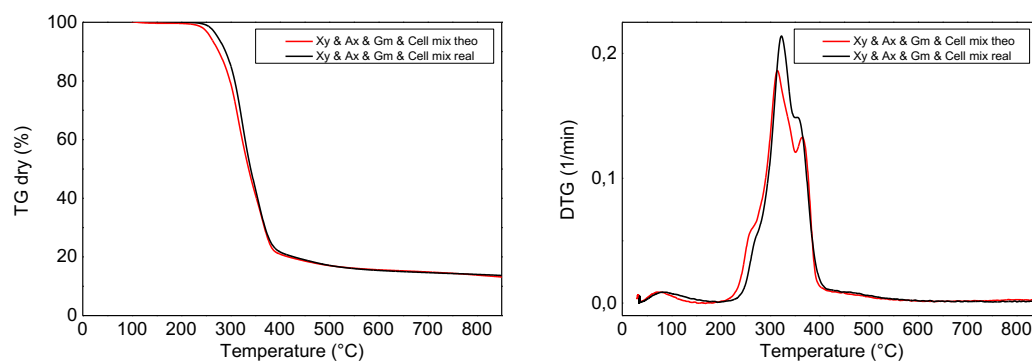


Figure 5.11: Xylan, arabinoxylan, glucomannan and cellulose mixture pyrolysis with a heating ramp of 20°C/min

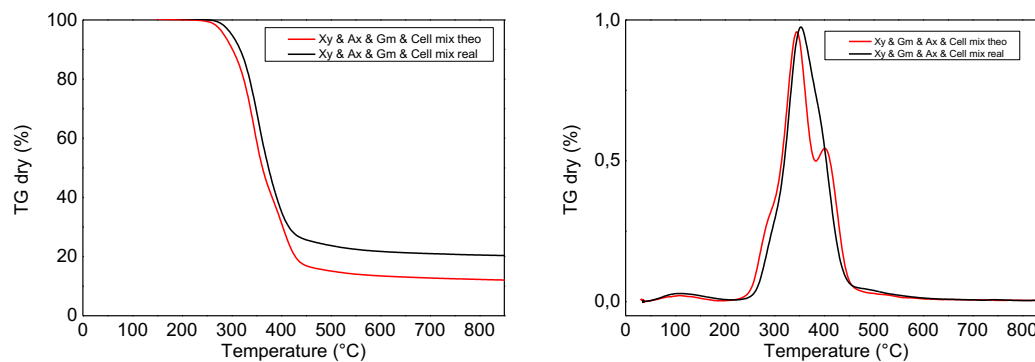


Figure 5.12: Xylan, arabinoxylan, glucomannan and cellulose mixture pyrolysis with a heating ramp of 100°C/min

The primary objective of this extensive analysis was to gain insights into the pyrolytic behavior of biomass mixtures, with a specific focus on those composed of diverse hemicelluloses. The aim was to discern whether the components within these mixtures exhibit an additive behavior, thereby eliminating the potential influence of mixing effects. To achieve this, data pertaining to the devolatilization of individual components were amalgamated to compute the anticipated behavior for a theoretical mixture. Subsequently, this theoretical projection was compared with experimental data.

Upon scrutinizing the TG and DTG curves at various heating rates, the evidence suggests that the mixtures do indeed adhere to an additive behavior. Each individual component appears to contribute distinctly to the overall behavior of the mixture. Examining the data reveals a consistent trend across all analyzed mixtures, with minimal discrepancies observed, particularly at higher heating rates.

A trend that was often observed it's a delay in the initial stage of xylan devolatilization. This could be due to the presence of glucuronic acids in the structure of this hemicellulose, which in the initial stage of the pyrolysis process are retained by the other component in the mixture which has not undergone gasification yet.

5.2. Speciation of pyrolysis products

After examining the devolatilization behavior of biomass mixtures, a detailed analysis was conducted to investigate mixture speciation. The goal was to comprehend the interactions among the components within the biomass and determine if their simultaneous presence influences the distribution of pyrolysis products. A campaign similar to the one conducted for individual biomasses, was carried out for this purpose.

Following the approach established for the speciation of individual hemicelluloses, two specific mixtures were investigated: xylan with cellulose, and xylan with glucomannan. Data on cellulose pyrolysis was previously collected in the research group.

Also in this case, the speciation results collected from mixtures were compared with those of individual components, collected from experiments on individual components, and those theoretically expected, assuming additivity and computed according to equation 5.2.

$$\text{mass yield}_{theo} = \text{mass yield}_i * w_i + \text{mass yield}_j * w_j \quad (5.2)$$

The same protocol employed for individual biomass samples was used for mixtures. A full quantitative speciation was achieved in terms of gas, water and heavy oxygenates collected in the Orbo™ trap. In contrast, the speciation of light oxygenates was performed only on a qualitative basis by identifying the species present in this phase, but without their quantification.

5.2.1. Xylan and Glucomannan mixture

In figure 5.13 and table 5.1, the quantification of products for the xylan and glucomannan mixture is illustrated. Mass yields for CO, CO₂, methane, methanol, water and levoglucosan are presented for the single components, the actual mixture, and the theoretical mixture, computed as weighted averages based on the mass fractions of the individual components.

As it is evident from the collected data, the behavior of the real mixture generally aligns with the anticipated pattern, with very small differences between mass yields values.

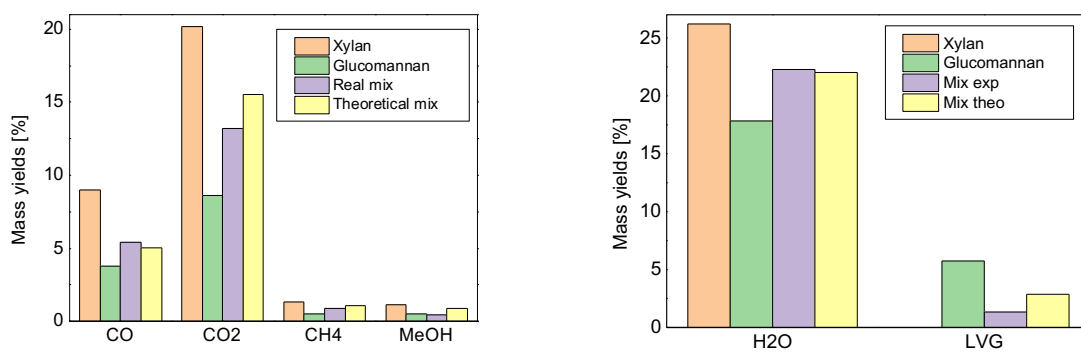


Figure 5.13: Xylan and glucomannan mixture product quantification

Table 5.1: Mass yields of xylan and glucomannan mixture products

	Mass yield on dry basis [%]			
	Xylan	Glucomannan	Theoretical mix	Real mix
CO	9.0	3.8	4.4	6.4
CO ₂	20.2	8.6	12.1	14.4
CH ₄	1.3	0.5	0.8	0.9
MeOH	1.15	0.5	0.7	0.8
H ₂ O	26.2	17.8	22.0	22.3
LVG	0	5.7	1.8	1.3

Despite not achieving satisfactory quantification results, a qualitative analysis for the bio-oil fraction remains feasible. This involves comparing the primary species identified in the vapor analysis of the mixture, as illustrated in figure 5.14 and table 5.2, with the species identified in the vapor analysis of xylan and glucomannan individually, detailed in tables 4.3 and 4.5. Notably, all the species identified in the mixture are also observed in the analysis of the individual components.

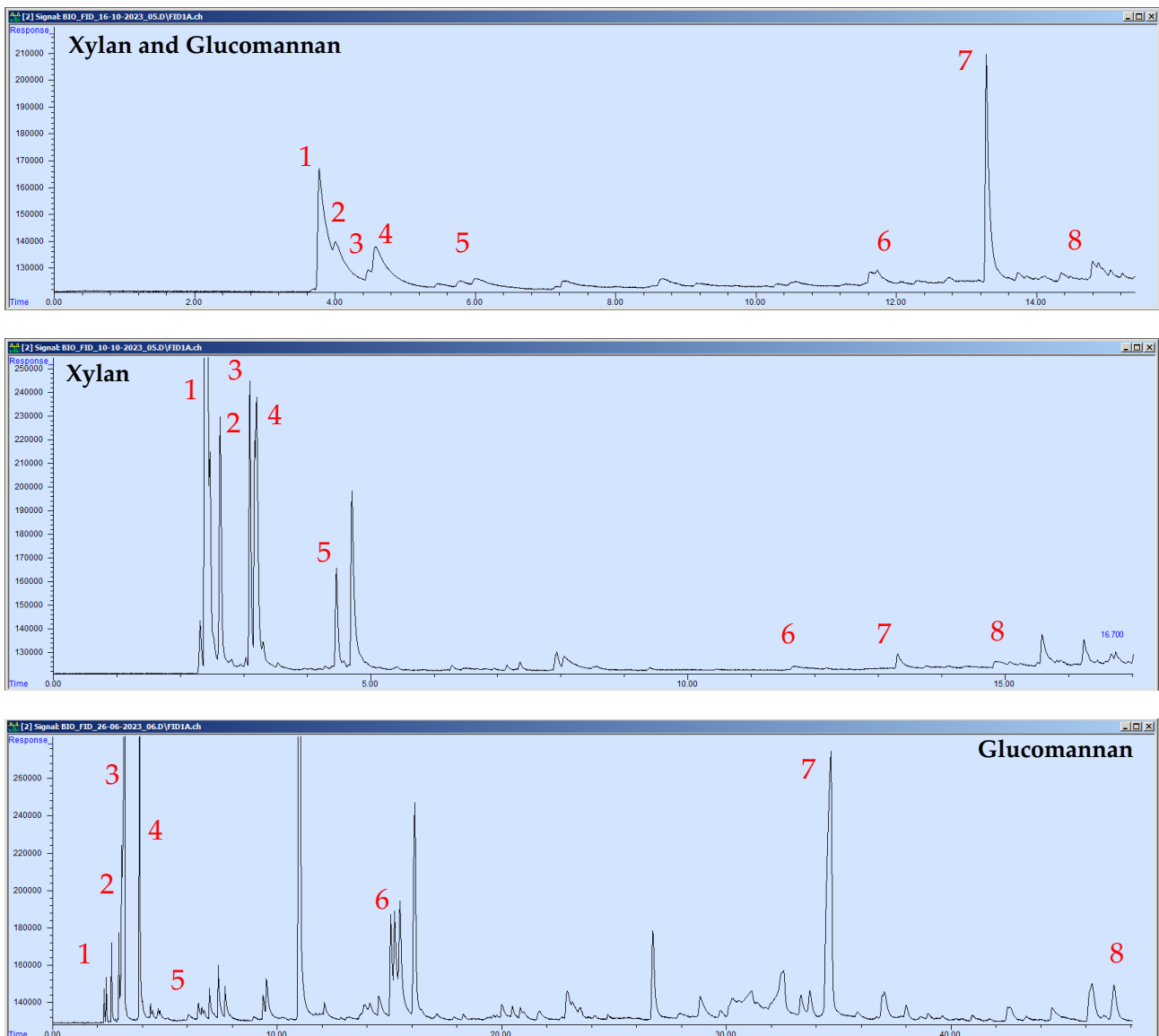


Figure 5.14: Chromatograms of xylan and glucomannan mixture, xylan and glucomannan vapor analysis with main species indicated by numbers

Table 5.2: Common species found in xylan, glucomannan and xylan and glucomannan mixture

Number	Species in the mixture
1	Acetaldehyde
2	Acetone + Furan
3	2,3 butanedione
4	Furan, 2-methyl
5	2,3-Pentanedione
6	2-Hydroxy-gamma-butyrolactone
7	Cyclopropyl carbinol
8	Catechol

The challenges encountered in quantifying mixture vapors can be attributed to the adherence of biomass components within the mixture to an additive behavior, as demonstrated during the analysis of thermogravimetric curves for devolatilization. To elucidate this, two crucial pieces of information must be recalled. Firstly, vapor analysis relies on a punctual collection of pyrolysis vapors from the Thermogravimetric Analyzer (TGA). Secondly, each biomass exhibits a distinct decomposition pathway, manifesting the highest volatiles production at different temperatures. For instance, xylan releases the most volatile species around 340°C, while glucomannan decomposition requires higher temperatures.

In the necessity to pinpoint the sampling moment for mixture vapors, a compromise must be struck. We endeavored to sample vapors at a temperature representing a midpoint between the decomposition peaks of the individual biomasses. However, it becomes evident that inaccuracies may arise from this process. If biomasses exhibit an additive behavior, participating separately in the devolatilization process, xylan may undergo excessive degradation, potentially hindering the detection of its products in the gas chromatography analysis. Conversely, glucomannan might not have commenced its decomposition at the chosen temperature, resulting in its contribution to pyrolysis products being absent from the chromatogram.

Given these considerations, it is apparent that following this sampling protocol for quantifying pyrolysis products would not yield representative results. Adjustments to the sampling protocol are imperative to obtain a meaningful quantification.

5.2.2. Xylan and Cellulose mixture

Similar trends and challenges were encountered in the case of the xylan and cellulose mixture, even if with less pronounced discrepancies.

In figure 5.15 and table 5.2 product quantification is reported. Mass yields for CO, CO₂, methane, methanol, water, levoglucosenone and levoglucosan are presented for individual biomasses, the actual mixture, and the theoretical mixture, computed as weighted averages based on the mass fractions of the individual compounds present in the mixture.

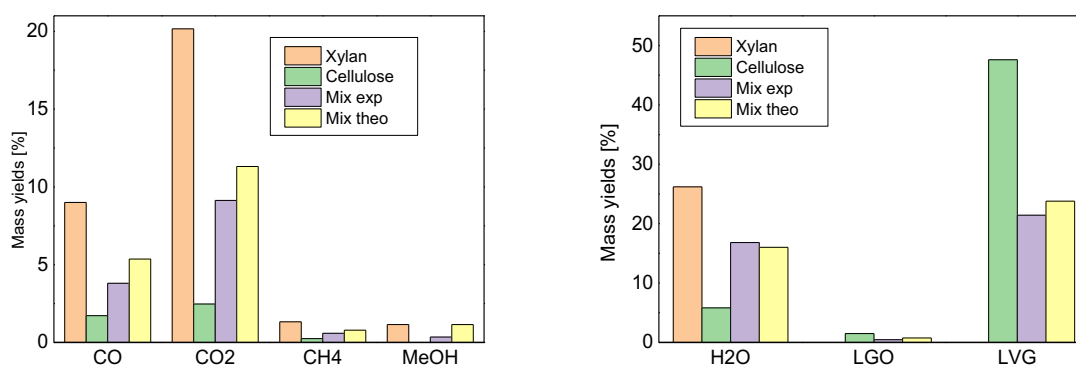


Figure 5.15: Xylan and cellulose mixture product quantification

Table 5.3: Mass yields of xylan and cellulose mixture products

	Mass yield on dry basis [%]			
	Xylan	Cellulose	Theoretical mix	Real mix
CO	9.0	1.7	5.4	3.8
CO₂	20.2	2.5	11.3	9.1
CH₄	1.3	0.2	0.8	0.6
MeOH	1.2	0.0	0.6	0.3
H₂O	26.2	5.8	16.0	16.8
LGO	0	1.5	0.8	0.5
LVG	0	47.6	23.8	21.4

Once again, challenges became more evident when quantifying light oxygenates. A qualitative analysis can be still carried out by comparing the species present in the gas chromatogram of the analyzed experimental mixture, shown in figure 5.16 and table 5.4, with the species present in xylan and cellulose samples. Notably, the majority of the species identified in the mixture are also observed in the analysis of the individual components.

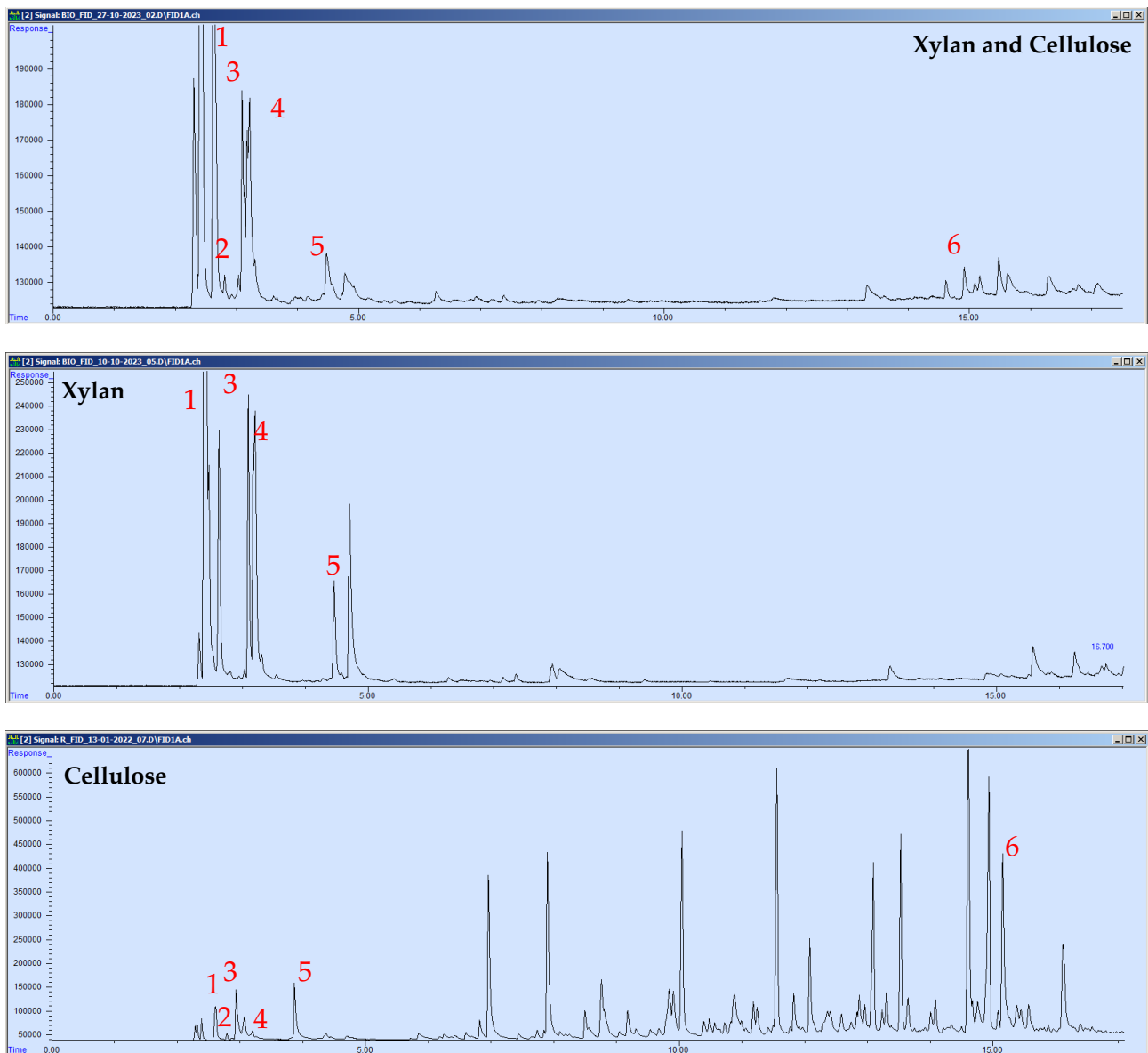


Figure 5.16: Chromatogram of xylan and cellulose mixture, xylan and cellulose vapor analysis with main species indicated by numbers

Table 5.4: Common species found in xylan, cellulose and xylan and cellulose mixture

Number	Species in the mixture
1	Acetone + Furan
2	Furan, 2,5- dihydro
3	2,3 butanedione
4	Furan, 2-methyl
5	2,3-Pentanedione
6	Levoglucosenone

In light of the considerations made thus far, it can be said that speciation experiments do not give strong evidence against additive behavior. However, it is also noticeable that a refinement in the experimental protocol is necessary to achieve a complete quantification of all the pyrolysis product and clearer indications towards additivity properties of mixture components.

It can be stated that the speciation of biomass mixtures still remains an ongoing challenge, requiring further in-depth investigation to achieve comprehensive and meaningful results.

6 Experiments in packed bed reactor

In the course of prior research activities, our group conducted pyrolysis experiments on cellulose, xylan, glucomannan, arabinoxylan, and their mixtures using a packed bed reactor configuration. This phase of our investigation involved the post-processing of experimental data gathered from these experiments, which will be here presented and discussed. The objective is to showcase data for the same biomasses previously analyzed, but in a different setup that allows for tests on a scale more representative than that achievable with thermogravimetric analysis.

The results are articulated in terms of integral mass yields, highlighting various pyrolysis product categories. The focus is on comparing the experimental mixture, the theoretical mixture, and the individual components to glean insights into the pyrolytic behavior of these biomasses under the new reactor configuration.

6.1. Xylan, Glucomannan and Cellulose comparison

In the first instance, a comparative analysis between xylan, glucomannan and cellulose pyrolysis products is provided below:

- Figure 6.1 illustrates the overall mass balance for the three biomasses. Xylan exhibits the most favorable balance closure, as well as the highest mass yields for gases and solid residue. Cellulose shows the opposite behavior, with higher production of bio-oil, in particular of the organic fraction. Glucomannan instead displays in general an intermediate behavior between the other two analyzed biomasses.
- In figure 6.2 the bio-oil fraction is compared: xylan and glucomannan exhibit greater water mass yield compared to cellulose, other than a higher production of aliphatic ketones and aldehydes. Cellulose on the other hand proves remarkably richer anhydrosugar with respect to glucomannan and in particular xylan, which in fact show lower bio-oil production. This is due to the presence of levoglucosan as the main cellulose pyrolysis product, with a mass yield higher than 40%.
- Figure 6.3 depicts the organic phase, revealing substantially higher mass yields of C6 species for cellulose, and comparable production of the other fractions.
- Finally, in figure 6.4, gaseous products are scrutinized, indicating similar yields for CO but considerably higher yields of CO₂ for xylan.

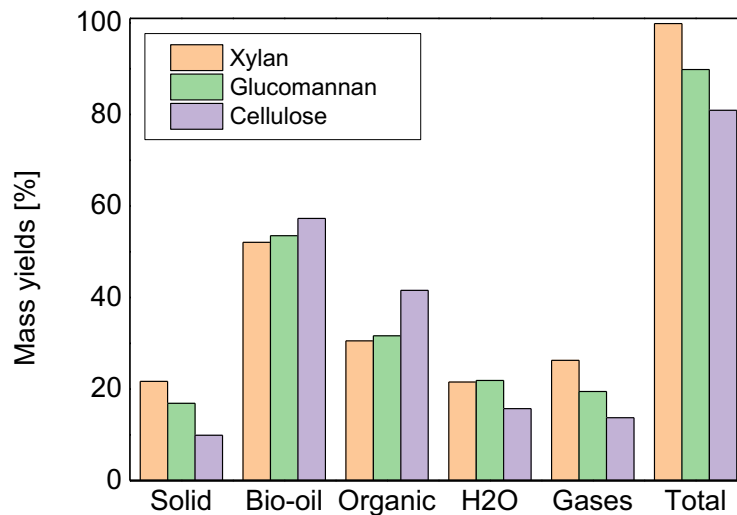


Figure 6.1: Xylan, glucomannan and cellulose pyrolysis products comparison

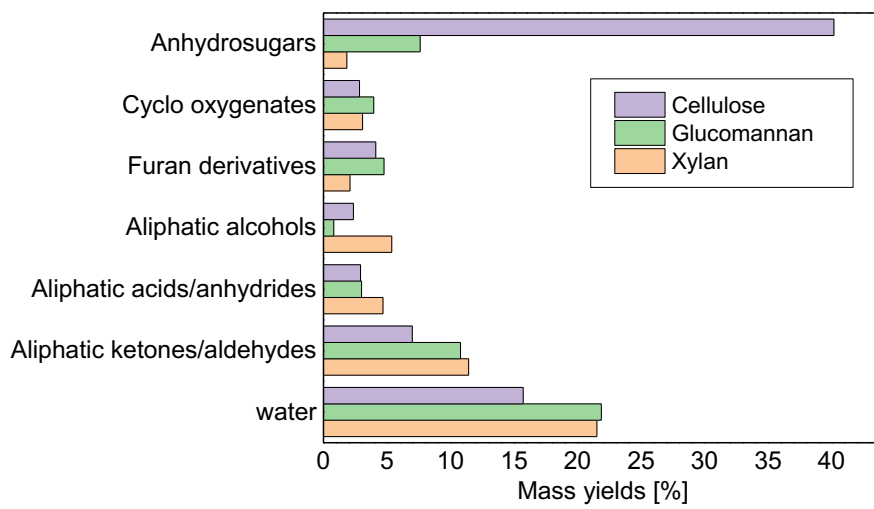


Figure 6.2: Xylan, glucomannan and cellulose bio-oil comparison

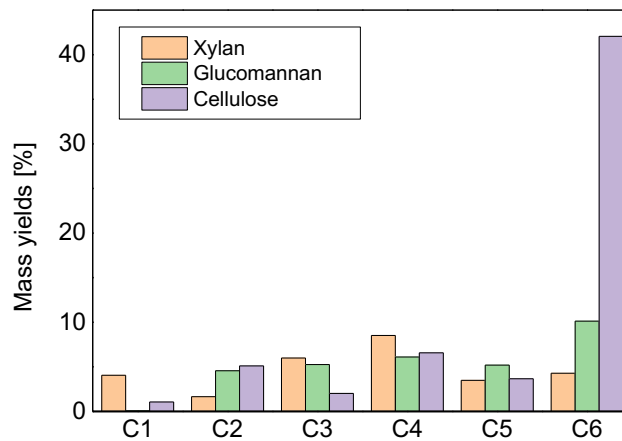


Figure 6.3: Xylan, glucomannan and cellulose organic phase comparison

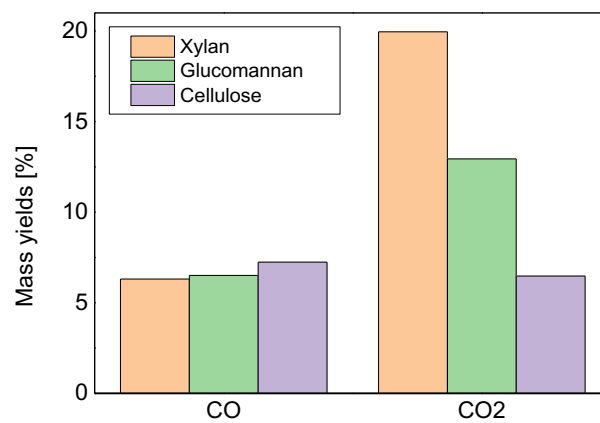


Figure 6.4: Xylan, glucomannan and cellulose gases comparison

At this stage, it would be extremely useful to compare the results obtained from the TGA experiments with those derived from the fixed bed configuration. Nevertheless, the inherent disparities between the two setups present challenges to such a comparison. For instance, the TGA tests employed a temperature ramp, while the fixed bed experiments maintained an isothermal condition. Furthermore, the fixed bed experiments may be subject to heat transfer limitations, resulting in a more intricate and less predictable temperature profile within the biomass bed. Given the fundamental influence of temperature in pyrolysis, this disparity is expected to introduce variations in the distribution of pyrolysis products.

Despite the complexity posed by these differences, conducting an integrated analysis of results from both the TGA and fixed bed reactor systems remains highly valuable. Notably, the trends observed in TGA results generally corresponded with those seen in the fixed bed reactor experiments. For example, cellulose exhibited the lowest yield of solid residual and the highest yield of bio-oil in both systems, with the primary product being the C6 anhydrosugar levoglucosan.

Similar agreement was observed for the two hemicelluloses. Xylan consistently displayed the largest solid residue, with products evenly distributed among solid, liquid, and gas phases. Notably, there was no prevalence of a particular family of species: both light and heavy oxygenates, were distributed more or less homogeneously across the whole C1-C9 range and various chemical functionalities.

Interestingly, glucomannan demonstrated a behavior intermediate between cellulose and xylan. This behavior could be attributed to its chemical structure, as glucomannan is a fully amorphous polysaccharide like xylan but is based on C6 monomers like cellulose. The significant production of levoglucosan, even in the case of glucomannan, suggests that the release of a C6 unit is also in this case more favored. These characteristics were consistently observed in both fixed bed and TGA experiments.

6.2. Xylan and Glucomannan mixture

In figures 6.5, 6.6, 6.7, 6.8 the mass yields for the pyrolysis products resulting from the xylan and glucomannan mixture are illustrated. Experimental outcomes are compared with theoretical values, computed as the weighted averages on the mass fraction of single components in the mixture. The aim is to investigate possible synergistic effects due to the presence of two different biomasses in the same sample.

- In figure 6.5, the comprehensive mass balance is presented. While the experimental mixture appears to align closely with the anticipated outcomes, the values plotted for the individual components, theoretical and experimental mixtures, exhibit striking similarities. Consequently, drawing conclusions about additivity is challenging, as the values fall within a narrow range, limiting our ability to discern meaningful distinctions.

- Figure 6.6 delves into the bio-oil fraction, revealing consistent mass yield values for both experimental and theoretical mixtures across all product categories. While similarities persist, the assessment of additivity becomes more certain when scrutinizing categories with the most pronounced discrepancies among the individual components, observed for example in the case of aliphatic alcohols. It's worth noting an exception to this trend in the anhydrosugars category, where the experimental mixture exhibits a lower value than anticipated. Even in this case however differences between all analyzed cases are too little to be a clear demonstration of additive behavior.
- Figure 6.7 illustrates the classification of the organic phase of the mixture according to the number of carbon atoms. In this case C3, C4 and C5 products show similar mass yields values for the experimental and theoretical mixtures, being the C4 category also representative for additivity considerations. The C6 products however fall short of meeting the expected value (5.20% vs. 7.20%), in line to what shown for the anhydrosugars category.
- In figure 6.8 pyrolysis gaseous products are reported. Here the experimental mixture shows a similar behavior to the theoretical one, pointing out interesting results in terms of additivity especially for CO₂ production.

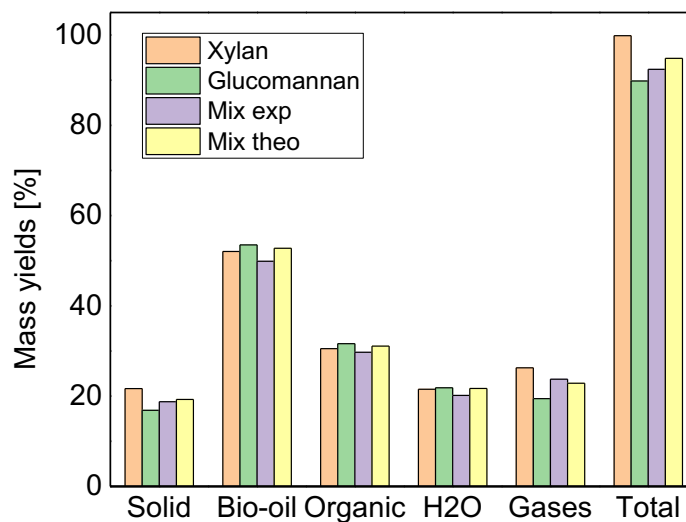


Figure 6.5: Xylan and glucomannan mixture main pyrolysis products

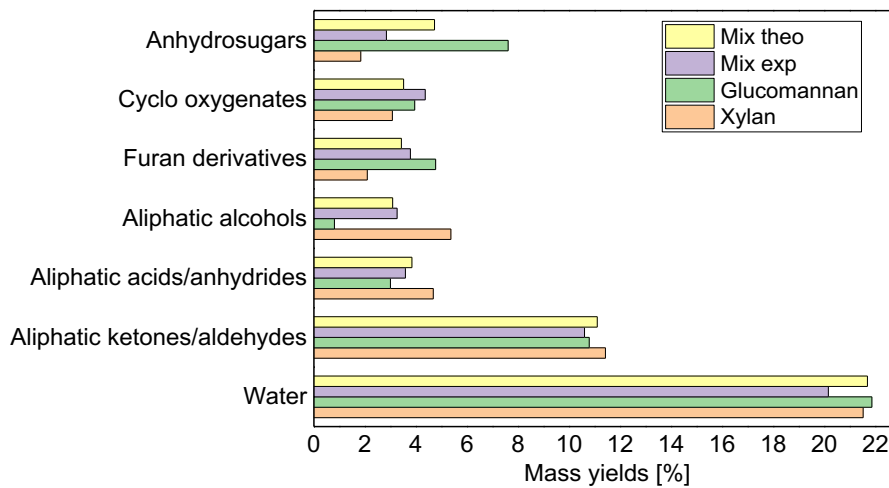


Figure 6.6: Xylan and glucomannan mixture bio-oil speciation

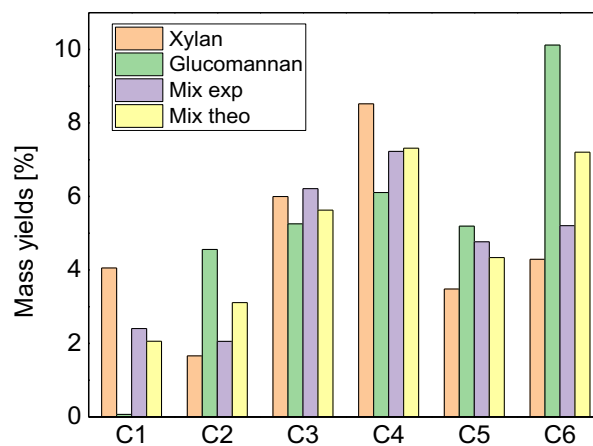


Figure 6.7: Xylan and glucomannan mixture organic phase speciation

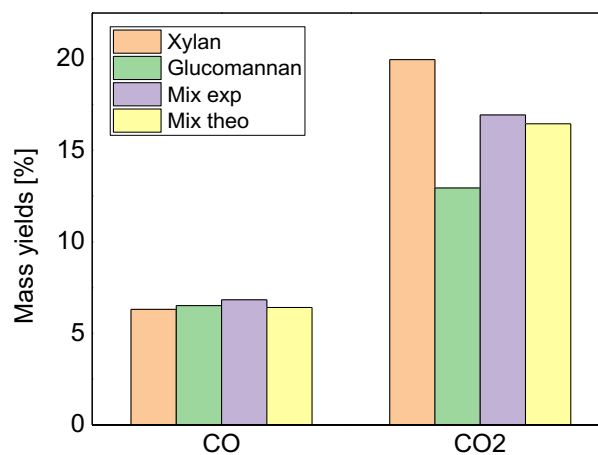


Figure 6.8: Xylan and glucomannan mixture gas speciation

6.3. Xylan and Cellulose mixture

Figures 6.9, 6.10, 6.11, and 6.12 depict the mass yields of pyrolysis products arising from the xylan and cellulose mixture. The experimental results are compared with theoretical values and results for individual components.

- Figure 6.9 presents the comprehensive balance, showcasing similar mass yield values between the experimental and theoretical mixtures across all categories, except for the bio-oil fraction. In this specific category, the experimental mixture exhibits lower values, a deficit that is noticeably reflected in the overall total mass balance. The general trend however shows no strong indication against an additive behavior.
- Figure 6.10 provides a detailed breakdown of the bio-oil from the xylan-cellulose mixture. In this instance, the mass yields for the actual mixture are slightly lower than anticipated across all product categories, though still relatively close to the expected values. Notably, an exception is observed in the anhydrosugars category, where the real mixture displays a significantly higher mass yield than expected. This deviation is likely attributed to the presence of cellulose, which, due to its pronounced production of levoglucosan, potentially amplifies the generation of anhydrosugars from xylan.
- Figure 6.11 illustrates the classification of the organic phase of the mixture, affirming and reflecting the trends observed in figure 6.10. The pyrolysis of the experimental mixture predominantly yields C6 species (36.51%), surpassing the expected value (21%). On the other hand, all the other categories present actual values lower than the theoretical ones.
- Figure 6.12 reports pyrolysis gas composition. The analyzed products include CO and CO₂, both showing similar values of mass yields for the real and expected cases.

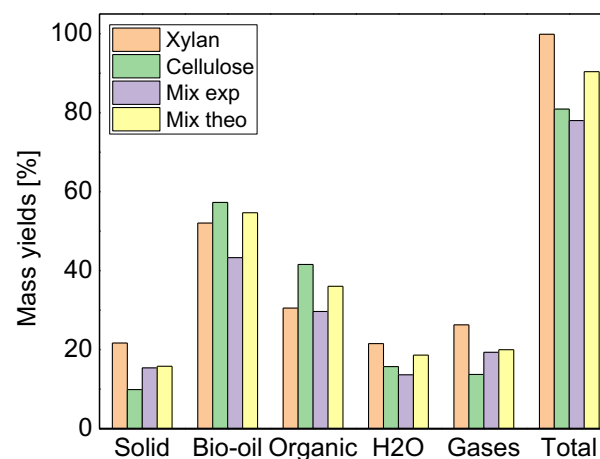


Figure 6.9: Xylan and cellulose mixture main pyrolysis products

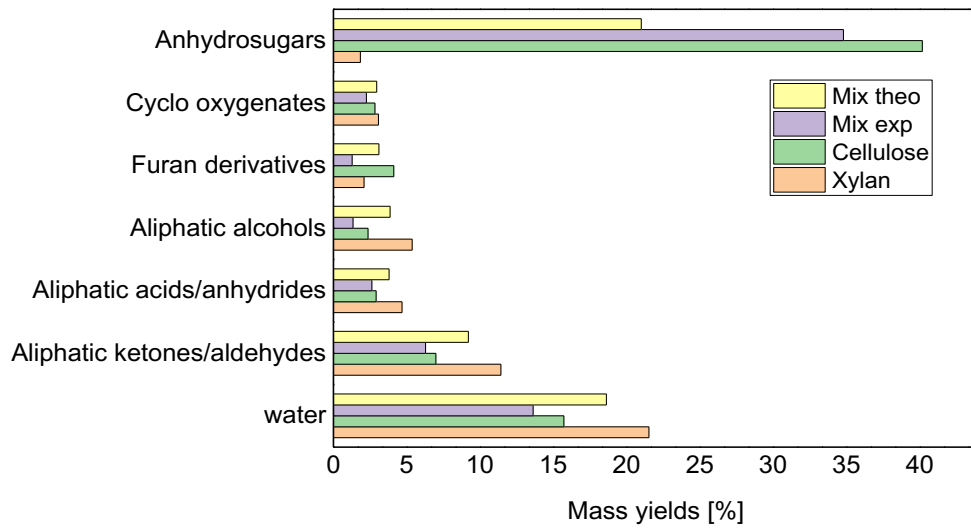


Figure 6.10: Xylan and cellulose mixture bio-oil speciation

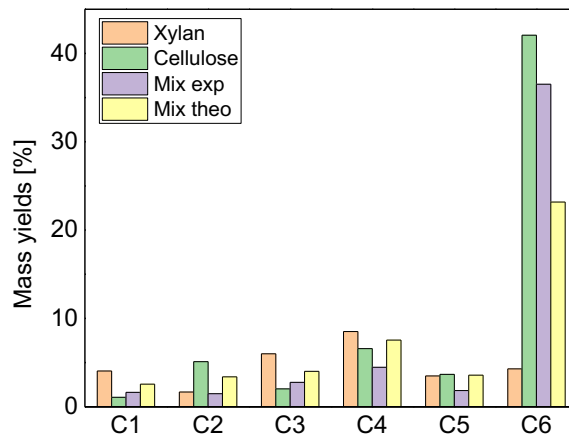


Figure 6.11: Xylan and cellulose mixture organic phase speciation

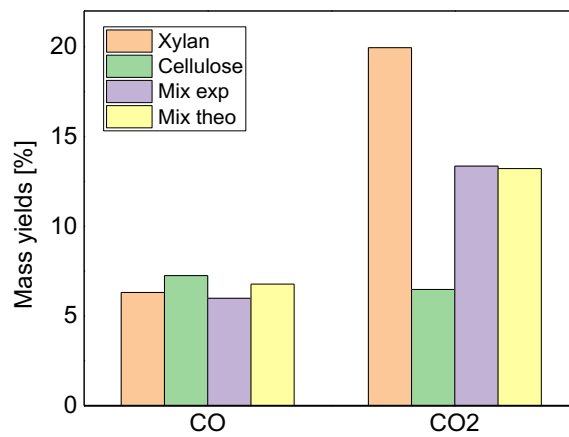


Figure 6.12: Xylan and cellulose mixture gas speciation

Once again, it is imperative to compare the results obtained from the TGA experiments with those derived from the fixed bed configuration. Nevertheless, it is crucial to emphasize again the inherent disparities between these two setups, posing notable challenges to a direct comparison.

Despite the intricacies introduced by these differences, conducting an integrated analysis of results from both the TGA and fixed bed reactor systems remains exceptionally valuable. Remarkably, the trends observed in TGA results generally align with those seen in the fixed bed reactor experiments. For example, the additive behavior of the individual components in the mixture, as evidenced by TG and DTG curves, is also apparent in experiments conducted within the fixed bed configuration.

Although some discrepancies require consideration and may warrant further investigation, the general trend does not strongly indicate the presence of mixing effects. Instead, it tends to affirm the initial hypothesis of additive behavior.

7 Conclusion

In the pursuit of sustainable solutions to mitigate the escalating challenge of high CO₂ emissions in the energy sector, the utilization of lignocellulosic biomass as a renewable feedstock emerges as a compelling strategy. Derived from abundant and diverse resources, it serves as a versatile raw material, that can be harnessed for the production of many valuable products, ranging from chemicals to fuels, making it a promising counterpart to fossil sources. The exploration of various valorization techniques has revealed the effectiveness of thermochemical routes in fully exploiting its potential. Among these processes, pyrolysis has emerged in the last years as one of the most promising technologies. By subjecting biomass to elevated temperatures in an inert atmosphere, pyrolysis yields biochar, bio-oil, and syngas—versatile energy carriers that can be utilized for heat, power generation, and even as precursors for bio-based chemicals. As we conclude this study, it becomes evident that the exploration of biomass pyrolysis not only contributes to the ongoing discourse on biomass utilization but also underscore the significance of such feedstock as integral player in the pursuit of a more sustainable and carbon-neutral energy landscape.

Within this broader context, this thesis has focused on the experimental investigation of hemicelluloses, a less-explored class of biomass components. Despite their large presence in nature alongside cellulose and lignin, they have often been overshadowed in the literature by their more extensively studied counterparts. This investigation was performed by carrying out pyrolysis experiments in a TGA-setup, aiming to collect kinetically relevant data on devolatilization trends and product speciation. Three hemicellulosic biomasses were studied – xylan, glucomannan, arabinoxylan – and compared to cellulose, used as reference biomass.

The first part of this exploration involved a meticulous examination of hemicellulose devolatilization. Through the application of Thermogravimetric Analysis (TGA), we tried to discern the intricacies of the process, with the ultimate goal of formulating kinetic models.

Analysis of three model hemicellulosic biomasses, including xylan, glucomannan, and arabinoxylan, revealed a complex devolatilization process. Thermogravimetric (TG) and derivative thermogravimetric (DTG) curves unveiled distinctive features, including changes in slope and multiple peaks, probably due to the compositional diversity of hemicelluloses, encompassing various monomer and lateral substituents.

Moreover, a lower pyrolysis onset temperature was observed with respect to cellulose, indicative of their branched and amorphous structure.

Finally, tests at varying heating rates demonstrated that an increase in the heating rate resulted in a shift of the onset temperature towards higher values, accompanied by a reduction in solid residue. This trend is primarily due to the dynamic nature of the pyrolysis experiment performed within the TGA, whose duration varies significantly with the selected heating rate, thereby varying also the extent of temperature control during the single run. These observations suggest the sensitivity of hemicellulose devolatilization to the rate of temperature increase during pyrolysis.

The second dimension of our investigation focused on the speciation of pyrolysis products employing different analytical techniques, including online mass spectrometry, offline gas chromatography and Orbo™ sorbent traps. Through a qualitative and quantitative analysis, we endeavored to quantify individual product yields and distribution of almost 50 species arising from hemicellulose degradation.

Pyrolysis products were firstly categorized in gases, bio-oil (comprising an organic phase and water), and solid residue. Product speciation was performed for xylan and glucomannan, and in both cases closure of mass balance achieved remarkable results, despite challenges encountered during the experiments and the high level of complexity of the analyzed systems, given the vast diversity of species individuated within the product slate.

The predominant observation that emerged was that bio-oil stood out as the primary pyrolysis product in glucomannan, exhibiting the highest mass yield, while for xylan a more homogenous distribution among all categories was observed. Given its significance, we delved into a detailed characterization of the organic fraction of bio-oil, which involved grouping species based on functional groups or the number of carbon atoms. Notably, distinctive product categories emerged for glucomannan and xylan. For glucomannan, anhydrosugars and furan derivatives, particularly C5 and C6 species, were prominent. In the case of xylan products were again distributed more homogeneously, but with much lower yields. Additionally, water was a significant component of the bio-oil of both biomasses, with a particularly high mass yield value for xylan. As for the gas phase CO, and CO₂ were the most significant components, with an especially high CO₂ production for xylan.

These initial insights into hemicellulose speciation underscore the complexity of the pyrolysis process and the challenges in characterizing diverse product profiles while shedding light on significant trends.

Another important outcome of this thesis involved investigating the pyrolysis of biomass mixtures, aiming to uncover potential interactions between various biomass components commonly found together in nature.

To comprehend the behavior of biomass mixtures, data acquired for single biomass components served as the basis for constructing average values, representing the behavior of a theoretical mixture. The initial hypothesis assumed an additive behavior, suggesting separate contributions of individual components to the overall behavior of the mixture. This theoretical framework was subsequently tested against experimental data to validate or challenge the assumption.

The first phase of the mixing effects investigation utilized thermogravimetric (TG) and derivative thermogravimetric (DTG) curves to characterize the devolatilization of various biomass mixtures. Remarkably, the experimental results consistently supported the hypothesis of additive behavior. The experimental curves closely matched the calculated ones, affirming that the real mixtures behaved with minimal irregularities.

The subsequent phase aimed to achieve a comprehensive product speciation of biomass mixtures. A protocol similar to that used for individual biomass samples was employed and quantitative results were obtained for gases and for heavy oxygenates, while for light oxygenates only a qualitative analysis was carried out. Quantification of vapors proved to be challenging due to the nature of the analysis, which relies on a differential sampling from the Thermogravimetric Analyzer (TGA) effluent, a characteristic that does not fit with the additive behavior of mixtures. Despite these challenges, also in this case the general trend observed was an alignment between the behavior of the real mixture and the expected one and no strong evidence was found against the hypothesis of additive behavior. However, unresolved challenges must be taken into consideration and may serve as a foundation for future investigations. A refinement in the experimental protocol is necessary to achieve a complete quantification and clearer indications towards additivity properties of mixture components.

The final phase of our investigation involved the post-processing of data gathered from experiments conducted within a fixed bed reactor configuration, which allowed tests on a scale more representative than that achievable with Thermogravimetric Analysis. The objective was to compare data for the same biomasses previously analyzed but in a different setup and diverse scale of testing. Conducting an integrated analysis of results from both the TGA and fixed bed reactor systems is highly valuable despite the complexity posed by inherent disparities between the two setups. Notably, the trends observed in TGA results generally corresponded with those seen in the fixed bed reactor experiments both for single components as well as for mixtures. For example, cellulose exhibited the lowest yield of solid residual and the highest yield of

bio-oil in both systems. Xylan consistently displayed the largest solid residue, with products evenly distributed among solid, liquid, and gas phases. Interestingly, glucomannan demonstrated behavior intermediate between cellulose and xylan. Moreover, the additive behavior of the individual components in the mixture, as evidenced by TG and DTG curves, is also apparent in experiments conducted within the fixed bed configuration. Although some discrepancies require consideration and may warrant further investigation, the general trend does not strongly indicate the presence of mixing effects. Therefore, the study of pyrolysis in an ideal configuration as that of TGA has proved to well mirror the behavior in larger scales; this confirms the high potential of TGA testing for the collection of controlled and kinetically valuable data on biomass pyrolysis.

In concluding this research journey, it is evident that exploring hemicellulose pyrolysis is both justified and enlightening. In a world increasingly committed to a green transition, where biomass stands as a cornerstone, the implications of this work extend beyond the laboratory, offering tangible contributions to the ongoing global effort for a more environmentally conscious future and leading the way for further innovations and breakthroughs in the dynamic field of biomass pyrolysis.

Bibliography

- [1] IEA, Paris <https://www.iea.org/data-and-statistics/charts/global-co2-emissions-by-sector-2019-2022>, IEA.
- [2] G. Manzolini, "Thermochemical processes", Solar and Biomass Power Generation
- [3] M.S. Galimberti, "Biomass", Chemistry for sustainable polymers
- [4] D. Mohan, C. U. Pittman, and P. H. Steele, "Pyrolysis of wood/biomass for bio-oil: A critical review," *Energy and Fuels*, vol. 20, no. 3. pp. 848–889, May 2006. doi: 10.1021/ef0502397.
- [5] Rui Katahira, Thomas J. Elder, Gregg T. Beckham; *Lignin Valorization: Emerging Approaches*, Chapter 1; 2018
- [6] Dallemand, Jean Francois; Taylor, Nigel George; Banja, Manjola. *Bioeconomy Observatory View project Energy from Waste in Croatia View project Nicolae Scarlat European Commission*. 2019.
- [7] Zadeh, Z.E.; Abdulkhani, A.; Aboelazayem, O.; Saha, B. Recent Insights into Lignocellulosic Biomass Pyrolysis: A Critical Review on Pretreatment, Characterization, and Products Upgrading. *Processes* 2020, 8, 799. <https://doi.org/10.3390/pr8070799>
- [8] Shurong Wang, Gongxin Dai, Haiping Yang, Zhongyang Luo, "Lignocellulosic biomass pyrolysis mechanism: A state-of-the-art review", *Progress in Energy and Combustion Science*, Volume 62, 2017, Pages 33-86, ISSN 0360-1285, <https://doi.org/10.1016/j.pecs.2017.05.004>.

- [9] Xu Chen, Qingfeng Che, Shujuan Li, Zihao Liu, Haiping Yang, Yingquan Chen, Xianhua Wang, Jingai Shao, Hanping Chen, "Recent developments in lignocellulosic biomass catalytic fast pyrolysis: Strategies for the optimization of bio-oil quality and yield", *Fuel Processing Technology*, Volume 196, 2019, 106180, ISSN 0378-3820, <https://doi.org/10.1016/j.fuproc.2019.106180>.
- [10] A. Demirbas, *Combustion of Biomass, Energy Sources, Part A: Recovery, Utilization, and Environmental Effects*, 29:6, 549-561, DOI: 10.1080/009083190957694
- [11] Hua-jun Huang, Xing-zhong Yuan, Recent progress in the direct liquefaction of typical biomass, *Progress in Energy and Combustion Science*, Volume 49, 2015, Pages 59-80, ISSN 0360-1285, <https://doi.org/10.1016/j.pecs.2015.01.003>.
- [12] Antonio Molino, Simeone Chianese, Dino Musmarra, Biomass gasification technology: The state of the art overview, *Journal of Energy Chemistry*, Volume 25, Issue 1, 2016, Pages 10-25, ISSN 2095-4956, <https://doi.org/10.1016/j.jechem.2015.11.005>.
- [13] Fahmy, T.Y.A., Fahmy, Y., Mobarak, F. et al. Biomass pyrolysis: past, present, and future. *Environ Dev Sustain* 22, 17–32 (2020). <https://doi.org/10.1007/s10668-018-0200-5>
- [14] Kiel, J. H., Van Paasen, S. V., Neeft, J. P., Devi, L., Ptasinski, K. J., Janssen, F. J., et al. (2004) Primary measures to reduce tar formation in fluidized-bed biomass gasifiers-final report SDE-project P1999-012". Report ECN-C-04-014, ECN, Petten.
- [15] Tao Kan, Vladimir Strezov, Tim J. Evans, Lignocellulosic biomass pyrolysis: A review of product properties and effects of pyrolysis parameters, *Renewable and Sustainable Energy Reviews*, Volume 57, 2016, Pages 1126-1140, ISSN 1364-0321, <https://doi.org/10.1016/j.rser.2015.12.185>.
- [16] François-Xavier Collard, Joël Blin, A review on pyrolysis of biomass constituents: Mechanisms and composition of the products obtained from the conversion of cellulose, hemicelluloses and lignin, *Renewable and Sustainable Energy Reviews*, Volume 38, 2014, Pages 594-608, ISSN 1364-0321, <https://doi.org/10.1016/j.rser.2014.06.013>.

- [17] D. Chen et al., "Insight into biomass pyrolysis mechanism based on cellulose, hemicellulose, and lignin: Evolution of volatiles and kinetics, elucidation of reaction pathways, and characterization of gas, biochar and bio-oil," *Combust Flame*, vol. 242, Aug. 2022, doi: 10.1016/j.combustflame.2022.112142.
- [18] M. Nasfi, M. Carrier, and S. Salvador, "Reconsidering the potential of micropyrolyzer to investigate biomass fast pyrolysis without heat transfer limitations," *J Anal Appl Pyrolysis*, vol. 165, 2022, doi: 10.1016/j.jaap.2022.105582i.
- [19] Tan Li, Jing Su, Cong Wang, Atsushi Watanabe, Norio Teramae, Hajime Ohtani, Kaige Wang, *Advances in the development and application of analytical pyrolysis in biomass research: A review*, *Energy Conversion and Management*, Volume 271, 2022, 116302, ISSN 0196-8904, <https://doi.org/10.1016/j.enconman.2022.116302>.
- [20] Ranzi, Eliseo & Cuoci, Alberto & Faravelli, Tiziano & Frassoldati, Alessio & Migliavacca, Gabriele & Pierucci, Sauro & Sommariva, Samuele. (2009). *Chemical Kinetics of Biomass Pyrolysis*. *Energy & Fuels*. 22. 4292-4300. 10.1021/ef800551t.
- [21] P. Debiagi, G. Gentile, A. Cuoci, A. Frassoldati, E. Ranzi, T. Faravelli, A predictive model of biochar formation and characterization, *Journal of Analytical and Applied Pyrolysis*, Volume 134, 2018, Pages 326-335, ISSN 0165-2370, <https://doi.org/10.1016/j.jaap.2018.06.022>.
- [22] Zhou, X., Li, W., Mabon, R., & Broadbelt, L. J. (2017). A critical review on hemicellulose pyrolysis. *Energy Technology*, 5(1), 52-79.
- [23] Ong, H. C., Chen, W. H., Singh, Y., Gan, Y. Y., Chen, C. Y., & Show, P. L. (2020). A state-of-the-art review on thermochemical conversion of biomass for biofuel production: A TG-FTIR approach. *Energy Conversion and Management*, 209, 112634.
- [24] Bahng, M. K., Mukarakate, C., Robichaud, D. J., & Nimlos, M. R. (2009). Current technologies for analysis of biomass thermochemical processing: A review. *Analytica chimica acta*, 651(2), 117-138.
- [25] Verma, Mausam & Godbout, Stéphane & Brar, Khushwinder & Solomatnikova, Olga & Lemay, S. & Larouche, Jean-Pierre. (2012). *Biofuels Production from Biomass*

by Thermochemical Conversion Technologies. *International Journal of Chemical Engineering*. 2012. 10.1155/2012/542426.

[26] Nanduri, A., Kulkarni, S. S., & Mills, P. L. (2021). Experimental techniques to gain mechanistic insight into fast pyrolysis of lignocellulosic biomass: A state-of-the-art review. *Renewable and Sustainable Energy Reviews*, 148, 111262.

[27] Mettler, M. S., Vlachos, D. G., & Dauenhauer, P. J. (2012). Top ten fundamental challenges of biomass pyrolysis for biofuels. *Energy & Environmental Science*, 5(7), 7797-7809.

[28] <https://www.megazyme.com>

[29] <https://www.sigmaaldrich.com/IT/it>

[30] Heal, G. R. (2002). Thermogravimetry and derivative thermogravimetry. *Principles of thermal analysis and calorimetry*, 52.

[31] <https://hha.hitachi-hightech.com/en/>

[32] Duckworth, H. E., Barber, R. C., & Venkatasubramanian, V. S. (1986). Mass spectroscopy.

[33] <https://www.mks.com/n/mass-spectrometry>

[34] <https://www.hidenanalytical.com>

[35] Bartle, K. D., & Myers, P. (2002). History of gas chromatography. *TrAC Trends in Analytical Chemistry*, 21(9-10), 547-557.

[36] Soria, Ana & Rodríguez-Sánchez, Sonia & Sanz, Jesús & Martínez-Castro, Isabel. (2014). Gas Chromatographic Analysis of Food Bioactive Oligosaccharides. 10.1002/9781118817360.ch20.

[37] <https://www.agilent.com>

[38] <https://www.alfatest.it/la-thermal-gravimetric-analysis-tga-e-la-simultaneous-thermal-analysis-sta/>

List of Figures

Figure 0.1: IEA, Global CO ₂ emissions by sector, 2019-2022 [1]	1
Figure 1.1: CO ₂ -neutral cycle [2]	4
Figure 1.2: Starch and cellulose [3]	4
Figure 1.3: Cellulose structure [3]	5
Figure 1.4: General hemicellulose structure [3]	5
Figure 1.5: Main monomeric units of hemicellulose [26]	6
Figure 1.6: Lignin general structure [5]	7
Figure 1.7: Biomass valorization routes [7]	9
Figure 1.8: Biomass combustion [10]	10
Figure 1.9: Basic reaction pathway for the liquefaction of biomass [11]	10
Figure 1.10: Processes in biomass gasification [12]	11
Figure 1.11: Primary mechanisms of the conversion of biomass constituents [16]	13
Figure 1.12: Reactions and evolution of lignin during pyrolysis [16]	15
Figure 1.13: Reactions and evolution of cellulose during pyrolysis [16]	16
Figure 1.14: Reactions and evolution of hemicellulose during pyrolysis [16]	17
Figure 1.15: Schematic description of a thermogravimetric analyzer [23]	18
Figure 1.16: Schematic description of a fixed bed reactor for biomass pyrolysis [25]	19
Figure 1.17: Schematic description of the pyrolizer [18]	20
Figure 1.18: Kinetic scheme of one-reaction model of hemicellulose pyrolysis [22]	23
Figure 1.19: Kinetic scheme of multi-component model of hemicellulose pyrolysis [22]	23
Figure 2.1: Xylan structure and aspect [28]	28
Figure 2.2: Arabinoxylan structure and aspect [28]	28
Figure 2.3: Glucomannan structure and aspect [28]	28
Figure 2.4: Cellulose structure and aspect [29]	29
Figure 2.5: Representation of a typical TGA instrument [38]	30

Figure 2.6: Hitachi STA7300 TG-DTA.....	31
Figure 2.7: TG and DTG curves for different biomass samples	32
Figure 2.8: Representation of a typical MS instrument [33].....	33
Figure 2.9: HPR-20 EGA mass spectrometer from HIDEN Analytical [34].....	34
Figure 2.10: MS analysis of pyrolysis gases of glucomannan.....	34
Figure 2.11: Gas Chromatograph with Flame Ionization Detection [36]	36
Figure 2.12: Agilent 6890, 5973 MSD Gas Chromatography-Mass Spectrometry with Flame Ionization Detection.....	37
Figure 2.13: MS chromatogram of glucomannan vapors	37
Figure 2.14: FID chromatogram of glucomannan vapors	38
Figure 2.15: Pairing of FID and MS chromatograms for glucomannan vapors.....	38
Figure 2.16: Orbo™ 32 – Large charcoal tubes [29].....	39
Figure 2.17: Orbo™ 23 – 2-HMP on Amberlite® XAD®-2 (20/40) [29].....	39
Figure 2.18: Orbo™ 609 Amberlite® XAD®-2 (20/50) sorbent [29]	40
Figure 3.1: TGA-based setup for biomass pyrolysis tests with complete product speciation.....	42
Figure 3.2: Calibration curve for helium.....	44
Figure 3.3: Conversion of raw data from mass spectrometer using the response factor	44
Figure 3.4: TG curve with dry mass definition	51
Figure 3.5: Example of the trend of CO ₂ (m/z=44) plotted to compute the integral area	57
Figure 3.6: Example of a GC-MS output where significant species have been detected using the online library provided by the analysis software	58
Figure 3.7: Example of mass spectrum for levoglucosan which can be associated to the corresponding peak on the GC-MS chromatogram.....	58
Figure 3.8: Example of coupling between GC-MS and GC-FID chromatograms.....	59
Figure 3.9: Example of the integration performed by the GC-FID	60
Figure 3.10: Example of the graphical char quantification	66
Figure 3.11: GC-MS at 10°C/min for glucomannan: ideal situation	69
Figure 3.12: GC-MS at 5°C/min for glucomannan: peaks are too low and less species are detected.	69

Figure 3.13: GC-FID at 10°C/min for glucomannan: peaks in the selected area are not well separated.....	69
Figure 3.14: GC-FID at 1°C/min for glucomannan: ideal situation	69
Figure 3.15: GC-FID Chromatogram using Orbo™ 32 – Large charcoal tubes	70
Figure 3.16: GC-FID Chromatogram using Orbo™ 23 – 2-HMP on Amberlite® XAD®-2 (20/40) tubes	71
Figure 3.17: GC-FID Chromatogram using Orbo™ 609 Amberlite® XAD®-2 (20/50) tubes	72
Figure 4.1: TG curves for glucomannan, xylan and arabinoxylan, under a heating rate of 100°C/min and with different carrier gas flowrate.....	77
Figure 4.2: TG curves for glucomannan, xylan and arabinoxylan under a heating rate of 100°C/min, 229ml/min of helium flowrate and with different mass values.....	79
Figure 4.3: TG (left) and DTG (right) curves for the different hemicellulose samples analyzed with a heating rate of 20°C/min	80
Figure 4.4: Mass loss curves for cellulose, arabinoxylan, glucomannan and xylan at varying heating rate.....	82
Figure 4.5: DTG curves for cellulose, arabinoxylan, glucomannan and xylan at varying heating rate	82
Figure 4.6: TG curves for xylan plotted as a function of time	83
Figure 4.7: Glucomannan main pyrolysis products.....	85
Figure 4.8: Glucomannan bio-oil speciation.....	86
Figure 4.9: Glucomannan organic phase speciation	86
Figure 4.10: Glucomannan gas speciation	87
Figure 4.11: Visual representation of standard deviation for glucomannan pyrolysis products.....	92
Figure 4.12: Xylan main pyrolysis products	93
Figure 4.13: Xylan bio-oil speciation	94
Figure 4.14: Xylan organic phase speciation	94
Figure 4.15: Xylan gas speciation.....	95
Figure 4.16: Visual representation of standard deviation for xylan pyrolysis products	98
Figure 4.17: Glucomannan and xylan pyrolysis products comparison	100
Figure 4.18: Glucomannan and xylan bio-oil comparison	101

Figure 4.19: Glucomannan and xylan organic phase comparison.....	101
Figure 4.20: Glucomannan and xylan gases comparison.....	101
Figure 5.1: Xylan and cellulose mixture pyrolysis with a heating ramp of 3°C/min	105
Figure 5.2: Xylan and cellulose mixture pyrolysis with a heating ramp of 20°C/min	105
Figure 5.3: Xylan and cellulose mixture pyrolysis with a heating ramp of 100°C/min	105
Figure 5.4: Xylan and glucomannan mixture pyrolysis with a heating ramp of 3°C/min	107
Figure 5.5: Xylan and glucomannan mixture pyrolysis with a heating ramp of 20°C/min.....	107
Figure 5.6: Xylan and glucomannan mixture pyrolysis with a heating ramp of 100°C/min.....	107
Figure 5.7: Xylan and arabinoxylan mixture pyrolysis with a heating ramp of 3°C/min	109
Figure 5.8: Xylan and arabinoxylan mixture pyrolysis with a heating ramp of 20°C/min	109
Figure 5.9: Xylan and arabinoxylan mixture pyrolysis with a heating ramp of 100°C/min.....	109
Figure 5.10: Xylan, arabinoxylan, glucomannan and cellulose mixture pyrolysis with a heating ramp of 3°C/min.....	111
Figure 5.11: Xylan, arabinoxylan, glucomannan and cellulose mixture pyrolysis with a heating ramp of 20°C/min.....	111
Figure 5.12: Xylan, arabinoxylan, glucomannan and cellulose mixture pyrolysis with a heating ramp of 100°C/min.....	111
Figure 5.13: Xylan and glucomannan mixture product quantification.....	113
Figure 5.14: Chromatograms of xylan and glucomannan mixture, xylan and glucomannan vapor analysis with main species indicated by numbers	114
Figure 5.15: Xylan and cellulose mixture product quantification.....	116
Figure 5.16: Chromatogram of xylan and cellulose mixture, xylan and cellulose vapor analysis with main species indicated by numbers.....	117
Figure 6.1: Xylan, glucomannan and cellulose pyrolysis products comparison	120
Figure 6.2: Xylan, glucomannan and cellulose bio-oil comparison.....	121
Figure 6.3: Xylan, glucomannan and cellulose organic phase comparison.....	121

Figure 6.4: Xylan, glucomannan and cellulose gases comparison.....	121
Figure 6.5: Xylan and glucomannan mixture main pyrolysis products	123
Figure 6.6: Xylan and glucomannan mixture bio-oil speciation	124
Figure 6.7: Xylan and glucomannan mixture organic phase speciation	124
Figure 6.8: Xylan and glucomannan mixture gas speciation.....	124
Figure 6.9: Xylan and cellulose mixture main pyrolysis products	125
Figure 6.10: Xylan and cellulose mixture bio-oil speciation	126
Figure 6.11: Xylan and cellulose mixture organic phase speciation.....	126
Figure 6.12: Xylan and cellulose mixture gas speciation.....	126

List of Tables

Table 1.1: Monomeric composition of hemicellulose [22]	6
Table 1.2: Biomass composition	7
Table 1.3: Pyrolysis process variants [4]	12
Table 2.1: Hemicellulose composition [28,29]	27
Table 3.1: Calibration factors for species in mass spectrometer	46
Table 3.2: Mother solution	47
Table 3.3: Response factors for different calibration solutions.....	48
Table 3.4: Moisture (%) of different biomasses	52
Table 3.5: Example of the numerical output of the GC software.	60
Table 3.6: Example of the quantification's results: in green the species considered as heavy products	62
Table 3.7: Temperature ramp used in the GC analysis of different biomass samples	68
Table 4.1: Solid residue for samples subjected to different carrier flowrates.....	78
Table 4.2: Solid residue for samples of different mass	79
Table 4.3: Glucomannan pyrolysis vapors products	87
Table 4.4: Standard deviation for glucomannan pyrolysis products	92
Table 4.5: Xylan pyrolysis vapors products	95
Table 4.6: Standard deviation for xylan pyrolysis products.....	99
Table 5.1: Mass yields of xylan and glucomannan mixture products.....	113
Table 5.2: Common species found in xylan, glucomannan and xylan and glucomannan mixture.....	115
Table 5.3: Mass yields of xylan and cellulose mixture products.....	116
Table 5.4: Common species found in xylan, cellulose and xylan and cellulose mixture	118

